ISSN: 0128-7680

Pertanika Journal of

SCIENCE & TECHNOLOGY

VOLUME 9 NO.2
JULY 2001

A scientific journal published by Universiti Putra Malaysia Press

Pertanika Journal of Science & Technology

About the Journal

Pertanika, the poineer journal of UPM, began publication in 1978. Since then, it has established itself as one of the leading multidisciplinary journals in the tropics. In 1992, a decision was made to streamline Pertanika into three journals to meet the need for specialised journals in areas of study aligned with the strengths of the univeristy. These ara **(i) Pertanika Journal of Tropical Agricultural Science, (ii) Pertanika Journal of Science and Technology (iii) Pertanika Journal of Social Science and Humanities**.

Aims and Scope

Pertanika Journal of Science and Technology welcomes full papers and short communications in English or Bahasa Melayu in the fields of chemisty, physics, mathematics and statistics, engineering, environmental control and management, ecology and computer science. It is published twice a year in January and July.

Articles must be reports of research not previously or simultaneously published in other scientific or technical journals.

Communications are notes of a significant finding intended for rapid publication. It should not exceed five double-spaced typerwritten pages and must be accompanied by a letter from the author justifying its publication as a communication.

Reviews are critical appraisals of literature in areas that are of interest to a broad spectrum of scientists and researchers. Review papers will be published upon invitation.

Submission of Manuscript

Three complete clear copies of the manuscript are to be submitted to

The Chief Editor
Pertanika Journal of Science and Technology
Universiti Putra Malaysia
43400 UPM Serdang, Selangor Darul Ehsan
MALAYSIA
Tel: 89486101 Ext: 1326; Fax (603)89416172

Proofs and Offprints

Page proofs, illustration proofs, the copy-edited manuscript and an offprint order form will be sent to the author. Proofs must be checked very carefully within the specified time as they will not be proofread by the Press editors.

Authors will receive 20 offprints of each article. Additional copies can be ordered from the Secretary of the Editorial Board by filling out the offprint order form.

Published by Universiti Putra Malaysia Press
ISSN No.: 0128-7680

Pertanika Journal of Science & Technology

Volume 9 No. 2, 2001

Contents

ISSN: 0128-7680
Pertanika J. Sci. & Technol. 9(2): 143 - 147 (2001)

Coumarins from *Hedyotis dichotoma* (Rubiaceae)

Rohaya Ahmad, Ahmad Sazali Hamzah, Halila Jasmani, Abdul Razak Baba, Nordin Hj. Lajis[1] and Masataka Konishi[2]

Faculty of Science, Universiti Teknologi MARA
40450 Shah Alam, Selangor, Malaysia
[1]Institute of Bioscience, Universiti Putra Malaysia
43400 UPM Serdang, Selangor, Malaysia
[2]School of Pharmaceutical Sciences, Toho University
Miyama 2-2-1, Funabashi, Chiba 274, Japan

Received: 23 February 1999

ABSTRAK

Kajian kimia ke atas akar-akar *Hedyotis dichotoma* menghasilkan dua kumarin, skopoletin dan fraksin, bersama-sama dengan empat metabolit tumbuhan yang diketahui; isoviteksin, asid ursolik, asid geniposidik, dan asid klorogenik serta dua antrakuinon; 1,4-dihidroksi-2,3-dimetoksiantrakuinon dan 2,3-dimetoksi-9-hidroksi-1,4-antrakuinon. Struktur kedua-dua kumarin dikenalpasti melalui teknik spektroskopi moden.

ABSTRACT

Chemical investigation on the roots of *Hedyotis dichotoma* yielded two coumarins, scopoletin and fraxin, along with four more known plant metabolites; isovitexin, ursolic acid, geniposidic acid and chlorogenic acid and two anthraquinones; 1,4-dihydroxy-2,3-dimethoxyanthraquinone and 2,3-dimethoxy-9-hydroxy-1,4-anthraquinone. The structures of both coumarins were elucidated using modern spectroscopic techniques.

Keywords: scopoletin, fraxin, coumarins, *Hedyotis dichotoma*, Rubiaceae

INTRODUCTION

Hedyotis or Oldenlandia is a large genus of herbs or somewhat shrubby plants of the family Rubiaceae which can be found throughout the tropics. There are approximately 180 species recorded of which 35 were identified in Malaysia (Ridley, 1923). These plants are often used for medicinal purposes and among the 35 Malaysian species, the most common representatives include *H. capitellata, H. dichotoma, H. diffusa, H. herbacea and H. verticillata* (Burkill 1966). Previous chemical studies on the genus *Hedyotis* include *H. verticillata, H. herbacea, H. chrysotricha, H. diffusa, H. corymbosa, H. lawsoniae* and *H. auricularia* (Hamzah *et al.*, 1996, Hamzah *et al* 1994, Fang *et al* 1992, Wu *et al* 1991, Ho *et al* 1986, Matsuda *et al* 1984, Puroshotaman *et al* 1981). Our interest has been mainly on *H. dichotoma* which is a small herb (0.1 - 0.2 m tall) commonly found in open places, especially in sandy areas. The leaves of the plant are sold locally and used as poultice. The roots of *H. dichotoma* have previously yielded two new anthraquinones; 1,4-dihydroxy-2,3-dimethoxyanthraquinone and 2,3-dimethoxy-9-hydroxy-1,4-anthraquinone (Hamzah *et al* 1997). As part of our continuing

interest in the constituents of *H. dichotoma*, we now report the isolation of two coumarins from the roots of the plant. Scopoletin or 7-hydroxy-6-methoxy-coumarin [1] and fraxin or 8-O-β-D-glucopyranosyl-7-hydroxy-6-methoxy-coumarin [2] have been identified using spectroscopic techniques. This is the first time a coumarin has been isolated from the genus *Hedyotis*.

MATERIALS AND METHODS

Plant Materials

H. dichotoma was collected from Gebeng, Kuantan, Malaysia and the voucher specimen was deposited at the herbarium of Biology Department, Universiti Putra Malaysia.

General

Melting points were determined on a Kofler hot stage apparatus and are uncorrected. UV spectra were recorded on Shidmazu UV-VIS 160 and IR spectra on Perkin Elmer 1600 FTIR spectrometers. Mass spectra were recorded on Jeol JMS DX 303. Ionization was induced by electron impact at 70 eV. ^{1}H-NMR and ^{13}C-NMR spectra were recorded on Jeol JNM A 500 spectrometer at 400 (^{1}H) and 100 (^{13}C) MHz, respectively. For column chromatography and analytical tlc, we utilized Merck 7734 and Merck DC-Plastikfollen 60 F_{254}, respectively.

Extraction and Isolation

The ground roots of *H. dichotoma* (300 g) were soaked in dichloromethane for forty-eight hours. The dichloromethane was removed by filtration and fresh dichloromethane was then added to the roots. The filtrates were combined and evaporated under reduced pressure to give a reddish viscous mass (1.6 g). The crude extract was subjected to column chromatography using dichloromethane with increasing amounts of methanol. Thirty-three fractions were collected. Fractions 25, 26 and 27 were combined and was subjected again to column chromatography using gradient elution with CH_2Cl_2/EtOAc. Preparative thin layer chromatography of fractions 8-11 using [EtOAc:CH_2Cl_2: MeOH(7:2:1)] afforded scopoletin [1]. Fractions 30 - 33 were combined and subjected to preparative thin layer chromatography using [CH_2Cl_2/EtOAc (95:5)] to afford fraxin [2].

Scopoletin [1]

Red crystals; mp 204-206°C; fabms m/z (%): 192(100), 177(75), 164(34), 149(53), 135(22), 120(23); UV λ_{max} (MeOH, log ε) 343.6(0.873), 252.6 (0.429) nm; IR ν_{max} (KBr disk): 3342, 2920, 2852, 1705, 1609, 1567, 1511, 1436, 1377, 1292 cm^{-1}; ^{13}C-NMR (100 MHz, $CDCl_3$): δ 161.41 (C-2), 150.28 (C-7), 149.68 (C-6), 143.99 (C-8), 143.26 (C-9), 113.44 (C-3), 111.50 (C-10), 107.48 (C-5), 103.21 (C-4), 56.41 (OMe); ^{1}H-NMR δ 7.59 (d, H-4), 6.92 (s, H-8), 6.85 (s, H-5), 6.28 (d, H-3), 3.96 (s, 3 OMe).

Fraxin [2]
White amorphous powder; mp 205-207°C; fabms m/z (%): 393(35), 371(10), 209(45), 177(60); UV λ_{max} (MeOH) 237, 297, 356 nm; IR ν_{max} (KBr disk): 3421, 2935, 2868, 1719, 1674, 1598, 1506, 1458, 1292, 1230, 1078 cm^{-1}.

TABLE 1
^{1}H-NMR & ^{13}C-NMR spectra of compound 2 (δ:ppm in CD_3OD)

Number	^{1}H	^{13}C
1		
2	6.24(1H,d,J=9.3Hz)	164.1
3	7.85(1H,d,J=9.3Hz)	111.4
4	6.98(1H,s)	146.7
5		106.6
6		148.5
7		146.7
8		133.7
9		144.6
10		110.9
OCH_3	3.91(3H,s)	56.8
1'	4.96(1H,d,J=7.7Hz)	105.8
2'	3.3-3.6 (4H,m)	75.5
3'		78.5
4'		71.0
5'		78.5
6'	3.71(1H,dd,J=5.1&12.1Hz)	62.3
	3.80(1H,dd,J=2.6&12.1Hz)	

RESULTS AND DISCUSSION

Chemical investigation on the dichloromethane extracts of the roots of *H. dichotoma* led to the isolation of two compounds. For compound [1], the FAB-MS spectrum showed the molecular ion peak at m/z 192 which analyzed for $C_{10}H_8O_4$. The fragment at m/z 177 indicated cleavage of a methyl group from the methoxy group. The IR spectrum showed an absorption band at 1705 cm^{-1} and 1567 cm^{-1} suggesting the presence of a carbonyl group and C-O stretching respectively. Aromatic stretching frequencies appeared at 1609 cm^{-1}. The UV

spectrum showed an absorption maximum at 343.6 nm which was shifted to 392 nm upon addition of alkaline ethanol. This is indicative of a coumarin-type compound (Abu-Eittah and El-Tawil, 1985). The ^{13}C-NMR spectrum showed the presence of ten carbon signals for the molecule and a peak at δ 161.4 ppm indicated the presence of a carbonyl group. The singlet at δ 56.4 ppm was attributed to a methyl signal of the methoxy group. In the ^{1}H-NMR spectrum, a singlet at 3.96 ppm integrated for three protons was due to the methoxy group. Two singlets at 6.85 and 6.92 ppm were assigned to the isolated aromatic protons (H-5 and H-8) in ring B of the coumarin. A doublet at 7.59 ppm was due to H-4 coupled to H-3. A similarly coupled doublet was observed for H-3 at 6.28 ppm (Pouchert *et al* 1993).

Compound [2], a white amorphous powder showed pseudo-molecular ion peaks at m/z 371 (M + H$^+$) and 393 (M + Na$^+$) which corresponded to a molecular formula of $C_{16}H_{18}O_{10}$. The peak at m/z 209 was assignable to the aglycone due to cleavage of the glucoside group and m/z 177 was demethylated aglycone. The UV spectrum showed absorption maxima at 237 nm and 356 nm. The IR spectrum displayed bands at 1674 cm^{-1} and 1598 cm^{-1} indicating the presence of a carbonyl group and C-O stretching respectively. The ^{13}C NMR spectrum was typical of a coumarin-type compound as seen in Table 1 (Chen *et al* 1984). In addition, there were signals due to the sugar moiety present in the molecule. In the ^{1}H-NMR spectrum, a doublet at 7.85 ppm was due to H-4 coupled to H-3. Similarly, a doublet at 6.24 was assigned as H-3. Although both were olefinic protons, this assignment was supported by the fact that β-proton resonates significantly lower field than α-proton in the α, β-unsaturated ketone. A singlet observed at 6.98 arises from the isolated proton at H-5. The methoxy proton resonated at 3.91 ppm. The proton signals of the sugar unit were also present in the upfield region. A doublet at 4.96 ppm with a *J* value of 7.7 Hz was due to the anomeric protons of the glucoside, suggesting that the sugar has an α-linkage to the coumarin skeleton (Dubois *et al* 1990).

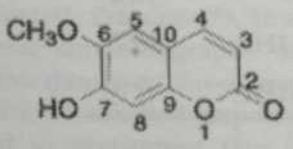

[1] Scopoletin

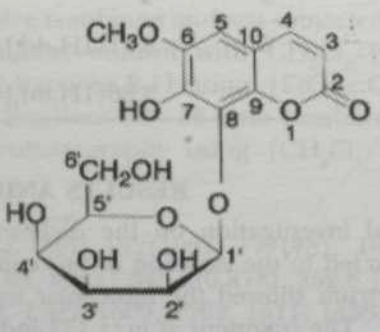

[2] Fraxin

ACKNOWLEDGEMENTS

The authors thank the Bureau of Research and Consultancy of Universiti Teknologi MARA for financial assistance.

REFERENCES

ABU-EITTAH, R.H. and A.H. EL-TAWIL. 1985. The electronic spectra of some coumarins. A molecular orbital treatment. *Can. J. Chem.* **63:** 1173-1179.

BURKILL, I.H. 1966. *A Dictionary of the Economic Products of the Malay Peninsula.* Vols 1 and 2: 1148-1150. London: Crown Agents for the Colonies.

CHEN, Y., T. TAKEDA and Y. OGIHARA. 1984. Studies on the constituents of *Xanthoceras sorbifolia* BUNGE. *Shoyakugaku Zasshi* **38(2):** 203-206

DUBOIS, M., M. WIEBER and H. WAGNER. 1990. Palustroside, a coumarin glucoside ester from *Ledum palustre. Phytochemistry* **29(10):** 3369-3371.

FANG, Z., Y. YIFANG and Z. GUISHENG. 1992. Isolation and identification of chemical constituents of *Hedyotis chrysotricha* (Palib.). *Zhongguo Zhongyao Zazhi* **17:** 98-100.

HAMZAH, A.S., H. JASMANI, R. AHMAD, A.R. BABA, N.H. LAJIS, N. AIMI, M. KITAJIMA and H. TAKAYAMA. 1997. New Anthraquinones from the roots of *Hedyotis dichotoma. Jour. Natural Products* **60:** 36-37.

HAMZAH, A.S., N. AIMI and N.H. LAJIS. 1996. Constituents of *Hedyotis herbaceae* (Rubiaceae). *Pertanika J.Sci. Technol.* **24(3)**: 273.

HAMZAH, A.S., N.H. LAJIS and M.V. SARGENT. 1994. Kaempferitrin from the leaves of *Hedyotis verticillata* and its biological activity. *Planta Med.* **60:** 388-389.

HO T.I., P.C. GEN, Y.M. LIN and F.A. CHEN. 1986. An anthraquinone from *Hedyotis diffusa. Phytochemistry* **25:** 1988-1999.

MATSUDA, S., S.KADOTA, T. TAI and T. KIKUCHI. 1984. Isolation and structure of hedyotisol-A, -B and -C. Novel dilignans from *Hedyotis lawsoniae. Chem. Pharm. Bull.* **32:** 5066-5069.

POUCHERT, C.J. and J. BEHNKE. 1993. *The Aldrich Library of ^{13}C-NMR and ^{1}H-NMR FT NMR. Spectra* **2:** 1314

PUROSHOTAMAN, K.K. and A. SARADA. 1981. Structure of auricularine, a bis-indole alkaloid from *Hedyotis auricularia. Phytochemistry* **20:** 351-352

RIDLEY, H.N. 1923. *The Flora of the Malay Peninsula.* London:Richard Clay and Sons

TAKAGI, S., M.YAMAKI, K.MASUDA, Y.NISHIHAMA K.SAKINA, 1981. Studies on the constituents of *Hedyotis corymbosa* Lam. *Yakugakuzasshi-Journal of the Pharmaceutical Society of Japan,* **101(7)**: 657-659

WU, A., X. TAO, Q. CHEN and X. LAU. 1991. Iridoids from *Hedyotis diffusa. J. Nat.Prod.* **54:** 254-256

ISSN: 0128-7680
Pertanika J. Sci. & Technol. 9(2): 149 - 155 (2001)

Kepadatan-F Kabur dalam Ruang Hausdorff Kabur

Abd. Fatah Wahab dan Abu Osman Md Tap[1]
Jabatan Matematik
Fakulti Sains dan Teknologi
Kolej Universiti Sains & Teknologi Malaysia (KUSTEM)
21030 Mengabang Telipot, Kuala Terengganu
Terengganu, Malaysia
[1]Pusat Pengajian Sains Matematik
Fakulti Sains dan Teknologi
Universiti Kebangsaan Malaysia
43600 UKM Bangi, Selangor DE., Malaysia

Diterima: 6 Julai 1996

ABSTRAK

Kepadatan-F kabur ditakrifkan dalam ruang Hausdorff kabur dan hubungannya dengan sifat minimum kabur, sifat tertutup mutlak kabur serta kepadatan-C kabur dikaji. Selanjutnya rim padat-F kabur diperkenalkan.

ABSTRACT

Fuzzy F-compactness is defined in a fuzzy Hausdorff space and its relationships with fuzzy minimality, fuzzy absolutely closed and fuzzy C-compactness are studied. Furthermore fuzzy rim F-compactness is introduced.

Kata kunci: kepadatan-F kabur, kepadatan-C kabur, rim padat-F kabur

PENDAHULUAN

Dalam topologi biasa, konsep kepadatan fungsian (ringkasnya kepadatan-F) telah diperkenalkan oleh Dickman & Zame (1969) yang kemudiannya diperluaskan oleh Goss & Viglino (1970). Sejak Zadeh (1965) memperkenalkan set kabur, banyak konsep di dalam topologi biasa telah diitlakkan kepada topologi kabur.

Dalam kertas ini kita akan terima pakai ruang topologi Chakraborty & Ahsanullah (1992) yang diubah suai dari ruang topologi Chang (1968). Kita juga terima pakai konsep Hausdorff oleh Srivastava *et al.* (1981). Kita lambangkan ruang topologi kabur (ringkasnya rtk) dengan (X,τ) atau X sahaja tanpa kekeliruan. Untuk pengetahuan asas mengenai konsep topologi kabur, kepadatan kabur dan lain-lain, pembaca dirujuk kepada Abd. Fatah (1992). Abd. Fatah & Abu Osman (1996a.b). Chakraborty & Ahsanullah (1992), Chang (1968), De Prada & Saralegui (1988), Pu & Liu (1980a), Srivastava *et al.* (1981), Wong(1973, 1974) dan Zadeh (1965).

Kertas ini akan memperkenalkan konsep kepadatan-F kabur dalam ruang topologi Hausdorff kabur (X,τ) dan mengkaji kaitannya dengan kepadatan-C kabur. Hausdorff minimum kabur dan tertutup mutlak kabur. Konsep rim padat-F kabur juga diperkenalkan dan kaitannya dengan padat-F kabur dikaji.

PADAT-F KABUR

Konsep kepadatan-F kabur dan sifatnya merupakan salah satu konsep kepadatan kabur yang dapat diperluas melalui hubungannya dengan asas turas kabur dalam X. Dalam bahagian ini, kita akan mengkaji pencirian ruang Hausdorff yang padat-F kabur dengan ruang Hausdorff minimum kabur dan serta mengkaji sifat- sifatnya melalui pemetaan kabur.

TAKRIF 1. *Turas Kabur* dalam rtk (X,τ) adalah famili subset kabur $\Im = \{F_i\}_{i\in I}$ bagi X dengan sifat-sifat seperti berikut:

i. Jika $F_i, F_j \in \Im$ maka $F_i \cap F_j \in \Im$;
ii. Jika $F_i \in \Im$ dan $F_i \subset F_j$ maka $F_j \in \Im$;
iii. $\emptyset \notin \Im$.

Subfamili β bagi $\Im$ dinamakan *asas turas kabur* dalam $\Im$ jika untuk sebarang $F \in \Im$, wujud $B \in \beta$ sehingga $B \subset F$.

TAKRIF 2. Ruang Hausdorff kabur (X,τ) dikatakan *padat-F* kabur jika apabila diberikan β suatu asas turas kabur dalam X sehingga $A = \cap \{B_i | B_i \in \beta\} = \cap\{Ttp(B_i)(B_i \in \beta\}$ maka β merupakan asas kabur untuk jiranan kabur bagi A.

TAKRIF 3. Ruang Hausdorff kabur (X,τ) dikatakan *tertutup mutlak kabur* jika untuk setiap f homeomorfisma kabur daripada X kepada suatu subruang kabur bagi ruang Hausdorff kabur Y, f[X] tertutup kabur dalam Y.

Langsung daripada takrif kepadatan-F kabur dengan sifat Hausdorff minimum kabur (Lihat Abd. Fatah & Abu Osman (1996a), dapat ditunjukkan hasil yang utama sebagai yang berikut.

TEOREM 1. *Setiap ruang Hausdorff padat-F kabur adalah Hausdorff minimum kabur dan dengan itu tertutup mutlak kabur.*

Sekarang, kita akan menulis sifat utama bagi ruang Hausdorff yang padat-F kabur yang dapat dicirikan seperti teorem yang berikut.

TEOREM 2. *Ruang Hausdorff kabur (X,τ) adalah padat-F kabur jika setiap fungsi selanjar kabur daripada X kepada suatu ruang Hausdorff kabur adalah tertutup kabur.*

Bukti. Misalkan ruang Hausdorff kabur (X,τ) padat-F kabur, (Y,σ) ruang Hausdorff kabur dan $f : (X,\tau) \to (Y, \sigma)$ fungsi selanjar kabur. Misalkan pula Q subset tertutup kabur dalam X dan andaikan f[Q] terbuka kabur sehingga wujud suatu titik kabur $y_t \in Ttp_y(f[Q]) \setminus f[Q])$. Misalkan pula $A=\{A_i | A_i$ subset terbuka kabur bagi Y, $y_t \in A_i\}$ dan $\beta = \{f^{-1}[A_i] \ | A_i \in A\}$. Dengan Teorem 1, X menjadi ruang Hausdorff minimum kabur dan tertutup mutlak kabur. Oleh kerana setiap imej selanjar kabur bagi ruang Hausdorff tertutup mutlak kabur adalah tertutup mutlak kabur, maka $f[X] = Ttp_Y(f[X])$. Dengan itu, didapati $y_t \in f[X]$. Jadi β merupakan pungutan subset terbuka kabur tak hampa bagi X.

Oleh yang demikian, β merupakan asas turas terbuka kabur dalam X. Seterusnya, oleh kerana Y ruang Hausdorff kabur, maka $\{f^{-1}[y_t]\} = \cap\{B_i \mid B_i \in \beta\} = \cap\{Ttp_Y(B_i) \mid B_i \in \beta\}$. Jadi dengan Takrif 1, β merupakan asas kabur untuk jiranan kabur bagi $\{F^{-1}[y_t]\}$. Maka wujud $B \in \beta$ sehingga $B \subseteq X \setminus Q$. Oleh kerana $B=f^{-1}[f[B]]$ untuk $B \in \beta$, maka f(B) merupakan subset terbuka kabur dalam f(X) dengan $y_t \in f^{-1}[B]$ dan $f[B] \cap f[Q] = \varnothing$. Ini suatu percanggahan. Oleh itu f[Q] adalah tertutup kabur.

Akasnya, misalkan setiap fungsi selanjar kabur daripada X kepada suatu ruang Hausdorff kabur adalah tertutup kabur, dan misalkan pula β merupakan asas turas kabur dalam X sehingga $A = \cap\{B_i \mid B_i \in \beta\} = \cap\{Ttp(B_i) \mid B_i \in \beta\}$. Misalkan seterusnya wujud J suatu subset terbuka kabur bagi X yang me-ngandungi A sehingga $(X \setminus J) \cap B_i \neq \varnothing$, $\forall B_i \in \beta$. Misalkan $Y = X \setminus A$ dan $f : X \to Y$ suatu pemetaan bersahaja kabur ke seluruh Y ditakrifkan dengan $x_s \in f[x_s]$ untuk setiap $x_s \in X$. Sekarang takrifkan U suatu asas untuk topologi kabur seperti berikut:

$U \in U \Leftrightarrow$ (i) $f^{-1}[U]$ merupakan subset terbuka kabur bagi $X \setminus A$, atau
(ii) $f^{-1}[U] \in U$

Maka Y dengan topologi kabur ini adalah ruang Hausdorff kabur dan $f:X \to Y$ selanjar kabur dan keseluruh. Dengan hipotesis, f tertutup. Perhatikan $f[X \setminus J]$ tidak tertutup kabur kerana f[A] set titik had kabur bagi $f[X \setminus J]$. Ini merupakan percanggahan. Maka (X,τ) adalah ruang Hausdorff padat -F kabur. Sebagai natijah Teorem 2, diperoleh hasil berikut:

KOROLARI 1. *Misalkan (X,τ) ruang Hausdorff kabur, (Z,σ) ruang Hausdorff padat-F kabur dan $h: Z \to X$ suatu fungsi selanjar kabur keseluruh. Maka (X,τ) adalah padat-F kabur juga.*

Bukti. Misalkan f fungsi selanjar kabur daripada X kepada suatu ruang Hausdoff kabur Y dan K subset tertutup kabur dalam X. Oleh kerana ruang Hausdorff kabur Z padat-F kabur, maka dengan Teorem 2, foh: $Z \to Y$ adalah tertutup kabur dan oleh itu, $f[K]=foh\ [h^{-1}[K]]$ merupakan subset tertutup kabur dalam Y. Jadi f adalah tertutup kabur dan sekali lagi dengan Teorem 2, X adalah ruang Hausdorff padat-F kabur.

Kita ketahui bahawa setiap subset tertutup kabur di dalam suatu ruang Hausdorff kabur adalah padat kabur (Lihat Abd. Fatah (1992)). Untuk ruang Hausdorff padat-F kabur pula diperlukan syarat tambahan seperti dalam kes topologi biasa. (Lihat Dickman & Zame (1969). Syarat tambahan tersebut ialah tertutup sekata kabur yang diperkenalkan oleh Azad (1981).

TAKRIF 4. Subset tertutup kabur K di dalam ruang Hausdorff kabur (X,τ) dikatakan *tertutup sekata kabur* jika untuk setiap titik kabur x_s dalam $X \setminus K$, wujud $N(x_s)$ jiranan kabur bagi x_s dengan sifat $Ttp\ (N(x_s) \cap (K = \varnothing$.

TEOREM 3. *Misalkan ruang Hausdorff kabur (X,τ) padat-F kabur dan K subset tertutup sekata kabur bagi X. Maka K adalah padat-F kabur.*

Bukti. Misalkan $\alpha = \{A_i\}$ asas turas kabur dalam subset tertutup sekata kabur K dalam X sehingga $\cap \{A_i \mid A_i \in \alpha\} = \{Ttp_K (A_i) \mid A_i \in \alpha\} = A$. Sekarang misalkan pula $\beta=\{B_i\}$ asas turas kabur dalam X sehingga $(B_i \cap K) \in \alpha$. Oleh kerana K subset tertutup sekata kabur dalam X, maka $A = \cap \{B_i \mid B_i \in \beta\} = \cap \{Ttp_x (B_i) \mid B_i \in \beta\}$. Oleh kerana (X,τ) ruang Hausdorff padat-F kabur, maka β merupakan asas kabur bagi jiranan kabur A. Oleh itu, α adalah asas kabur untuk jiranan kabur A relatif kepada K. Oleh yang demikian K adalah padat-F kabur.

Sekarang kita akan mencirikan ruang padat-F kabur dengan konsep tudung terbuka kabur seperti berikut.

TEOREM 4. Misalkan (X,τ) ruang Hausdorff padat-F kabur. Jika diberikan K subset tertutup sekata kabur bagi X. O tudung terbuka kabur bagi X\K dan U jiranan terbuka kabur bagi, maka wujud $O_i \in O$, i =1,2, ..., n sehingga

$$X = U \cup Ttp_x\left(\bigcup_{i=1}^{n} O_i\right).$$

Bukti. Misal (X,τ) ruang Hausdorff padat-F kabur dan K suatu subset tertutup sekata kabur bagi X. Misalkan O tudung terbuka kabur bagi X\K, maka $X\backslash K \subset \cup O_i$, $O_i \in O$. Misalkan U jiranan terbuka kabur bagi K. Maka takrif dan Teorem 1, wujud $O_i \in O$ 1,2,..., n sehingga $X = U \cup Ttp_x\left(\bigcup_{i=1}^{n} O_i\right)$.

TEOREM 5. Misalkan ruang Hausdorff F-padat kabur (X,τ) tertutup mutlak kabur dan seminormal sekata kabur. Jika diberikan K suatu subset tertutup sekata kabur bagi X dan Q tudung terbuka kabur bagi X\K dan N suatu jiranan terbuka kabur bagi K, maka wujud $Q_i \in O$ i = 1,2,..., n sehingga

$$X = U \cup Ttp_x\left(\bigcup_{i=1}^{n} Q_i\right).$$

Bukti. Misalkan K suatu subset terbuka sekata kabur bagi X dan Q tudung terbuka kabur bagi X\K. Misalkan N suatu jiranan kabur bagi K. Pilih suatu subset terbuka sekata kabur S dan $Q_i \in Q$ dengan i = 1,2,..., n sehingga $K \subset S \subset N$ dan $X\ Ttp\left(\bigcup_{i=1}^{n} Q_i\right)$. Oleh kerana S suatu subset terbuka sekata kabur, maka didapati $Ttp\ (S)\backslash S \subset Ttp_x\left(\bigcup_{i=1}^{n} Q_i\right)$. Oleh itu $X = N \cup Ttp_x\left(\bigcup_{i=1}^{n} Q_i\right)$.

Sekarang, dalam bahagian ini kita akan melihat hubungan kepadatan-F kabur dengan kepadatan-C kabur dalam ruang Hausdorff kabur. Bagi tujuan tersebut kita takrifkan kepadatan-C kabur sebagai berikut:

TAKRIF 5. Ruang topologi kabur (X,τ) dikatakan *padat-C kabur* jika diberikan Q subset tertutup kabur dalam X dan O tudung terbuka kabur bagi Q, wujud O_i, i = 1, 2, ..., n bagi O terbuka kabur bagi Q, dengan $Q \subset \mathrm{Ttp}_x\left(\bigcup_{i=1}^{n} O_i\right)$.

Hubungan antara ruang Hausdorff yang padat-C kabur dengan ruang Hausdorff yang padat-F kabur dapat dinyatakan sebagai hasil berikut.

TEOREM 6. *Ruang Hausdorff padat-C kabur adalah juga padat-F kabur.*

Bukti. Misalkan (X,τ) ruang Hausdorff padat-C kabur dan $\beta = \{B_i\}$ asas turas terbuka kabur dalam X. Misalkan pula $A=\cap\{\mathrm{Ttp}(B_i) \mid B_i \in \beta\}$ subset tertutup kabur dalam X. Oleh kerana X padat-C kabur, maka $A \subset \mathrm{Ttp}\left(\bigcup_{i=1}^{n} B_i\right)$. Sekarang misalkan N jiranan kabur bagi A sehingga $N_A = \mathrm{Ttp}\left(\bigcup_{i=1}^{n} B_i\right)$. Maka β merupakan asas kabur dalam jiranan kabur A dan dengan Takrif 2, X adalah padat-F kabur.

Akas bagi teorem ini adalah tidak benar. (Lihat Dickman & Zame, 1969 dan Viglino, 1969).

RIM PADAT-F KABUR

Dalam Abd. Fatah & Abu Osman (1996b), kepadatan-C kabur dapat dihubungkan sebagai gabungan rim padat-C kabur dengan tertutup mutlak kabur. Sekarang diperkenalkan pula konsep rim padat-F kabur dan diperlihatkan hubungannya dengan kepadatan-F kabur. Bagi tujuan tersebut, dilihat dahulu takrif berikut:

TAKRIF 6. Misalkan M subset kabur bagi X. Suatu tudung terbuka kabur $\{O_i\}_{i\in I}$ bagi M dinamakan *tudung sekata kabur* jika $X \setminus \bigcup_{i\in I} O_i$ merupakan subset tertutup sekata kabur.

TAKRIF 7. Ruang Hausdorff kabur (X,τ) dinamakan *rim padat-F kabur* jika wujud suatu sistem jiranan kabur bagi setiap titik kabur dalam X yang terdiri daripada subset tertutup kabur V, dengan syarat diberikan Q sebagai subset tertutup kabur bagi Ttp (V)\V dan V suatu tudung sekata kabur bagi Q, maka wujud $V_i \in V$.

$i = 1,2,..., n$ dengan $Q \subset Ttp_x\left(\bigcup_{i=1}^{n} V_i\right)$.

Seperti yang dinyatakan di atas, kepadatan-F kabur dapat dihubungkan dengan sifat rim padat-F kabur dan tertutup mutlak kabur sebagai berikut.

TEOREM 7. Ruang Hausdorff kabur (X,τ) adalah padat-F kabur jika X rim F-padat kabur dan tertutup mutlak kabur.

Bukti. Misalkan $U \in U$ yang U tudung terbuka sekata kabur bagi X. Untuk setiap titik kabur $y_t \in U$, pilih $N(y_t)$ jiranan rim padat-F kabur bagi y_t dengan $N(y_t) \subset U$. Pilih daripada tudung kabur $(U \setminus \{U\}) \cup \{N(y_t) \mid y_t \in U\} = N_y$, unsur $N_i \in U \setminus \{U\}$. $i = 1,2,..., k$ dan $Ny_j \in \{N(y_t) | y_t \in U\}$, $j=1,2,...,m$ dengan $X = Ttp\left(\bigcup_{i=1}^{k} N_i \cup \bigcup_{j=1}^{m} N_{y_j}\right)$

Misalkan $N_s^{(i)} \in U \setminus \{U\}, s = 1,2,..,k_i$, sehingga $Ttp((N_y)) \setminus U \subset Ttp\left(\bigcup_{s=1}^{k_i} N_S^{(i)}\right)$,

$i=1,2,...,m$. $X = UUTtp\left(\left(\bigcup_{i=1}^{k} N_i\right) \cup \left(\bigcup_{\substack{i=1,2,...,m \\ s=1,2,...,k_i}} N_S^{(i)}\right)\right)$. Oleh yang demikianruang Hausdorff kabur (X,τ) adalah padat-F kabur.

RUJUKAN

Abd Fatah, W.1992. Beberapa konsep kepadatan kabur dalam ruang topologi kabur. Master Thesis UKM.

Abd Fatah, W. & M. T. Abu Osman. 1998. Beberapa Keputusan dalam Ruang Hausdorff kabur. *Sains Malaysiana* **27**: 83-91.

Abd Fatah, W. & M.T. Abu Osman. 1996b. On Fuzzy C-compactness in a fuzzy Hausdorff space. *Ematika* **15(2)**: 127-134.

Berri, M.P. 1963. Minimal topological spaces. *Trans. Amer. Maths Soc.* **108**: 97-105

Bourbaki. 1966. *General Topology* (Part I). Reading, Massachusetts: Addison-Wesley Publishing Company.

Chakraborty, M.K. & T.M.G. Ahsanullah. 1992. Fuzzy topology on fuzzy sets and tolerance topology. *Fuzzy Sets and Systems* **45**: 103-108.

Chang, C.L. 1968. Fuzzy topological spaces. *J. Math. Anal. Appl.* **24**: 97-105.

Chen-Tun Liu.1968. Absolutely closed spaces. *Trans. Amer. Maths. Soc.* **130**: 86-104.

De Prada, M.A. & M. Saralegui. 1988. Fuzzy filters. *J. Math. Anal. Appl.* **129**: 560-568.

DICKMAN, R.F. & A. ZAME. 1969. Functionally compact spaces. *Pacific J. Maths.* **31(2)**: 300-311

PU PAO-MING & LIU YING-MING. 1980. Fuzzy topology I: Neighbourhood structure of fuzzy point and Moore-Smith convergence. *J. Math. Anal. Appl.* **76**: 571-599

SARKAR, M. 1981. On fuzzy topological spaces. *J. Math. Anal. Appl.* **79**: 384-389.

Srivastava, R., Lal, S.N.& Srivastava, A.K. 1981. Fuzzy Hausdorff topological spaces. *J. Math. Anal. Appl.* **81**: 497-506.

VIGLINO, G. 1969. C-compact spaces. *Duke J. Math.* **36(4)**: 761-764.

VIGLINO, G. 1971. Seminormal & C-compact spaces. *Duke J.Math.* **38**: 57-61.

WONG, C.K. 1973. Covering properties of fuzzy topological spaces. *J. Math. Anal. Appl.* **43**: 697-704.

WONG, C.K. 1974. Fuzzy points and local properties f fuzzy topology. *J. Math. Anal. Appl.* **46**: 316-328.

ZADEH, L.A. 1965. Fuzzy sets. *J. Inform. Control* **8**: 338-353.

ISSN: 0128-7680
Pertanika J. Sci. & Technol. 9(2): 157 - 167 (2001)

On the Non-Commutative Neutrix Product $\Gamma^{(r)}(x_+) \circ x_+^r \ln x_+$

Adem Kiliçman
Department of Mathematics
Universiti Putra Malaysia
43400 UPM, Serdang
Selangor, Malaysia

Received: 14 July 1998

ABSTRAK

Dalam kertas ini, fungsi Gamma $\Gamma(x)$ dan fungsi Gamma yang berkaitan $\Gamma(x_+)$ ditakrifkan sebagai taburan dan hasil darab neutrix $\Gamma^{(s)}(x_+) \circ x_+^r \ln x_+$ akan dinilaikan. Misalkan f, g taburan dalam D' dan biarkan dengan $\{\}$ jujukan tertentu yang menumpukan ke fungsi Dirac-delta. Hasil darab neutrix komutatif fog dikatakan wujud dan sama dengan h apabila

$$N\text{-}\lim_{n\to\infty}\langle f g_n, \phi\rangle = \langle h, \phi\rangle$$

untuk semua ϕ di D.

ABSTRACT

In this work, the Gamma function $\Gamma(x)$ and the associated Gamma functions $\Gamma(x_+)$ are defined as distributions and neutrix product $\Gamma^{(s)}(x_+) \circ x_+^r \ln x_+$ is evaluated. Let f, g be distributions in D' and let $f_n = f * \delta_n, g_n = g * \delta_n$, where $\{\delta_n\}$ is a certain sequence converging to the Dirac delta-function. The non-commutative neutrix product f o g is said to exist and be equal to h if

$$N\text{-}\lim_{n\to\infty}\langle f g_n, \phi\rangle = \langle h, \phi\rangle$$

for all ϕ in D.

Keywords: distribution, delta-function, Gamma function, neutrix, neutrix limit, neutrix product. AMS (Subject Classification (2000): 33B10, 46F10

INTRODUCTION

In the following, we let N be the neutrix, van der Corput [1], having the domain N' = {1, 2,.., n,...} and range the real numbers, with negligible functions finite linear sums of the functions

$$n^{\lambda}\ln^{r-1}n, \quad \ln^r n \text{ for } \quad \lambda > 0, \quad r = 1,2,\ldots$$

[1]This research has been partially supported by UPM under the grant 50438-97-10.

and all functions which converge to zero in the normal sense as n tends to infinity.

We now let $\rho(x)$ be any infinitely differentiable function having the following properties:

i. $\rho(x) = 0$ for $|x| \geq 1$,

ii. $\rho(x) \geq 0$,

iii. $\rho(x) = \rho(-x)$,

iv. $\int_{-1}^{1}\rho(x)dx=1$

Putting $\delta_n(x) = n\rho(nx)$ for n = 1, 2,..., it follows that $\{\delta_n(x)\}$ is a regular sequence of infinitely differentiable functions converging to the Dirac delta-funtion $\delta(x)$.

Now let D' be the space of infinitely differentiable functions with compact support and let D' be the space of distributions defined on D. Then if f is an arbitrary distributions in D', we define

$$f_n(x)=(f*\delta_n)(x)=\langle f(t),\delta_n(x-t)\rangle$$

for $n = 1,2,....$ It follows that $\{f_n\}$ is a regular sequence of infinitely differentiable functions converging to the distribution f.

A first extension of the product of a distributions and an infinitely differentiable function is the following, example [2].

DEFINITION 1. *Let f and g be distributions in D' for which on the interval (a,b), f is the k-th derivative of a locally summable functions F in L^p (a,b) and $g^{(k)}$ is a locally summable function in $L^q(a,b)$ with $1/p + 1/q = 1$. Then the product fg = gf of f and g is defined on the interval (a,b) by*

$$fg=\sum_{i=0}^{k}\binom{k}{i}(-1)^i[Fg^{(i)}]^{(k-i)}$$

The following definition for the non-commutative neutrix product of two distributions was given in [4] and generalizes Definition 1.

DEFINITION 2. *Let f and g be distributions in D' and let $g_n = g * \delta n$. We say that the neutrix product f o g of f and g exists and is equal to the distributions h on the interval (a,b) if*

$$N\text{–}\lim_{n\to\infty}\langle fg_n,\phi\rangle=\langle h,\phi\rangle$$

for all functions ϕ in D with support contained in the interval (a,b).

Note that if

$$\lim_{n\to\infty} \langle fg_n,\phi\rangle=\langle h,\phi\rangle,$$

we simply say that the product f.g exists and equals h.

This definition of the neutrix product is in general non-commutative. A commutative neutrix product, denoted by f □ g, was considered in [3].

It is obvious that if the product *f.g* exists then the neutrix product $f\circ g$ exists and $f.g = f\circ g$. Further, it was proved in [4] that if the product fg exists by Definition 1 then the product $f\circ g$ exists by Definition 2 and $fg = f\circ g$.

The following theorem holds in [5].

METHOD AND RESULTS

THEOREM 1 Let f and g be distributions in D' and suppose that the neutrix products $f\circ g^{(i)}$ (or $f^{(i)}\circ g$) exist on the interval (a,b) for i = 0,1,2,...,r. Then the neutrix products $f^{(k)}\circ g$ (or $f\circ g^{(k)}$) exist on the interval (a,b) for k = 1,2,..,r and

$$f^{(k)}\circ g=\sum_{i=0}^{k}\binom{k}{i}(-1)^i(f\circ g^{(i)})^{(k-i)} \tag{1}$$

or

$$f^{(k)}\circ g=\sum_{i=0}^{k}\binom{k}{i}(-1)^i(f^{(i)}\circ g)^{(k-i)} \tag{2}$$

on the interval (a,b) for k = 1,2,...,r.

The distributions x^{-1} is defined by

$$\langle x^{-1},\phi\rangle=\int_0^\infty x^{-1}\left[\phi(x)-\phi(-x)\right]dx$$

whenever $\phi\in D$, see [6].

In the following theorem, which was proved in [5], the distributions x_+^{-r} and x_-^{-r} are defined by

$$x_+^{-r}=\frac{(-1)^{r-1}}{(r-1)!}(\ln x_+)^{(r)},\quad x_-^{-r}=\frac{1}{(r-1)!}(\ln x_-)^{(r)},$$

for r = 1,2,... and is distinct from the definition given by Gel'fand and Shilov [6].

THEOREM 2 The neutrix products $x_+^r \circ x_-^{-s}$ and $x_+^{-s} \circ x_+^r$ exist and

$$x_+^r \circ x_+^{-s} = x_+^{-s+r} + L_n \delta^{(s-r-1)}(x), \tag{3}$$

$$x_+^{-s} \circ x_+^r = x_+^{-s+r} + L_n' \delta^{(s-r-1)}(x), \tag{4}$$

where

$$L_n = \frac{(-1)^{r+s}[c_1 - \psi(s-1) - \psi(s-r-1)]}{(s-r-1)!}$$

$$L_n' = L_n - \sum_{i=r+1}^{s} \binom{s}{i} \frac{(-1)^{s+i} r! \psi(i-r-1)]}{2(s-1)!}$$

for s = 1,2,... and r = 0,1,...,s –1, and

$$c_1(\rho) = \int_0^1 \text{In } t\varphi(t)dt,$$

$$\psi(r) = \begin{cases} 0, & r=0, \\ \sum_{i=1}^{r} i^{-1}, & r \geq 1. \end{cases}$$

Now let us consider the Gamma function $\Gamma(x)$. This function is defined for $x > 0$ by

$$\Gamma(x) = \int_0^\infty t^{x-1} e^{-t} dt$$

and it follows that $\Gamma(x + 1) = x\,\Gamma(x)$ for $x > 0$. $\Gamma(x)$ is then defined by

$$\Gamma(x) = x^{-1}\Gamma(x+1)$$

for $-1 < x < 0$. Further we can express this function as follows

$$\Gamma(x) = x^{-1} + f(x)$$
$$= x^{-1} + \sum_{i=1}^{\infty} \frac{\Gamma^{(i)}(1)}{i!} x^{i-1},$$

where x^{-1} is interpreted in the distributional sense. The distribution $\Gamma(x)$ is of course an ordinary summable function for $x > 0$.

The related distribution $\Gamma(x_+)$ by equation

$$\Gamma(x_+)=x_+^{-1}+f(x_+)$$
$$=x_+^{-1}+\sum_{i=1}^{\infty}\frac{\Gamma^{(i)}(1)}{i!}x_+^{i-1}, \tag{5}$$

and the distribution $\Gamma(x_-)$ by equation

$$\Gamma(x_-)=x_-^{-1}+f(x_-)$$
$$=x_-^{-1}+\sum_{i=1}^{\infty}\frac{\Gamma^{(i)}(1)}{i!}x_-^{i-1}, \tag{6}$$

where x_+^{-1}, x_-^{-1} are interpreted in the distributional sense, see [8]. It follows that

$$\Gamma(x)=\Gamma(x_+)-\Gamma(x_-) \tag{7}$$

Differentiating equation (5) s times, we have

$$\Gamma^{(s)}(x_+)=(-1)^s s!x_+^{-s-1}+f^{(s)}(x_+)$$
$$=(-1)^s s!x_+^{-s-1}+\sum_{i=0}^{\infty}\frac{\Gamma^{(s+i+1)}(1)}{(s+i+1)i!}x_+^i, \tag{8}$$

and diffrentiating equation (6) s times we have

$$\Gamma^{(s)}(x_-)=s!x_-^{-s-1}+f^{(s)}(x_-)$$
$$=(-1)^s s!x_-^{-s-1}+\sum_{i=0}^{\infty}\frac{\Gamma^{(s+i+1)}(1)}{(s+i+1)i!}x_-^i. \tag{9}$$

The following two theorems were proved in [7], [10] respectively.

THEOREM 3 The neutrix products $\ln x_+ \circ \Gamma^{(s)}(x_-)$ and $\Gamma^{(s)}(x_-)\circ \ln x_+$ exist and

$$\ln x_+ \circ \Gamma^{(s)}(x_-)=\left(c_2+c_1\psi(s)-\frac{\pi^2}{12}\right)\delta^{(s)}(x) \tag{10}$$

$$=\Gamma^{(s)}(x_-)\circ \ln x_+ \tag{11}$$

$$=(-1)^s \ln x_- \circ \Gamma^{(s)}(x_+)=(-1)^s \Gamma^{(s)}(x_+)\circ \ln x_- \tag{12}$$

for $s=0,1,2...$ where

$$\psi(s)=\begin{cases}0, & s=0,\\ \sum_{i=1}^{s}\frac{1}{i}, & s\geq 1.\end{cases}$$

***THEOREM* 4** The neutrix products $\ln x_+ \circ x_+^{-s}, x_+^{-s}\circ$ and x_+^{-r}, x_+^{-s} exist for r, s = 1, 2, ... In particular,

$$\begin{aligned}&\ln x_+ \circ x_+^{-1} = x_+^{-1}\ln x_+,\\ &\ln x_+ \circ x_+^{-2} = x_+^{-2}\ln x_+ + (c_1-1)\delta'(x).\end{aligned} \tag{13}$$

It was in fact proved in [10] that

$$\ln x_+ \circ x_+^{-s} = x_+^{-s}\ln x_+ - \frac{\Lambda_s+\psi_1(s-1)}{(s-1)!}(-1)^s\delta^{(s-1)}(x), \tag{14}$$

where

$$\Lambda_s = -c_1\psi(s-1)+\frac{1}{2}\left[\chi(s-1)-\psi^2(s-1)\right]$$

for s = 1, 2, ... and

$$\chi(s)=\begin{cases}0, & s=0,\\ \sum_{i=1}^{s}1/i^2, & s\geq 1.\end{cases}$$

It was later in [9] that

$$x_+^{-r}\circ x_+^{-s} = x_+^{-r-s} + M_{rs}\delta^{(r+s-1)}(x), \tag{15}$$

for r , s = 1 , 2,... where

$$M_{rs}=\sum_{i=0}^{r-1}\binom{r-1}{i}\left[\frac{2c_1}{s+i+1}+\frac{c_1}{s+i}+\frac{\psi(s+i)}{s+i+1}-\frac{1}{(s+i)^2}\right]\frac{(-1)^{s+i}}{(r-1)!(s-1)!}.$$

We now prove the following theorem

***THEOREM* 5** The neutrix products $(x_+^r \ln x_+)\circ\Gamma^{(s)}(x_+)$ and $\Gamma^{(s)}(x_+)\circ(x_+^r \ln x_+)$ exist and

$$\begin{aligned}(x_+^r \ln x_+)\circ\Gamma^{(s)}(x_+) &= x_+^{-s+r}\ln x_+ + N_{rs}\delta^{(s-r-1)}(x)+\\ &+\sum_{i=r+1}^{s-1}\frac{(-1)^{r+s}r!(i-r-1)!M_{i-r,1}}{i!(s-i-1)!}\delta^{(s-r-1)}(x),\end{aligned} \tag{16}$$

$$\Gamma^{(i)}(x_+)\circ(x_+^r \ln x_+)=x_+^{-s+r}\ln x_+ + N_{rs}\delta^{(s-r-1)}(x)+$$
$$+\sum_{i=r+1}^{s-1}\left[\frac{(-1)^{r+s}r!(i-r-1)!M_{1,i-r}}{i!(s-i-1)!}+\frac{(-1)^{s+i}r!s\psi(r)\psi(i-r-1)!M_{1,i-r}}{2i!(s-i)!}\right]\delta^{(s-r-1)}(x)\quad(17)$$

where

$$N_{rs}=(-1)^{r+s}\frac{c_2+2c_1-\psi(r)\left[\psi(s-1)+\psi(s-r-1)+c_1\right]}{(s-r-1)!}+$$
$$-\sum_{i=0}^{r-1}\frac{(-1)^{s+i}}{r!i!(s-i-1)!(r-i)^2}$$

for r = 1, 2,... and s = r + 1 , r+ 2,...

Proof. We define the function f (x+,r) by

$$f(x_+,r)=\frac{x_+^r \ln x_+ -\psi(r)x_+^r}{r!}$$

and it follows easily by induction that

$$f^{(i)}(x_+,r)=f(x_+,r-i),$$

for i = 1 , 2 ,..., r. In particular,

$$f^{(r)}(x_+,r)=\ln x_+,$$

so that

$$f^{(i)}(x_+,r)=(-1)^{i-r-1}(i-r-1)!x_+^{-i+r},$$

for i = r + 1 , r + 2, ... Now the product of the functions x_+^i and x_+^i In x_+ and the distribution x_+^{-1} exist by Definition 1 and it is easily seen that

$$x_+^i x_+^{-1}=x_+^{i-1},$$
$$(x_+^i \ln x_+^{-1}=x_+^{-1}\ln x_+,$$

for i = 1 , 2,...Thus

$$f^{(i)}(x_+,r)x_+^{-1} = \frac{x_+^{r-i-1}\ln x_+ - \psi(r-i)x_+^{r-i-1}}{(r-i)!}$$
$$= \frac{x_+^{r-i-1}\ln x_+ - \psi(r-i-1)x_+^{r-i-1} - (r-i)^{-1}x_+^{r-i-1}}{(r-i)!}$$
$$= \frac{f(x_+,r-i-1)}{r-i} + \frac{x_+^{r-i-1}}{(r-i)(r-i)!}, \tag{18}$$

for i = 0, 1, ..., r − 1.

Using equation (9) we have

$$f^{(i)}(x_+,r)\circ x_+^{-1} = x_+^{-1}\ln x_+ - (c_2+2c_1)\delta(x) \tag{19}$$

and using equation (12) we have

$$f^{(i)}(x_+,r)\circ x_+^{-1} = (-1)^{i-r-1}(i-r-1)!\left[x_+^{-i+r-1} - M_{i-r,1}\delta^{(i-r)}(x)\right], \tag{20}$$

for i = r + 1, r + 2 ,...

Using equation (2), it follows that

$$(-1)^{s-1}(s-1)!f(x_+,r)\circ x_+^{-s} = \sum_{i=0}^{s-1}\binom{s-1}{i}(-1)^i\left[f^{(i)}(x_+,r)\circ x_+^{-1}\right]^{(s-i-1)}.$$

Noting that

$$f(x_+,r)\circ x_+^{-s} = \frac{x_+^{-s+r}\ln x_+ - \psi(r)x_+^{-s+r}}{r!}$$

on any interval not containing the origin, it now follows on using equations (15), (16) and (17) that

$$f(x_+,r)\circ\Gamma^{(s)}(x_+) = \frac{x_+^{-s+r}\ln x_+ - \psi(r)x_+^{-s+r}}{r!} - \sum_{i=0}^{r-1}\frac{(-1)^{s+i}}{i!(s-i-1)!(r-i)^2}\delta^{(s-r-1)}(x) +$$
$$+\frac{(-1)^{r+s}(c_2+2c_1)}{r!(s-r-1)!}\delta^{(s-r-1)}(x) + \sum_{i=r+1}^{s-1}\frac{(-1)^{r+s}(i-r-1)!M_{i-r,1}}{i!(s-i-1)!}\delta^{(s-r-1)}(x).$$

Finally, since

$$f(x_+,r)\circ\Gamma^{(s)}(x_+) = \frac{(x_+^r\ln x_+)\circ x_+^{-s} - \psi(r)x_+^r\circ\Gamma^{(s)}(x_+)}{r!},$$

equation (13) follows on using equation (3).

As above, we have

$$x_+^{-1} f^{(i)}(x_+,r)=\frac{f(x_+,r-i-1)}{r-i}+\frac{x_+^{r-i-1}}{(r-i)(r-i)!}, \tag{21}$$

for i = 0, 1, ..., r − 1, using equation (10) we have

$$x_+^{-1}\circ f^{(r)}(x_+,r)=x_+^{-1}\ln x_+ +(c_2+2_{c1})\delta(x) \tag{22}$$

and using equation (12) we have

$$x_+^{-1}\circ f^{(i)}(x_+,r)=(-1)^{i-r-1}(i-r-1)!\left[x_+^{-i+r-1}+M_{1,i-r}\delta^{(i-r)}(x)\right]. \tag{23}$$

Using equation (1), it follows that

$$(-1)^{s-1}(s-1)!\Gamma^{(s)}(x_+)\circ f(x_+,r)=\sum_{i=0}^{s-1}\binom{s-1}{i}(-1)^i\left[x_+^{-1}\circ f^{(i)}(x_+,r)\right]^{s-i-1}.$$

It now follows as above that

$$\Gamma^{(s)}(x_+)\circ f(x_+,r)=\frac{x_+^{-s+r}\ln x_+ -\psi(r)x_+^{-s+r}}{r!}-\sum_{i=0}^{r-1}\frac{(-1)^{s+i}}{i!(s-i-1)!(r-i)^2}\delta^{(s-r-1)}(x)+$$
$$-\frac{(-1)^{r+s}(c_2+2c_1)}{r!(s-r-1)!}\delta^{(s-r-1)}x+\sum_{i=r+1}^{s-1}\frac{(-1)^{r+s}(i-r-1)!M_{1,i-r}}{i!(s-i-1)!}\delta^{(s-r-1)}(x).$$

Finally, since

$$\Gamma^{(s)}(x_+)\circ f(x_+,r)=\frac{\Gamma^{(s)}(x_+)\circ(x_+^r\ln x_+)-\psi(r)\Gamma^{(s)}(x_+)\circ x_+^r}{r!},$$

equation (14) follows on using equation (4).

Corollary 1 The neutrix products $(x_-^r \ln x_-)\circ\Gamma^{(s)}(x_-)\circ(x_-^r\ln x_-)$ exist and

$$(x_-^r\ln x_-)\circ\Gamma^{(s)}(x_-)=x_-^{-s+r}\ln x_-(-1)^{r+s}N_n\delta^{(s-r-1)}(x)+$$
$$-\sum_{i=r+1}^{s-1}\frac{r!(i-r-1)!M_{i-r,1}}{i!(s-i-1)!}\delta^{(s-r-1)}(x), \tag{24}$$

$$\Gamma^{(s)}(x_-)\circ(x_-^r \ln x_-)=x_-^{-s+r}\ln x_- -(-1)^{r+s}N_n\delta^{(s-r-1)}(x)+$$
$$-\left[\sum_{i=r+1}^{s-1}\frac{r!(i-r-1)!M_{1,i-r}}{i!(s-i-1)!}+\frac{(-1)^{r+1}r!s\psi(r)\psi(i-r-1)}{2i!(s-i)!}\right]\delta^{(s-r-1)}(x) \quad (25)$$

for r = 1, 2, ... and s = r + 1, r + 2 ,...

Proof. Replacing x by and $x_+^r \ln x_+$, $\Gamma^{(s)}(x_+)$ and $\delta^{(s-r-1)}(x)$ gives us $x_-^r \ln x_-$, $\Gamma^{(s)}(x_-)$ and $(-1)^{r+s-1}\delta^{(s-r-1)}(x)$ respectively. The results now follow immediately from the theorem 5.

Corollary 2 The neutrix products $(x^r \ln|x|)\circ\Gamma^{(s)}(x)$ and $\Gamma^{(s)}(x)\circ(x^r \ln|x|)$ exist and

$$(x^r \ln|x|)\circ\Gamma^{(s)}(x) = x^{-s+r}\ln|x| \quad (26)$$
$$= \Gamma^{(s)}(x)\circ(x^r \ln|x|), \quad (27)$$

for r = 1, 2,... and s = r + 1, r + 2,....

Proof. Noting that the neutrix product is clearly distributive with respect to addition, we have

$$(x^r \ln|x|)\circ\Gamma^{(s)}(x)=\left[x_+^r \ln x_+ +(-1)^r x_-^r \ln x_-\right]\circ\left[\Gamma^{(s)}(x_+)+(-1)^{(s)}(x_-)\right]$$
$$=(x_+^r \ln x_+)\circ\Gamma^{(s)}(x_+)+(-1)^s(x_+^r \ln x_+)\circ\Gamma^{(s)}(x_-)+$$
$$+(-1)^r(x_-^r \ln x_-)\circ\Gamma^{(s)}(x_+)+(-1)^{r+s}(x_-^r \ln x_-)\circ\Gamma^{(s)}(x_-),$$

for r = 1, 2 ,... and s = r + 1 , r + 2,... Equation (24) now follows from these equations and equations (5), (6), (14) and (22). Equation (25) follows similarly using equations (7), (8), (15) and (23).

REFERENCES

VAN DER CORPUT, J.G. 1959-60. Introduction to the neutrix calculus. *J.Analyse Math.* **7**: 291-398.

FISHER, B. 1971. The product of distributions. *Quart. J. Math. Oxford* (2), **22**: 291-298.

FISHER, B. 1974. The neutrix distribution product $x_+^{-r}\delta^{(r-1)}(x)$. *Studia Sci. Math. Hungar.* **9**: 439-441.

FISHER, B. 1982. A non-commutative neutrix product of distributions. *Math. Nachr.* **108**: 117-127.

FISHER, B., E. SAVAS, S. PEHLIVAN and E. OZCAG. 1993. Results on the non-commutative neutrix product of distributions. *Math. Balkanica* **7**: 347-356.

GEL'FAND, I.M and G.E. SHILOV. 1964. *Generalized Functions*. Vol. I. Academic Press.

KILIÇMAN, A. 2000. Some results on the non-commutative neutrix product distributions and $\Gamma^{(r)}(x)$. *Bulletin of Malaysian Math. Soc.* **23**: 69-78.

KILIÇMAN, A. and B. FISHER. 1998. The commutative neutrix product of $\Gamma^{(r)}(x)$ and $\delta^{(r)}(x)$. *Punjab J. Math.* **3**: 1-12.

B. FISHER and A. KILIÇMAN. 1995. On the non-commutative neutrix product $x_+^{-r} \circ x_+^{-s}$. *Punjab J. Math.* **28**: 122-131.

B. FISHER, A.KILIÇMAN, B. DAMYANOV and C.J. AULT. 1996. On the non-commutative neutrix product $\ln x_+ \circ x_+^{-s}$. *Comment. Math. Univ. Carolin.* **37(2)**: 229-239.

ISSN: 0128-7680
Pertanika J. Sci. & Technol. 9(2): 169 - 188 (2001)

A Parametric Bootstrap Simulation Study in EGARCH Model

Choo Wei Chong[1], Muhammad Idress Ahmad[2], Habshah Midi[3]
[1]Jabatan Pengurusan dan Pemasaran
Fakulti Ekonomi dan Pengurusan
[2]Jabatan Matematik, Fakulti Sains dan Pengajian Alam Sekitar
[3]Jabatan Matematik, Fakulti Sains dan Pengajian Alam Sekitar
Universiti Putra Malaysia
Serdang, Selangor Darul Ehsan, Malaysia

Received: 26 February 1998

ABSTRAK

Kami membentangkan satu penggunaan baru bagi kaedah butstrap berparameter untuk memeriksa ciri-ciri taburan anu bagi parameter-parameter bagi Model Teritlak Autoregresi dan heteroskedastisiti bersyarat. Kertas ini juga mengkaji kaedah pilihan bagi butstrap berparameter untuk menentukan ralat piawai dan membina selang keyakinan bagi anggaran parameter-parameter model. Berdasarkan kajian simulasi bustrap berparameter, kami mendapati bahawa taburan empirikal bagi parameter-parameter adalah pencong dan leptokurtik. Oleh itu, kaedah butstrap berparameter yang tidak bergantung ke atas anggaran taburan normal adalah pendekatan pilihan yang boleh dipercayai dalam penentuan ralat piawai dan pembinaan selang keyakinan.

ABSTRACT

We present a new application of the parametric bootstrap method to examine the characteristics of the unknown underlying populations of the parameters of the exponential Generalized Autoregressive Conditional Heteroscedasticity Model. This paper also studies the alternative method of parametric bootstrap to evaluate the standard errors and to construct the confidence intervals of the parameter estimates of the model. From the parametric bootstrap simulation study, we observe that the unknown empirical distributions of the parameters are skewed and leptokurtic. Hence, the parametric bootstrap estimation method, which does not rely on the normality assumption, is one of the reliable alternative approaches for standard errors evaluation and construction of confidence intervals.

Keywords: parametric bootstrap, percentile method, EGARCH, standard error, confidence intervals, time series

INTRODUCTION

The exponential GARCH or EGARCH model, proposed by Nelson (1991), has two advantages in modelling the stock market volatility. First, there is no restriction such as nonnegative constraints on the parameters in the EGARCH model (Nelson and Cao 1992). Second, this non-linear model can cope with the skewness in the distribution of returns, especially the stock market indices that are commonly skewed, as well as effectively remove the excess kurtosis in returns. Choo (1997), Choo (1998) and Choo *et al.* (1999) also have studied

these. They found that the EGARCH performs better than the other models in describing the observed skewness in stock market indices and in out-of-sample (one-step-ahead) forecasting.

The GARCH regression model for the series of rate of return, r_t can be written as

$$r_t = \mu + \varepsilon_t$$
$$\varepsilon_t = \sqrt{h_t}.e_t$$
$$e_t \sim N(0,1)$$

The parameter μ reflects a constant term, which in practice is typically estimated to be close or equal to zero. The conditional variance, h_t, is an asymmetric function of lagged disturbances, ε_{t-i}:

$$\ln(h_t) = \omega + \sum_{i=1}^{q} \alpha_i g(e_{t-i}) + \sum_{j=1}^{p} \beta_j \ln(h_{t-j})$$

where

$$g(e_t) = \theta e_t + \gamma[|e_t| - E|e_t|]$$
$$e_t = \varepsilon_t / \sqrt{h_t}$$

The coefficient of the second term in $g(e_t)$ is set to be 1 (γ = 1) in this formulation. Note that $E|e_t| = (2/\pi)^{1/2}$ if $e_t \sim N(0,1)$.

The EGARCH model is estimated using the maximum likelihood method. The log-likelihood function is computed from the product of all conditional densities of the prediction errors,

$$l = \sum_{t=1}^{N} \frac{1}{2}[-\ln(2\pi) - \ln(h_t) - \frac{\varepsilon_t^2}{h_t}]$$

where $e_t = r_t - \mu$ and h_t is the conditional variance. It is attractive that this method enables the rate of return and variance processes being estimated jointly (Engle,1982). However, this method estimates the parameters and confidence intervals of EGARCH model by assuming the normality of the underlying population of the parameters.

Our interest is to examine an alternative approach to the maximum likelihood method. Through a simulation study, artificial series covering the extreme points of the parameter space of the EGARCH(1,1) model were generated and submitted to the use of the parametric bootstrap method to assess the standard error and confidence intervals for the parameters of the model.

Bootstrap – an Overview

Efron (1979) introduced a non-parametric computer-intensive statistics technique, which allows a description of the variability of a statistic, based on a unique finite sample. It is used when finite sample theory is impossible or

difficult to derive, or when only asymptotic theory is available. This occurs especially with the financial time series. This new general statistical procedure is known as 'bootstrap'.

It enjoys the advantage of being completely automatic. The bootstrap estimate of standard error and confidence interval requires no theoretical calculations, and is available no matter how mathematically complicated the estimator may be.

The bootstrap is a technique used to estimate the standard errors by resampling with replacement the original finite sample. Through the process of resampling, the so-called 'pseudo-data' or 'bootstrap sample' is obtained and submitted to the estimation of the statistics of interest, called 'bootstrap estimates'. This technique has been successfully used in various applied statistical problems, although not many applications have been reported in the area of time series.

PROCEDURE

Simulation Study

The essence of the proposed simulation procedure is to obtain an empirical distribution of the specified statistic via parametric bootstraps. Then, the fitted model is used to repeatedly generating many samples, each of which has the same number of observations as the original data.

In some cases, starting values of the generating process may also be important. However, if the process is stationary, the effects of any starting values will be negligible, provided that we discard certain data points at the beginning of a generating exercise. This is stated in Tsay (1992).

In the simulation procedure, the parametric model used consists of a mathematical form with the known parameters and a known probability distribution for the innovations.

In this study, we used $B = 1000$ replications, which is the smallest number of replications in construction of the reliable confidence intervals as suggested by Efron and Tibshirani(1993). The observed daily series used including Composite Index and Finance Index. This data is collected from 1 January 1989 to 9 October 1990. Source of data is Investors Digest, published by Kuala Lumpur Stock Exchange (KLSE).

The algorithm of simulation is as follows:

1. Estimate the unknown parameters, $\hat{\mu}$, $\hat{\omega}$, $\hat{\alpha}$, $\hat{\beta}$ *and* $\hat{\theta}$ in the EGARCH(1,1) model using the maximum likelihood method from the observed daily series of the indices.
2. Generate 1000 series of $\varepsilon_t \sim N(0.1)$ with the sample size of $n = 433$.
3. To start up the recursion, use the pre-sample estimates for h_t and ε_t^2, $t \leq 0$. Calculate the starting values for ε_0 and h_0 as suggested by Bollerslev (1986),

$$\varepsilon_0^2 = h_0 = T^{-1} \sum_{t=1}^{T} \varepsilon_t^2$$

4. Calculate h_1 using the equation,

$$\ln(h_1) = \hat{\omega} + \hat{\alpha}(\hat{\theta}e_0 + |e_0| - (\frac{2}{\pi})^{1/2}) + \hat{\beta}\ln(h_0)$$

where $e_0 = \frac{\varepsilon_0}{\sqrt{h_0}} = 1$

5. Calculate the rate of return,

$$r_1 = \hat{\mu} + \sqrt{h_1}.e_1$$

6. Calculate h_2, using the equation,

$$\ln(h_2) = \hat{\omega} + \hat{\alpha}(\hat{\theta}e_1 + |e_1| - (\frac{2}{\pi})^{1/2}) + \hat{\beta}\ln(h_1)$$

7. Calculate the rate of return,

$$r_2 = \hat{\mu} + \sqrt{h_2}.e_2$$

8. Repeat the calculation process of h_t and r_t until the desirable sample size, n (n = 433 in this study)
9. With this simulated series of size n = 433, estimate the parameters of EGARCH(1,1) model using the maximum likelihood method.
10. Repeat step 3 until step 9 for 1000 times in order to obtain 1000 parametric bootstrap estimates of the parameters of the EGARCH(1,1) model from the 1000 bootstrap samples of size, n = 433.

Bootstrap Standard Errors

Using non-parametric bootstrap to evaluate the standard error has been studied by researchers such as Efron *et. al.* (1986&1993), Abdullah (1995). Efron and Tibshirani (1993) proposed that the minimum number of replications to obtain a reliable standard error is 200. In order to obtain the comparisons, we use B equals 25, 50, 100, 250, 500, 800 and 1000 replications respectively in this study.

The algorithm of parametric bootstrap for estimating standard errors is as follows:

1. Generate B independent bootstrap data sets r^{*1}, r^{*2}, ..., r^{*B} by drawing B samples of size n from the parametric estimate of the population $\hat{F}$:

$$\hat{F}_{par} \dashrightarrow (r_1^*, r_2^*, r_3^*, \ldots, r_n^*)$$

where $\hat{F}_{par}$ is an estimate of F derived from a parametric model for the observed data.

2. Evaluate the bootstrap replication corresponding to each bootstrap sample, $\hat{T}^*(b) = s(r^{*b})$ where b=1,2,3,...,B.
3. Evaluate the parametric bootstrap estimate of standard error $se_{\hat{F}_{par}}(\hat{T})$ by the sample standard deviation of the B replications:

$$\overset{\Lambda}{se}_B = \{\sum_{b=1}^{B} [\hat{T}^*(b) - \hat{T}^*(.)]^2 / (B-1)\}^{1/2}$$

where

$$\hat{T}^*(.) = \sum_{b=1}^{B} \hat{T}^*(b)/B.$$

Confidence Intervals

Properties of Confidence Intervals

Two properties associated with all the confidence intervals are their lengths and shapes, respectively,

$$length = \hat{T}_u - \hat{T}_l,$$

$$shape = \frac{\hat{T}_u - \hat{T}}{\hat{T} - \hat{T}_l}.$$

A confidence interval with a shorter length is always preferred to a confidence interval with longer length. "Shape" measures the asymmetry of the interval about the point estimate, $\hat{T}$. Shape > 1 indicates asymmetry with greater distance from $\hat{T}_u$ to $\hat{T}$ than from $\hat{T}$ to $\hat{T}_l$. The standard intervals are symmetrical about $\hat{T}_l$, having shape = 1 by definition. Exact intervals, when they exist, are often quite asymmetrical. The most serious errors made by standard intervals are due to their enforced symmetry.

There are various methods to construct bootstrap confidence intervals, such as in Efron (1987), Hall (1986), Hall (1987), Masarotto (1990) and Thombs *et. al.* (1990). We will study two methods of bootstrap confidence intervals, namely standard normal intervals using bootstrap estimates (symmetry bootstrap) and bootstrap percentile intervals.

Standard Normal Intervals

Let $\hat{T}$ be the usual plug-in estimate of a parameter T and $\hat{se}$ be its estimated standard error. Consider the standard normal confidence interval $[\hat{T} - z^{(1-\alpha)}.\hat{se}, \hat{T} - z^{(\alpha)}.\hat{se}]$. The end points of this interval can be described in a way that is particularly convenient for bootstrap calculations. Let $\hat{T}^*$ indicate a random variable drawn from the distribution $N(\hat{T}, \hat{se}^2)$,

$$\hat{T}^* \sim N(\hat{T}, \hat{se}^2).$$

Then, $\hat{T}_l = \hat{T} - z^{(1-\alpha)}.\hat{se}$ and $\hat{T}_u = \hat{T} - z^{(\alpha)}.\hat{se}$ are the $100\alpha th$ and $100(1-\alpha)th$ percentiles of $\hat{T}^*$. In other words,

$\hat{T}_l = \hat{T}^{*(\alpha)} = 100.\alpha th$ percentile of $\hat{T}^*$'s distribution,

$\hat{T}_u = \hat{T}^{*(1-\alpha)} = 100.(1-\alpha)th$ percentile of $\hat{T}^*$'s distribution.

Let $\hat{T} = 86.85$, the mean of the sample. The bootstrap standard error of $\hat{T}$ is 25.23, so if we choose, say, $\alpha = 0.05$, then the standard 90% normal confidence interval for the true mean T is [86.85 - (1.645)25.23, 86.85 + (1.645)25.23] =[45.3, 128.4].

This is a good approximation intervals if the underlying distribution of T is normal. If it is not, the other intervals are preferred, such as percentile intervals.

Percentile Intervals

Through the use of the bootstrap we can obtain accurate intervals without having to make a normal theory assumption. The percentile method can be thought of as a computational algorithm for extending the range of effectiveness of the standard intervals.

The computational algorithm of the parametric bootstrap percentile intervals is as follows:

1. Instead of sampling with replacement from the observed data, we generate B independent bootstrap data sets r^{*1}, r^{*2}, ..., r^{*B} by drawing B samples of size n from the parametric estimate of the population $\hat{F}$:

   $$\hat{F}_{par} --> (r_1^*, r_2^*, r_3^*, \ldots, r_n^*)$$

   where $\hat{F}_{par}$ is an estimate of F derived from a parametric model for the observed data.
2. Compute the bootstrap replication corresponding to each bootstrap sample,

   $$\hat{T}^*(b) = s(r^{*b}) \quad \text{where} \quad b = 1,2,3,\ldots B.$$
3. Let $\hat{T}_B^{*(\alpha)}$ be the *100.αth* empirical percentile of the $\hat{T}^*(b)$ values, that is the *B.αth* value in the ordered list of the B replication of $\hat{T}^*$.

   So if B = 1000 and α = 0.05, $\hat{T}_B^{*(\alpha)}$ is the *50th* ordered value of the replications.
4. Likewise let $\hat{T}_B^{*(1-\alpha)}$ be the *100.(1- α)th* empirical percentile
5. The approximate *(1-2α)* percentile interval is

   $$[\hat{T}_{\%,l}, \hat{T}_{\%,u}] \approx [\hat{T}_B^{*(\alpha)}, \hat{T}_B^{*(1-\alpha)}].$$

If the bootstrap distribution of $\hat{T}^*$ is roughly normal, then the standard normal and percentile intervals will nearly agree. The central limit theorem tells us that as $n \to \infty$, the bootstrap histogram will become normal shaped, but for small samples it may look non-normal. In this case, percentile intervals are preferred over the standard normal intervals because they have the advantage of automatically making the transformation from non-normal to normal (Efron and Tibshirani, 1993).

Percentile Interval: Advantages and Properties

1. The less erratic property

   The percentile intervals are less erratic in actual practice, but have less satisfactory coverage properties.

2. The range-preserving property

   For some parameters, there is a restriction on the values that the parameter can take. For example, the values of the correlation coefficient lie in the interval [-1, +1]. Clearly, it would be desirable if a confidence procedure always produced intervals that fall within the allowable range : such an interval is called *range-preserving*.

   The percentile intervals are range-preserving, since a) the plug-in estimate $\hat{T}$ obeys the same range restriction as T, and b) its endpoints are values of the bootstrap statistic $\hat{T}^*$, which again obey the same range restriction as T. In contrast, the standard interval need not be range-preserving. Confidence procedures that are range-preserving tend to be more accurate and reliable.

3. The transformation-respecting property

   The percentile interval is *transformation-respecting*: the percentile interval for any (monotone) parameter transformation $\psi=m(T)$ is simply the percentile interval for T mapped by $m(T)$:

   $$[\hat{\psi}_{\%,l},\hat{\psi}_{\%,u}] = [m(\hat{T}_{\%,l}), m(\hat{T}_{\%,u})]$$

   The advantage of the percentile method is that we do not need to know the correct transformation. All we assume is that such a transformation exists and will be transformed automatically.

RESULTS AND DISCUSSION

By using the 1000 simulated series of Composite Index, we showed some characteristics of 1000 parametric bootstrap estimates of the parameters of EGARCH(1,1) model in Table 1. The distributions of the parameters are shown in *Fig. 1, 2, 3, 4* and *5*. Even though the histogram of $\hat{\mu},\hat{\alpha}$ and $\hat{\theta}$ shown the normality of the distribution, the skewness and kurtosis in Table 1 clearly suggest that the bootstrap histograms of the parameters are non-normal. In other words, the unknown distributions of the parameters are skewed and leptokurtic. This indicates that the normality assumption of the underlying populations of the parameters could be a serious error in parameter estimation and construction of confidence intervals.

By using the 1000 simulated series of Finance Index, we present characteristics of 1000 parametric bootstrap estimates of the parameters of the EGARCH(1,1) model in Table 2. The distributions of the parameters are shown in Figure 6, 7, 8, 9 and 10. From Table 2 and the histograms, the distributions of the parameters are clearly non-normal, especially the histograms of $\hat{\omega}$ and $\hat{\beta}$ for

Finance Index. The kurtosis of the distributions for $\hat{\omega}$ and $\hat{\beta}$ are 72.967 and 71.574 respectively whereas the kurtosis of standard normal distribution is only 3.

Using 433 daily observed data for Composite Index and Finance Index, taken from Investor Digest, KLSE, from 1 January 1989 to 9 October 1990, we estimate the parameters of EGARCH(1,1) model using maximum likelihood method. With 1000 simulated series of Composite Index and Finance Index, with each series of size, $n = 433$, the bootstrap parameter estimates are obtained using the mean of the 1000 parametric bootstrap estimates of the parameters of the EGARCH(1,1) model. These results are shown in Table 1 and Table 2 too respectively. The parameter estimates using parametric bootstrap are very close to the parameter estimates using the maximum likelihood for both Composite Index and Finance Index.

Using the 1000 simulated series of Composite Index and 1000 simulated series of Finance Index, the parametric bootstrap estimates of standard error for $\hat{\mu}$, $\hat{\omega}$, $\hat{\alpha}$, $\hat{\beta}$ and $\hat{\theta}$ as B increased from 25 to 1000 replications are shown in Table 3 and Table 4. Table 3 and Table 4 too present the standard error of the parameter estimates of EGARCH(1,1) model for the observed Composite Index and the observed Finance Index respectively using the maximum likelihood estimation method. The standard errors of the parameter estimates for 433 observed daily series using the maximum likelihood method are compared with the standard errors of the parameter estimates for 1000 simulated series using parametric bootstrap approach. The parametric bootstrap standard errors of $\hat{\mu}$

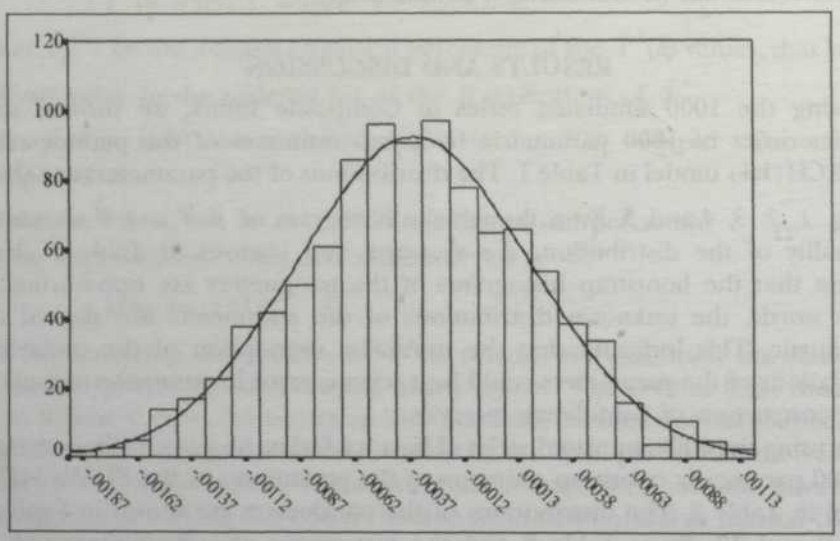

Fig. 1. Histogram, with normal curve, for 1000 parametric bootstrap replications of $\hat{\mu}$, using 1000 Simulated Series of Composite Index

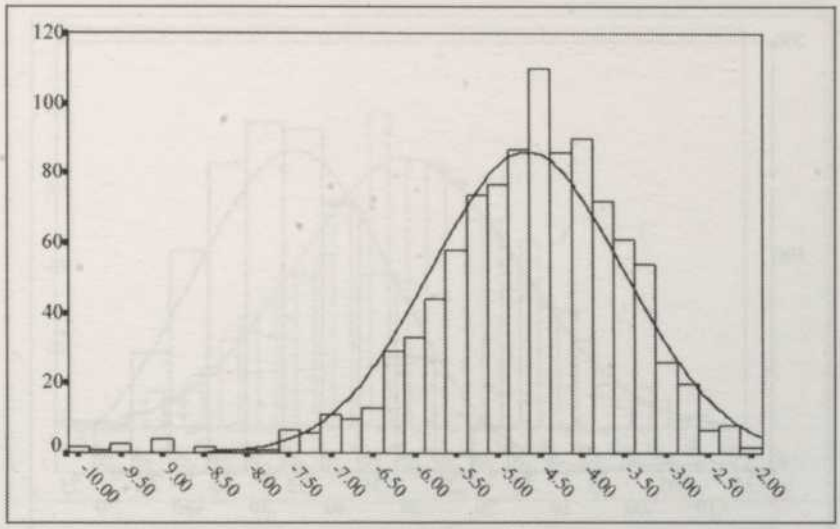

$\hat{\omega}$

Fig. 2. Histogram, with normal curve, for 1000 parametric bootstrap replications of $\hat{\omega}$, using 1000 Simulated Series of Composite Index

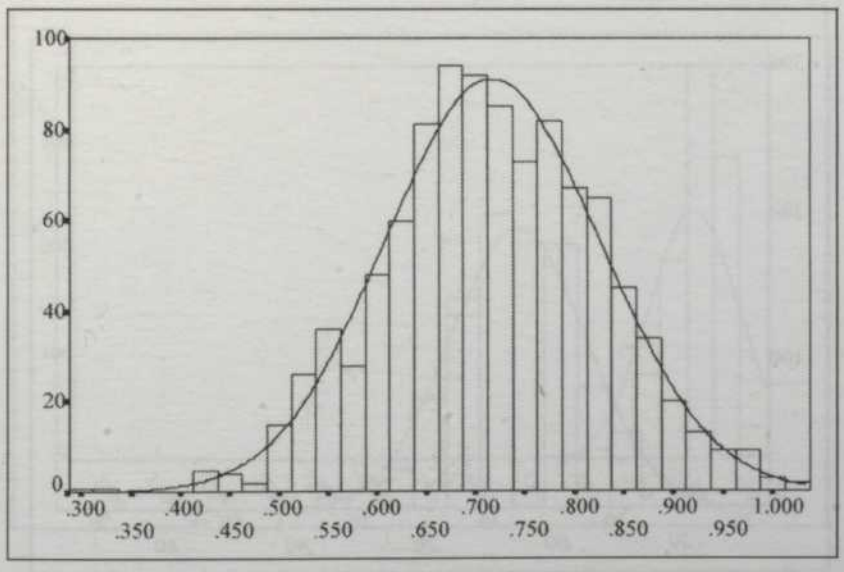

$\hat{\alpha}$

Fig. 3. Histogram, with normal curve, for 1000 parametric bootstrap replications of $\hat{\alpha}$, using 1000 Simulated Series of Composite Index

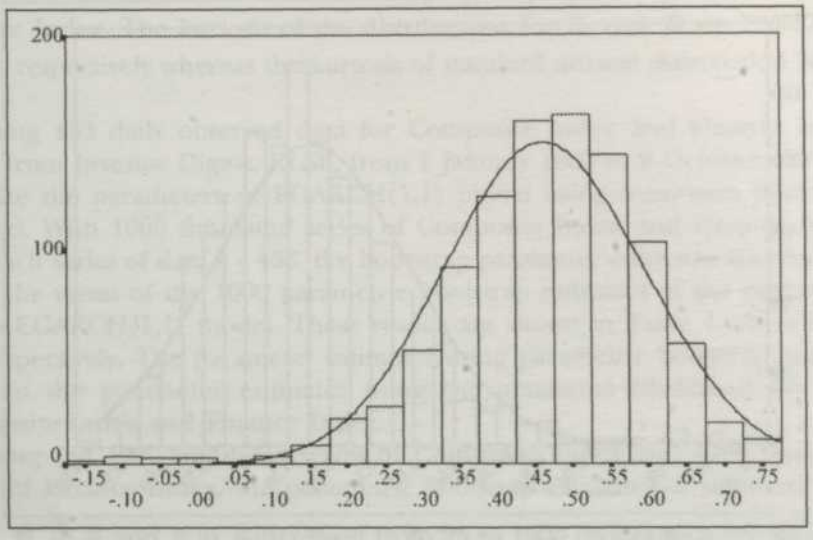

Fig. 4. Histogram, with normal curve, for 1000 parametric bootstrap replications of $\hat{\beta}$, using 1000 Simulated Series of Composite Index

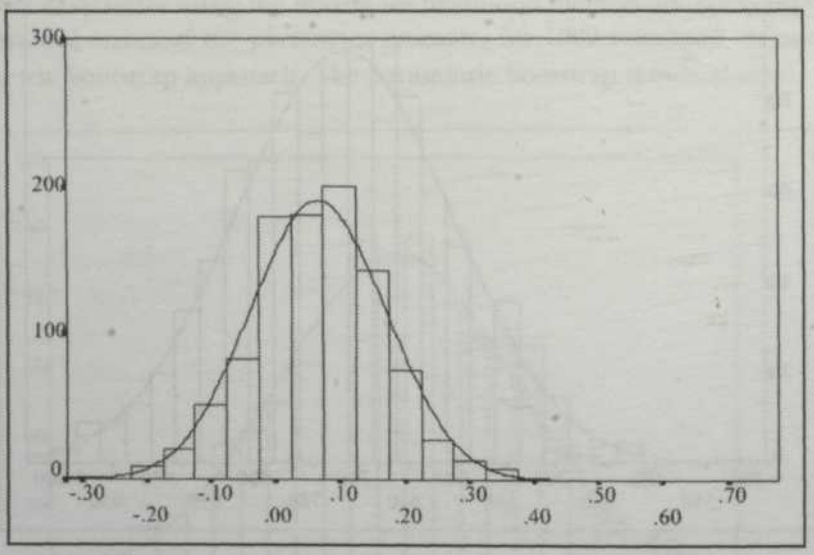

Fig. 5. Histogram, with normal curve, for 1000 parametric bootstrap replications of $\hat{\theta}$, using 1000 Simulated Series of Composite Index

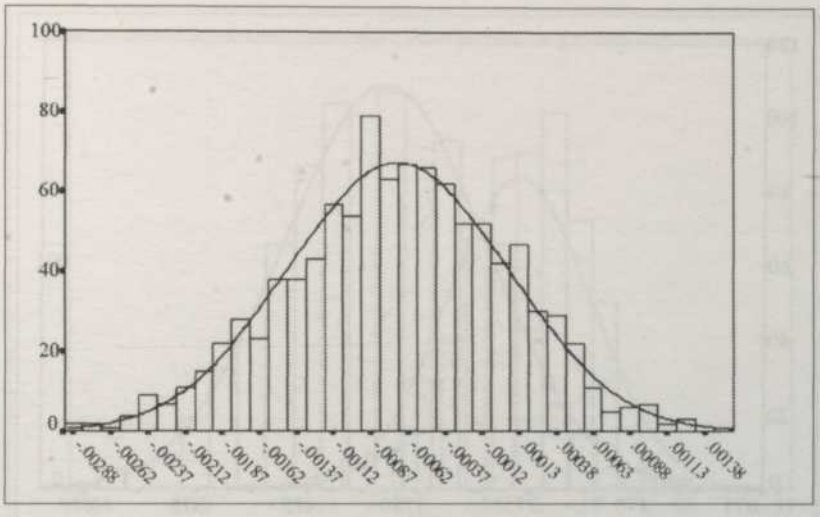

$\hat{\mu}$

Fig. 6. Histogram, with normal curve, for 1000 parametric bootstrap replications of $\hat{\mu}$, using 1000 Simulated Series of Finance Index

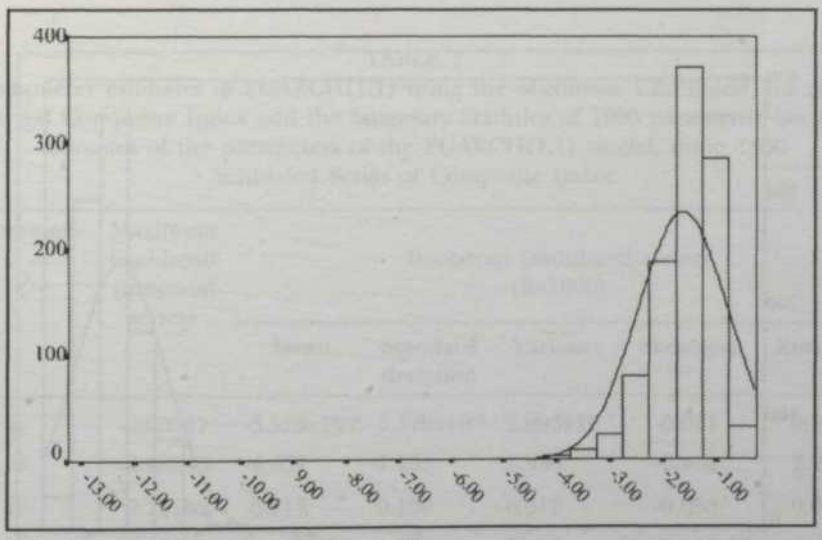

$\hat{\omega}$

Fig. 7. Histogram, with normal curve, for 1000 parametric bootstrap replications of $\hat{\omega}$, using 1000 Simulated Series of Finance Index

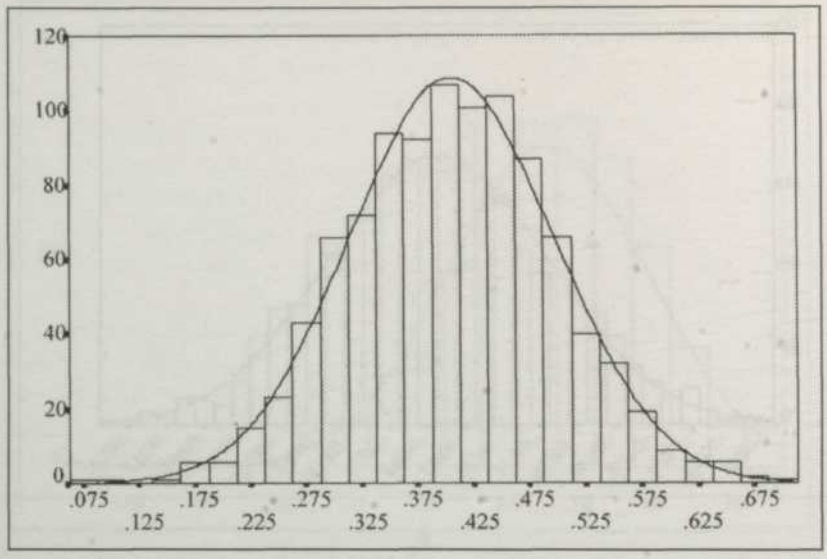

$\hat{\alpha}$

Fig. 8. Histogram, with normal curve, for 1000 parametric bootstrap replications of $\hat{\alpha}$, using 1000 Simulated Series of Finance Index

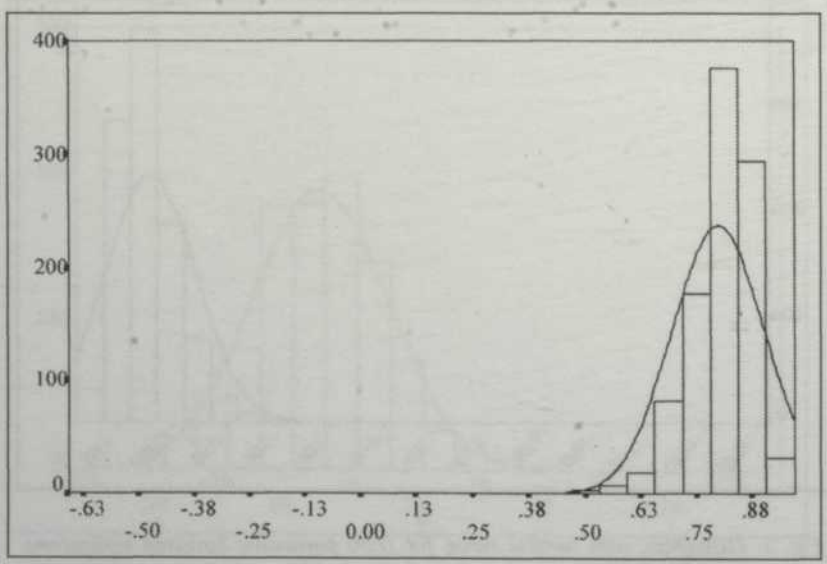

$\hat{\beta}$

Fig. 9. Histogram, with normal curve, for 1000 parametric bootstrap replications of $\hat{\beta}$, using 1000 Simulated Series of Finance Index

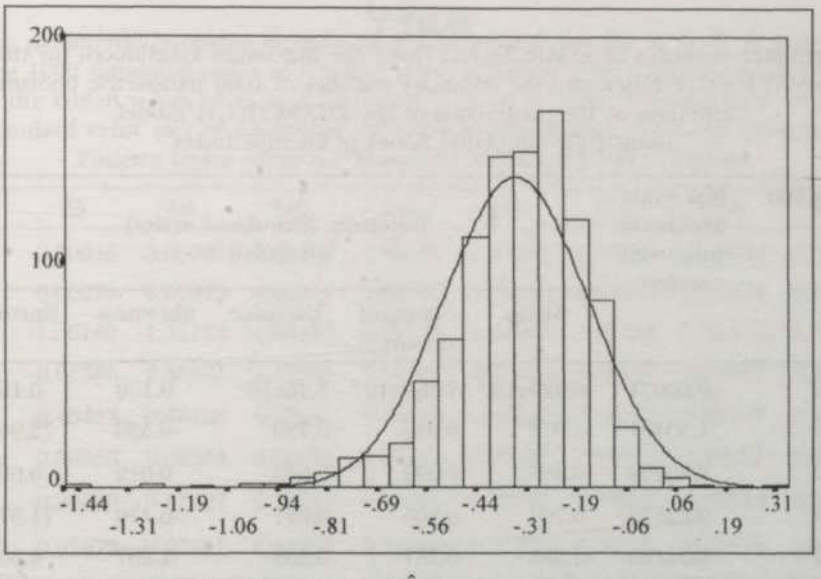

Fig. 10. Histogram, with normal curve, for 1000 parametric bootstrap replications of $\hat{\theta}$, using 1000 Simulated Series of Finance Index

TABLE 1
Parameter estimates of EGARCH(1,1) using the Maximum Likelihood, for the Observed Composite Index and the Summary Statistics of 1000 parametric bootstrap estimates of the parameters of the EGARCH(1,1) model, using 1000 Simulated Series of Composite Index

Parameter	Maximum likelihood (observed series)	Bootstrap (simulated series) (B=1000)				
		Mean	Standard deviation	Variance	Skewness	Kurtosis
$\hat{\mu}$	-0.00037	-3.529×10^{-4}	5.379×10^{-4}	2.893×10^{-7}	-0.011	-0.184
$\hat{\omega}$	-4.48246	-4.651	1.155	1.334	-0.932	2.242
$\hat{\alpha}$	0.72132	0.717	0.109	0.012	-0.053	0.017
$\hat{\beta}$	0.48133	0.463	0.133	0.018	-0.906	2.175
$\hat{\theta}$	0.06026	0.066	0.105	0.011	0.305	2.178

TABLE 2
Parameter estimates of EGARCH(1,1) using the Maximum Likelihood, for the Observed Finance Index and the summary statistics of 1000 parametric bootstrap estimates of the parameters of the EGARCH(1,1) model, using 1000 Simulated Series of Finance Index

Parameter	Maximum likelihood (observed series)	Bootstrap (simulated series) (B=1000)				
		Mean	Standard deviation	Variance	Skewness	Kurtosis
$\hat{\mu}$	-0.00071	-6.920×10^{-4}	7.389×10^{-4}	5.46×10^{-7}	-0.100	-0.161
$\hat{\omega}$	-1.40131	-1.616	0.849	0.720	-6.539	72.967
$\hat{\alpha}$	0.40728	0.406	0.092	0.008	0.019	0.081
$\hat{\beta}$	0.82576	0.799	0.105	0.011	-6.470	71.574
$\hat{\theta}$	-0.31108	-0.338	0.181	0.033	-1.207	4.360

TABLE 3
The parametric bootstrap estimate of standard error (*se*) for $\hat{\mu}$, $\hat{\omega}$, $\hat{\alpha}$, $\hat{\beta}$ and $\hat{\theta}$, using 1000 Simulated Series of Composite Index. A run of 1000 bootstrap replications gave the tabled values of *se* as B increased from 25 to 1000. A comparison with the standard error (*se*) of parameter estimates of EGARCH(1,1) for the observed composite index using the Maximum Likelihood (ML) Method

B:	25	50	100	250	500	800	1000	ML
$\hat{\mu}$:	-.00019	-.00036	-.00040	-.00034	-.00035	-.00034	-.00035	-0.00037
se $\hat{\mu}$:	.00059	.00060	.00059	.00057	.00056	.00053	.00054	0.00013
$\hat{\omega}$:	-4.75573	-4.64047	-4.77596	-4.71238	-4.68712	-4.64875	-4.65141	-4.48246
se $\hat{\omega}$:	1.46219	1.24390	1.29393	1.13209	1.10190	1.13338	1.15498	0.85589
$\hat{\alpha}$	.71969	.71450	.72397	.71843	.71964	.71782	.71714	0.72132
se $\hat{\alpha}$:	.10442	.10694	.10809	.11104	.11036	.10994	.10939	0.15375
$\hat{\beta}$	.45140	.46345	.44842	.45604	.45844	.46285	.46262	0.48133
se $\hat{\beta}$:	.16804	.14252	.14727	.12949	.12672	.13034	.13277	0.09754
$\hat{\theta}$	.08106	.06450	.06331	.06860	.06377	.06672	.06644	0.06026
se $\hat{\theta}$:	.10045	.10344	.10291	.09898	.09936	.10466	.10466	0.11359

TABLE 4

The parametric bootstrap estimate of standard error (*se*) for $\hat{\mu}$, $\hat{\omega}$, $\hat{\alpha}$, $\hat{\beta}$ and $\hat{\theta}$, using 1000 simulated series of finance index. A run of 1000 bootstrap replications gave the tabled values of se as B increased from 25 to 1000. A comparison with the standard error (se) of parameter estimates of EGARCH(1,1) for the Observed Finance Index using the Maximum Likelihood (ML) Method

B:	25	50	100	250	500	800	1000	ML
$\hat{\mu}$:	-0.00046	-0.00069	-0.00074	-0.00066	-0.00068	-0.00068	-0.00069	-0.00071
se $\hat{\mu}$:	0.00078	0.00079	0.00081	0.00075	0.00076	0.00073	0.00074	0.00071
$\hat{\omega}$:	-1.56149	-1.51123	-1.68422	-1.66130	-1.62888	-1.62551	-1.61616	-1.40131
se $\hat{\omega}$:	0.62386	0.56321	1.17545	1.11842	0.87356	0.89111	0.84867	0.31832
$\hat{\alpha}$	0.40453	0.40468	0.40941	0.40429	0.40692	0.40713	0.40577	0.40728
se $\hat{\alpha}$:	0.08983	0.08334	0.09094	0.09182	0.09007	0.09197	0.09157	0.07189
$\hat{\beta}$	0.80690	0.81227	0.79117	0.79426	0.79797	0.79831	0.79949	0.82576
se $\hat{\beta}$:	0.07672	0.06961	0.14359	0.13697	0.10716	0.10991	0.10472	0.03876
$\hat{\theta}$	-0.34871	-0.34723	-0.34000	-0.33782	-0.33986	-0.33682	-0.33784	-0.31108
se $\hat{\theta}$:	0.18111	0.16356	0.17468	0.18088	0.17413	0.17821	0.18059	0.10384

and $\hat{\alpha}$ for Finance Index are relatively close to those of the maximum likelihood standard errors. For Composite Index, the standard errors of $\hat{\mu}$ and $\hat{\beta}$ are quite close in both methods. However, the parametric bootstrap standard errors of $\hat{\alpha}$ and $\hat{\theta}$ are smaller than the maximum likelihood standard errors. Hence, for standard error of the parameter estimates of EGARCH(1,1) model, the parametric bootstrap approach, which does not rely on the normality assumption, is one of the reliable alternatives to the maximum likelihood method, especially when the underlying population of the parameters is unknown.

The corresponding 90% and 95% confidence intervals of the parameter estimates of EGARCH(1,1) model for Composite Index based on the standard normal theory using the maximum likelihood estimates (symmetry ML), the parametric bootstrap percentile method and the standard normal theory using bootstrap estimates (symmetry bootstrap) are presented in Table 5 and Table 6.

The lengths of the 90% and 95% bootstrap percentile intervals of $\hat{\alpha}$ and $\hat{\theta}$ are the shortest following by symmetry bootstrap intervals and symmetry ML intervals for Composite Index. However, the lengths of the 90% and 95% symmetry ML intervals of $\hat{\mu}$, $\hat{\omega}$ and $\hat{\beta}$ are shorter than the bootstrap percentile intervals. The lengths of the 90% and 95% symmetry bootstrap intervals of $\hat{\mu}$, $\hat{\omega}$ and $\hat{\beta}$ are the longest intervals among those considered for Composite Index.

For Finance Index, the corresponding 90% and 95% confidence intervals of the parameter estimates are presented in Table 7 and Table 8. The lengths

TABLE 5
90% confidence interval of the parameter estimates of EGARCH(1,1) for Composite Index

	Parameter	Estimate	Lower	Upper	Length	Shape
Symmetry	$\hat{\mu}$	-0.00037	-0.0006	-0.0001	0.0005	1.0000
ML	$\hat{\omega}$	-4.48246	-5.8904	-3.0745	2.8159	1.0000
	$\hat{\alpha}$	0.72132	0.4684	0.9742	0.5058	1.0000
	$\hat{\beta}$	0.48133	0.3209	0.6418	0.3209	1.0000
	$\hat{\theta}$	0.06026	-0.1266	0.2471	0.3737	1.0000
Bootstrap	$\hat{\mu}$	-0.00035	-0.0014	0.0007	0.0021	0.9307
Percentile	$\hat{\omega}$	-4.65141	-6.6219	-3.0262	3.5957	0.8248
(B=1000)	$\hat{\alpha}$	0.71714	0.5352	0.8950	0.3597	0.9775
	$\hat{\beta}$	0.46262	0.2349	0.6530	0.4182	0.8359
	$\hat{\theta}$	0.06644	-0.1028	0.2302	0.3330	0.9675
Symmetry	$\hat{\mu}$	-0.00035	-0.0012	0.0005	0.0018	1.0000
Bootstrap	$\hat{\omega}$	-4.65141	-6.5514	-2.7515	3.7999	1.0000
(B=1000)	$\hat{\alpha}$	0.71714	0.5372	0.8971	0.3599	1.0000
	$\hat{\beta}$	0.46262	0.2442	0.6810	0.4368	1.0000
	$\hat{\theta}$	0.06644	-0.1057	0.2386	0.3443	1.0000

TABLE 6
95% confidence interval of the parameter estimates of EGARCH(1,1) for Composite Index

	Parameter	Estimate	Lower	Upper	Length	Shape
Symmetry	$\hat{\mu}$	-0.00037	-0.0006	-0.0002	0.0002	1.0000
ML	$\hat{\omega}$	-4.48246	-6.1600	-2.8049	3.3551	1.0000
	$\hat{\alpha}$	0.72132	0.4200	1.0227	0.6027	1.0000
	$\hat{\beta}$	0.48133	0.2902	0.6725	0.3824	1.0000
	$\hat{\theta}$	0.06026	-0.1624	0.2829	0.4453	1.0000
Bootstrap	$\hat{\mu}$	-0.00035	-0.0013	0.0005	0.0018	0.9420
Percentile	$\hat{\omega}$	-4.65141	-7.2802	-2.7886	4.4916	0.7086
(B=1000)	$\hat{\alpha}$	0.71714	0.5050	0.9359	0.4309	1.0316
	$\hat{\beta}$	0.46262	0.1718	0.6824	0.5106	0.7557
	$\hat{\theta}$	0.06644	-0.1413	0.2763	0.4177	1.0101
Symmetry	$\hat{\mu}$	-0.00035	-0.0014	0.0007	0.0021	1.0000
Bootstrap	$\hat{\omega}$	-4.65141	-6.9152	-2.3876	4.5275	1.0000
(B=1000)	$\hat{\alpha}$	0.71714	0.5027	0.9315	0.4288	1.0000
	$\hat{\beta}$	0.46262	0.2024	0.7229	0.5205	1.0000
	$\hat{\theta}$	0.06644	-0.1387	0.2716	0.4103	1.0000

TABLE 7
90% confidence interval of the parameter estimates of EGARCH(1,1) for Finance Index

	Parameter	Estimate	Lower	Upper	Length	Shape
Symmetry	$\hat{\mu}$	-0.00071	-0.0019	0.0005	0.0023	1.0000
ML	$\hat{\omega}$	-1.40131	-1.9249	-0.8777	1.0473	1.0000
	$\hat{\alpha}$	0.40728	0.2890	0.5255	0.2365	1.0000
	$\hat{\beta}$	0.82576	0.7620	0.8895	0.1275	1.0000
	$\hat{\theta}$	-0.31108	-0.4819	-0.1403	0.3416	1.0000
Bootstrap	$\hat{\mu}$	-0.00069	-0.0019	0.0005	0.0024	0.9280
Percentile	$\hat{\omega}$	-1.61616	-2.6933	-0.8242	1.8691	0.7353
(B=1000)	$\hat{\alpha}$	0.40577	0.2610	0.5566	0.2956	1.0417
	$\hat{\beta}$	0.79949	0.6657	0.8964	0.2307	0.7241
	$\hat{\theta}$	-0.33784	-0.6529	-0.1015	0.5513	0.7501
Symmetry	$\hat{\mu}$	-0.00069	-0.0019	0.0005	0.0024	1.0000
Bootstrap	$\hat{\omega}$	-1.61616	-3.0122	-0.2201	2.7921	1.0000
(B=1000)	$\hat{\alpha}$	0.40577	0.2551	0.5564	0.3013	1.0000
	$\hat{\beta}$	0.79949	0.6272	0.9717	0.3445	1.0000
	$\hat{\theta}$	-0.33784	-0.6349	-0.0408	0.5941	1.0000

TABLE 8
95% confidence interval of the parameter estimates of EGARCH(1,1) for Finance Index

	Parameter	Estimate	Lower	Upper	Length	Shape
Symmetry	$\hat{\mu}$	-0.00071	-0.0021	0.0007	0.0028	1.0000
ML	$\hat{\omega}$	-1.40131	-2.0252	-0.7774	1.2478	1.0000
	$\hat{\alpha}$	0.40728	0.2664	0.5482	0.2818	1.0000
	$\hat{\beta}$	0.82576	0.7498	0.9017	0.1519	1.0000
	$\hat{\theta}$	-0.31108	-0.5146	-0.1075	0.4071	1.0000
Bootstrap	$\hat{\mu}$	-0.00069	-0.0022	0.0007	0.0028	0.9014
Percentile	$\hat{\omega}$	-1.61616	-3.0493	-0.7254	2.3238	0.6215
(B=1000)	$\hat{\alpha}$	0.40577	0.2280	0.5843	0.3563	1.0043
	$\hat{\beta}$	0.79949	0.6212	0.9100	0.2887	0.6199
	$\hat{\theta}$	-0.33784	-0.7606	-0.0628	0.6978	0.6506
Symmetry	$\hat{\mu}$	-0.00069	-0.0021	0.0008	0.0029	1.0000
Bootstrap	$\hat{\omega}$	-1.61616	-3.2796	0.0472	3.3268	1.0000
(B=1000)	$\hat{\alpha}$	0.40577	0.2263	0.5853	0.3590	1.0000
	$\hat{\beta}$	0.79949	0.5942	1.0047	0.4105	1.0000
	$\hat{\theta}$	-0.33784	-0.6918	0.0161	0.7079	1.0000

of the 90% and 95% symmetry ML intervals of all the parameter estimates are the shortest, followed by bootstrap percentile intervals and symmetry bootstrap intervals.

For both series of Composite Index and Finance Index, the shapes of the 90% and 95% symmetry Ml intervals and symmetry bootstrap intervals of all the parameter estimates are 1. These should be the expected results since the standard normal intervals are symmetrical about the point estimate $\hat{T}$, having shape = 1 by definition.

The 90% bootstrap percentile intervals of all the parameters in the Composite Index indicate some degree of asymmetry with greater distances from the lower limits, $\hat{T}_l$ to the point estimate $\hat{T}$ than from $\hat{T}$ to the upper limits, $\hat{T}_u$.

The 95% bootstrap percentile intervals of $\hat{\alpha}$ and $\hat{\theta}$ for the Composite Index are asymmetrical with greater distances from the upper limits, $\hat{T}_u$ to the point estimate, $\hat{T}$ than from $\hat{T}$ to the lower limits, $\hat{T}_l$ whereas the intervals of $\hat{\mu}$, $\hat{\omega}$ and $\hat{\beta}$ have the shape < 1.

For Finance Index, the 90% and 95% bootstrap percentile intervals of all the parameter estimates have the shape < 1 except $\hat{\alpha}$ with the shape > 1.

SUMMARY AND CONCLUSION

Using 433 daily observed series for Composite Index and Finance Index, we generated the maximum likelihood estimates of the parameters to generate 1000 artificial time series corresponding to EGARCH(1,1) model. These simulated series are then submitted to the use of the parametric bootstrap method to examine the characteristics of the unknown underlying populations of the parameters, including skewness and kurtosis. This paper also studies the standard error and confidence intervals for the parameters of the model via the parametric bootstrap approach.

From the histograms, skewness and kurtosis of the parameter estimates, we observe that the unknown (empirical) distributions of the parameters are skewed and leptokurtic. Hence, the parametric bootstrap estimation method, which does not rely on the normality assumption of the underlying population of the parameter, is one of the reliable alternative approaches to obtain the interval estimate of the parameters and to obtain the standard errors of the parameter estimates of the EGARCH(1,1) model.

The most serious errors made by the standard normal intervals, either using the maximum likelihood estimates (symmetry ML) or bootstrap estimates (symmetry bootstrap), are due to their enforced symmetry on the unknown underlying population of the parameters. These is the case of the parameter of EGARCH(1,1) model. Therefore, the parametric bootstrap percentile method is one of the reliable alternatives to construct the confidence intervals of the parameter estimates of the EGARCH(1,1) model.

Limitations of the Study: Problem of Dependence

Independence between observational units is often an important assumption in data analysis and is usually present in bootstrap-based inferences. Lack of independence can reduce the accuracy of inferences. There is no easy solution

to the problems of dependence as in the case of time series. We cannot simply resample from the individual observations, as this would destroy the correlation that we are trying to capture.

In order to rectify this problems, Efron and Tibshirani (1993) proposed to model the dependence in some way, and then draw inferences from the model. It is called "the moving blocks bootstrap" that has the advantage of being less "model dependent" or more model-free in handling dependence. With the moving block bootstrap, the idea is to choose a block size l large enough so that observations more than l time units apart will be nearly independent. By sampling the blocks of length l, we retain the correlation present in observations less than l units apart. However, the choice of block size l can be quite important, and effective methods for making this choice have not yet been developed.

Souza *et. al.* (1996) using a non-parametric bootstrap method to resample the simulated time series of ARMA(p,q) structures. However, the problem of dependence still remains a question in the study.

An alternative approach to deal with the problems of dependence is using the resampling algorithm via parametric bootstrap. Instead of sampling with replacement from the observed data, we generate B independent bootstrap data sets r^{*1}, r^{*2}, ..., r^{*3} by drawing B samples of size n from the parametric estimate of the population $\hat{F}$:

$$\hat{F}_{par} - - > (r_1^*, r_2^*, r_3^*, \ldots, r_n^*)$$

where $\hat{F}_{par}$ is an estimate of the cumulative distribution function, F derived from a parametric model for the observed data. From each pseudo-data, r^{*b} where $b = 1,2,\ldots,B$, we can evaluate the desired statistic of interest, $\hat{T}^*(b)$.

It might seem strange to use a bootstrap resampling algorithm when a text book formula could be used to estimate the parameters of a model. However, according to Efron and Tibshirani (1993), when the bootstrap sampling used in parametric mode, it provides more accurate answer than textbook formulae because it does not depend on the asymptotic results and the normality assumption of the underlying process. Furthermore, it can provide answers to problems for which no text book formulae exist. Besides, in the case of time series, it can help solving the problems of dependence.

In this study, $\hat{F}_{par}$ is the generated daily rate of return of stock market indices and parameters of interest are the parameters of the EGARCH(1,1) model such as μ, ω, α, β and θ.

REFERENCES

ABDULLAH, M. 1995. On bootstrap methods in orthogonal regression model. *Pertanika J. Sci. Technol.* **3(2):** 349-359.

BOLLERSLEV, T. 1986. Generalized autoregressive conditional heteroscedasticity. *J. Econometric* **31:** 307-327.

CHOO, W. C. 1997. Stock market models: A comparison. *Proceedings of Seminar Statistics 1997.* Institut Statistik Malaysia.

CHOO, W. C. 1998. Generalised autoregressive conditional heteroscedasticity (GARCH) models for stock market volatility. Master of Science thesis, Department of Mathematics, Faculty of Science and Environmental Studies, Universiti Putra Malaysia.

CHOO, W. C. 1999. Performance of GARCH models in forecasting stock market volatility. *J. Forecasting* **18:** 333-343.

EFRON, B. 1979. Bootstrap methods: another look at the Jacknife. *Annals of Statistics* **7:** 1-26.

EFRON, B. 1987. Better bootstrap confidence intervals. *J. Amer. Statistical Association* **82:** 171-200.

EFRON, B. and R. J. TIBSHIRANI, 1986. Bootstrap methods for standard errors, confidence intervals and other measures of statistical accuracy. *Statistical Sci.* **1:** 54-77.

EFRON, B. and R. J. Tibshirani. 1993. *An Introduction to the Bootstrap.* New York: Chapman and Hall.

ENGLE, R. F. 1982. Autoregressive conditional heteroscedasticity with estimates of the variance of UK inflation. *Econometrica* **50:** 987-1008.

HALL, P. 1986. On the bootstrap and confidence intervals. *Ann. Statistics* **14:** 1431-1452.

HALL, P. 1987. On the bootstrap and likelihood-based confidence intervals. *Biometrika* **74:** 481-493.

MASAROTTO, G. 1990. Bootstrap prediction intervals for autoregressions. *Inter. J. of Forecasting* **6:** 229-239.

NELSON, D. B. 1991. Conditional heteroscedasticity in asset returns: A new approach. *Econometrica* **59:** 347-370.

NELSON, D. B. and C. Q. CAO, 1992. Inequality constraints in the univariate GARCH model. *J. Business and Econ. Statistics* **10:** 229-235.

SOUZA, R. C. and A. C. Neto, 1996. A bootstrap simulation study in ARMA(p,q) structures. *J. Forecasting* **15**: 343-353.

THOMBS, L. A. and W. R. SCHUCANY, 1990. Bootstrap prediction intervals for autoregression. *J. Amer. Statistical Association* **85:** 486-492.

TSAY, RUEY. S. 1992. Model checking via parametric bootstraps in time series analysis. *Applied Statistics* **41**: 1-15.

Pertanika J. Sci. & Technol. 9(2): 189 - 195 (2001)
ISSN: 0128-7680

Effects of Filter Positioning in an Er^{3+}-doped Fibre Ring Laser

Teyo Tuan Chin, M.K. Abdullah and H. Ahmad
Telekom Malaysia Photonics Research Centre
Department of Physics, University of Malaya
50603 Kuala Lumpur

Received: 20 April 1998

ABSTRAK

Kesan kedudukan turas dalam laser gelanggang fiber terdop Er telah dibuktikan dengan jelas. Tenaga output serta keefisienan cerun dalam kes-kes apabila turas ditempatkan selepas runcing (FAT) lebih tinggi daripada sebelum runcing (FBT), dan cahaya bergerak mengikut arah pusingan jam (CCW). Tenaga maksimum setinggi 16.3 mW boleh dicapai dalam kes biasa. Manakala dalam kes yang kemudiannya, tenaga yang dikeluarkan hanya 10.7 mW. Keefisienan cerun masing-masing adalah 13.3% dan 8.8%.

ABSTRACT

Effects of filter positioning in an Er^{3+}-doped fibre ring laser (EDFL) are demonstrated. The output power as well as the slope efficiency in the cases when the filter is placed after the taper (FAT) is higher than that of before taper (FBT), and the light oscillates in counter-clockwise (CCW) direction. Maximum power as high as 16.3 mW could be achieved in former case while latter case gave only 10.7 mW. The slope efficiencies were 13.3 % and 8.8 %, respectively.

Keywords: Er^{3+}–doped fibre, fibre laser

INTRODUCTION

Er^{3+}-doped fibre lasers and amplifiers at the 1550 nm band have many important applications in telecommunication and other fields [1,2]. Several EDFL systems have been demonstrated with wide tuning range using different methods [3,4,5]. In our study, a bandpass filter was used to realise the tunability of the laser system. Oscillation mode in a laser cavity can be selected or controlled when the centre wavelength of a tuneable filter in an EDFL is changed.

In previous work [6], the effects of filter positioning were done as a function of coupler reflectivity. The experimental results showed that the FAT case gave a better performance in term of output power for the reflectivity. In this paper, however, filter-positioning study was carried out as a function of pump power. A different feature was observed in the amplified spontaneous emission (ASE) level and side mode suppression ratio (SMSR).

EXPERIMENTAL SET-UP

The block diagram of an erbium-doped fibre ring laser is shown in *Fig. 1*. The laser system consists of two 980/1550-nm wavelength division multiplexers

(WDMs), a 1550 nm coupler (taper) with the ratio of 50/50, a Fabry-Perot (FP) tuneable filter and an optical isolator. The laser output was fed to an optical spectrum analyser (OSA) set at 0.5 nm of resolution. An optical isolator was used to ensure a unidirectional oscillation of laser modes in the cavity. It was placed in such a direction (*Fig. 1*) to provide a counter-propagating of cavity configuration. In order to have a co-propagating configuration, points A and B were exchange. An erbiumñdoped fibre (EDF) with a cut-off wavelength of 950 nm, refractive index of 1.473, core diameter of 1.68 (m and ion concentration of +240 ppm was placed in between WDMs as an active (gain) medium in the fibre laser system. A Nortel diode laser with 980 nm wavelength was used as a pumping source. The extra 980-nm pump source, as an excess power, was measured by a power meter from WDM II. The cavity length was about 15m without taking into account the EDF length. The EDF length used was 8.7 m.

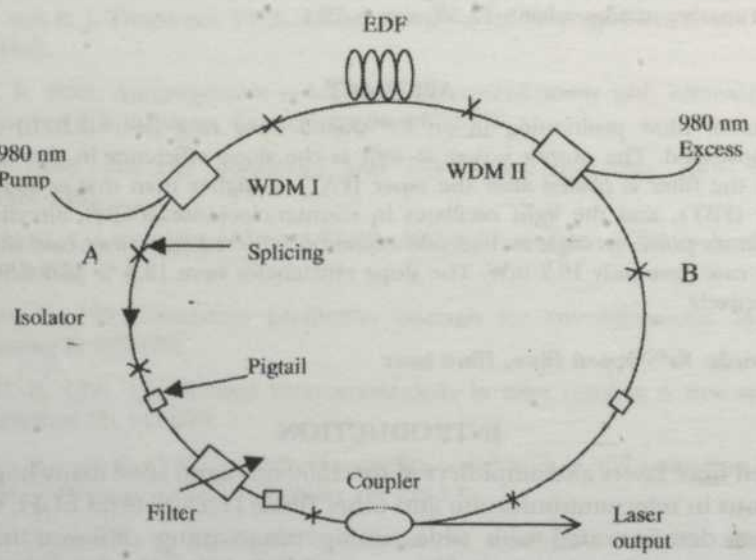

Fig. 1. Set-up of an erbium-doped fibre laser system

RESULTS AND DISCUSSION

Experiment results show that different filter positions give different laser performances. The output power in the case when filter is placed before the taper (FBT) is obviously lower than that of filter after the taper (FAT), corresponding to counter-clockwise (CCW) direction, as shown in *Fig. 2*. The maximum output power for both cases are 10.7 mW and 16.3 mW respectively at the maximum pump power of 124.5 mW. By placing the filter at the position before the taper, the total oscillating laser light would experience loss after passing through the filter, before being coupled-out from one of the taper's

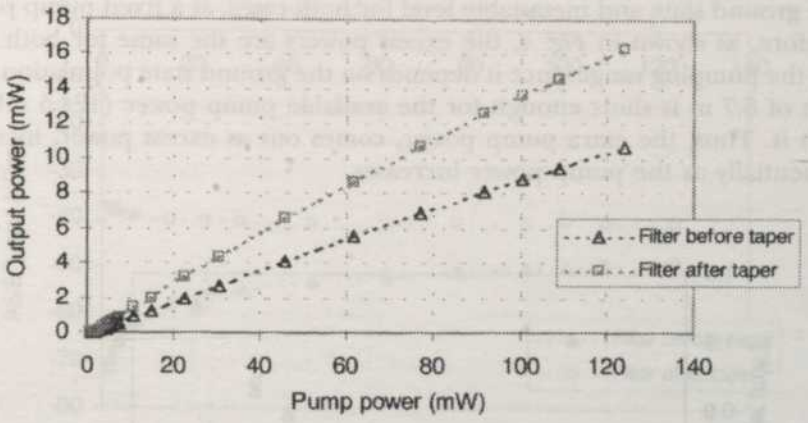

Fig 2. Output power versus pump power

leg. In the case of FAT, there is only 50% of the oscillating light would be suppressed by filter, giving a higher output power. Therefore, the latter case gives higher slope efficiency, 13.3% as compared to former case that gives 8.8% only. It is expected that improvement in the output performance can be achieved by further EDF length and reflectivity optimisation. The power spectrums for the both cases are presented in *Fig. 3.* The presence of the filter before the taper not only suppresses the peak power but also ASE level. Without the filter, a wider band and higher ASE level are obtained.

The intensity of circulating light before entering the EDF end at WDM II is the same for both the filter positions. This result in the same population of ion

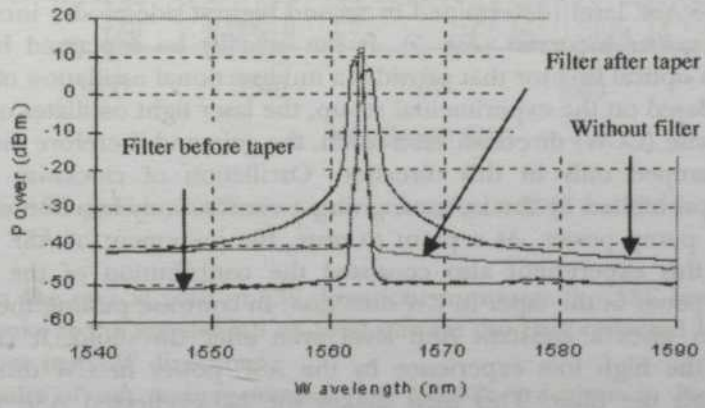

Fig. 3. Power spectrum for the case of filter before taper, filter after taper and without filter

in the ground state and metastable level for both cases, at a fixed pump power. Therefore, as shown in *Fig. 4*, the excess powers are the same for both cases along the pumping range since it depends on the ground state population. EDF length of 8.7 m is short enough for the available pump power (124.5 mW) to bleach it. Thus, the extra pump power, comes out as excess power, increases exponentially as the pump power increases.

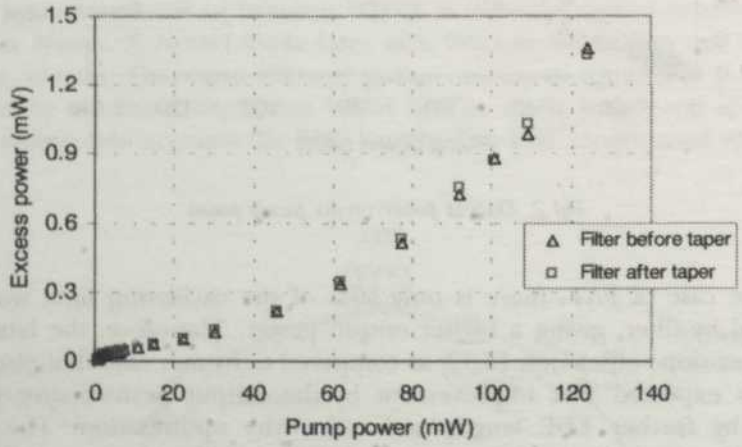

Fig. 4. Excess pump power as a function of pump power

From the laser theory, it is known that the population difference ΔN_{th} ($\equiv N_2 - N_1$) is clamped at the threshold after lasing [7,8]. Since the ASE level is population dependent, it should remain unchanged along the pumping range after the threshold. However, this is not the case in our study, in the case of FBT, where the ASE level (determined by second highest side mode) increases as the pump power increases (*Fig. 5*). It can actually be explained by the presence of an optical isolator that provides a unidirectional oscillation of light in the cavity. Based on the experimental set-up, the laser light oscillates only in counter-clockwise (CCW) direction. As a result, the gain and therefore the ASE power are clamped only in this direction. Oscillation of clockwise (CW) direction are prohibited by the isolator, giving a continuously increase of ASE level with the pump power. As a point to note, the increment of ASE levels measured in this experiment also consisted the contribution of the back-reflected ASE power at the taper in CW direction. In contrast, putting the filter after the taper gives a constant ASE level even after threshold. It can be attributed to the high loss experience by the ASE power in CW direction passing through the filter. This then makes the back-reflected ASE power negligible. The graph in *Fig. 5* reveals a steady output of ASE level in this case.

The ASE spectrum in CW direction, as shown in *Fig. 6*, were measured by exchanging the 50% and 100% of taper legs in the cavity. The presence of the

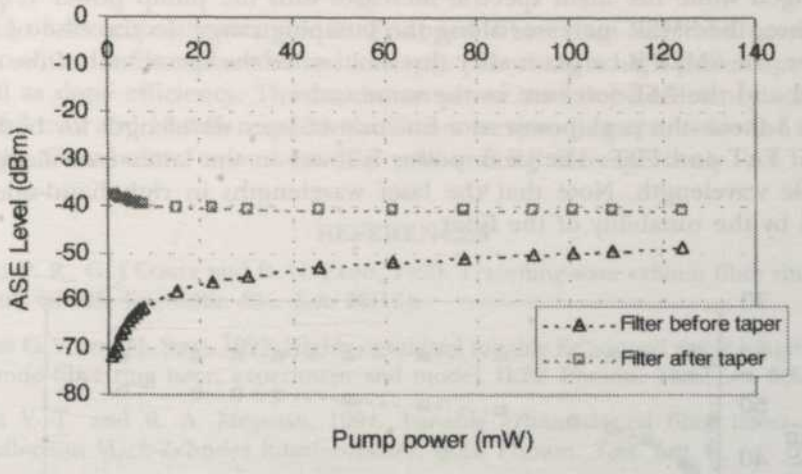

Fig. 5. ASE level as a function of pump power

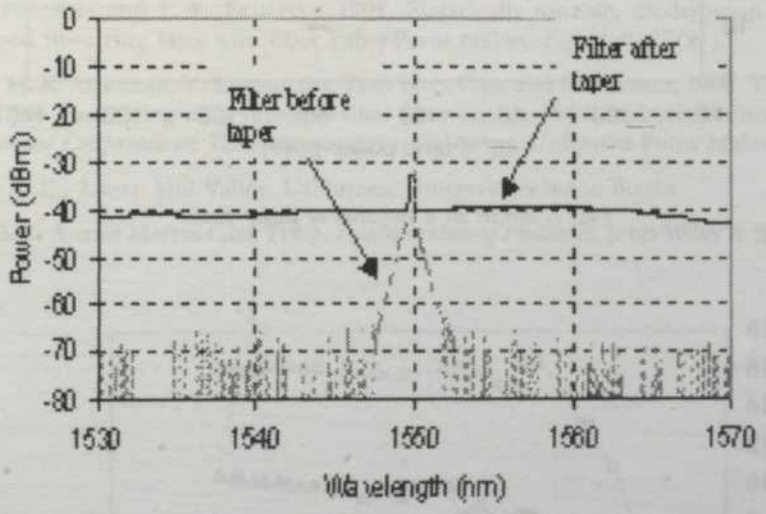

Fig. 6. ASE spectrum for CW direction by exchanging the 50% and 100% legs of coupler

filter in the optical path of CW direction suppresses the ASE level of > 20dB. The peaks at the wavelength of 1550 nm are the back-reflected laser signal at the taper in CCW direction.

Results of *side mode suppression ratio* (SMSR) are given in *Fig. 7*. SMSR is defined as the ratio of main spectral to the second highest side mode (or the highest ASE level). This parameter actually represents the signal-to-noise ratio of a laser system. In the case of FAT, the ASE levels as shown in *Fig. 7* remain

unchanged while the main spectral increases with the pump power (*Fig. 2*). Therefore, the SMSR increases along the pumping range. In the case of FBT, however, the SMSR is constant after threshold since the increment of the main spectral and the ASE level are in the same order.

Fig. 8 shows the peak power as a function of laser wavelength for both the cases of FAT and FBT. The peak power is lower in the latter case along the tuneable wavelength. Note that the laser wavelengths in right-hand-side are limited by the tunability of the filter.

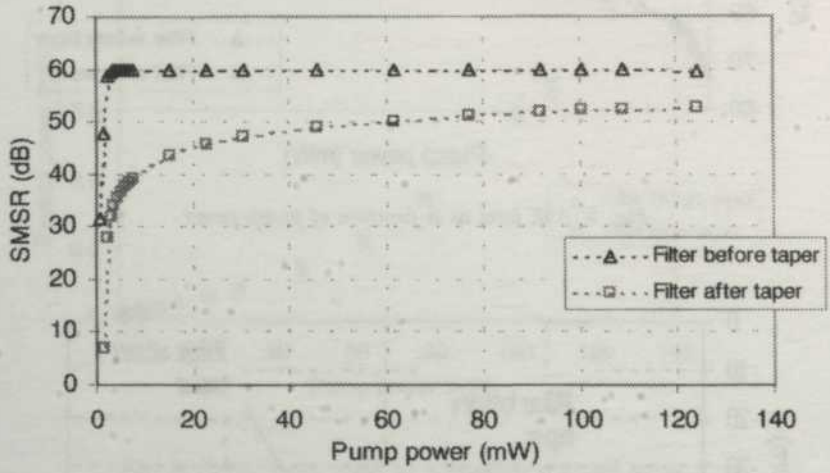

Fig. 7. SMSR as a function of pump power

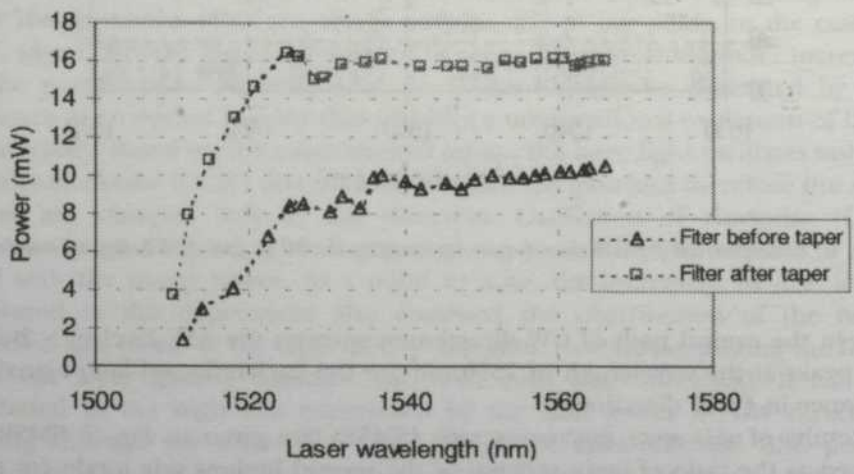

Fig. 8. Output power spectral for the both cases of FAT and FBT

CONCLUSION

Effects of filter positioning in an Er-doped fibre ring laser are presented. System with the filter placed after the taper promising a high power operation as well as slope efficiency. The maximum power and slope efficiency achieved was 16.3 mW and 13.3 % respectively. The corresponding results for the system with the filter before taper were 10.7 mW and 8.8 % respectively.

REFERENCES

MORKEL P. R., G. J COWLE and D. N. PAYNE, 1990. Travelling-wave erbium fiber ring laser with 60 kHz linewidth. *Elec. Lett.* **26(10)**.

POULSEN C. V. and M. SEJKA, 1993. Highly optimized tunable Er^{3+}-doped single-longitudinal-mode fiber ring laser, experiment and model, IEEE Photon. *Tech. Lett.* **5(6)**.

CHIENG Y. T. and R. A. MINASIAN, 1994. Tunable erbium-doped fiber lasers with a reflection Mach-Zehnder interferometer, IEEE Photon. *Tech. Lett.* **6**.

HUMPHREY P. D. and J. E. BOWERS, 1993. Fiber-birefringence tuning technique for an erbium-doped fiber ring laser, IEEE Photon. *Tech. Lett.* **5**.

ZYSKIND P. R., W. SULHOFF, J. STONE, D. J. DIGIOVANNI, L. W. STULZ, H. M. PRESBY, A. PICCIRILLI and P. E. PRAMAYAN; 1991. Electrically tunable, diode-pump erbium-doped fiber ring laser with fiber Fabry-Perot etalon. *Elec. Lett.* 27(21).

ISNIN F., M. K. ABDULLAH, V. SINIVASAGAM, TEYO TUAN CHIN and H. AHAMAD, 1998. The effect of filter positioning on a tuneable fiber laser system, IEEE Malaysia Section. In 2nd *National Conference on Telecommunications Technology*, Universiti Putra Malaysia.

SIEGMAN A. E., *Lasers*. Mill Valley, California: University Science Books.

SALLEH B. E. A. and MALVIN CARL TEICH. *Fundamentals of Photonics*. John Wiley & Sons, Inc.

Pertanika J. Sci. & Technol. 9(2): 197 - 206 (2001)
ISSN: 0128-7680

Application of Electrical Resistivity Method in Assessment of Groundwater Pollution at Seri Petaling Landfill, Selangor

Abdellatif Mukhtar Ahmed, Wan Norazmin Sulaiman, Shaharin Ibrahim[1], Puziah Abdul Latif and M. M. Hanafi[2]

Depatment of Environmental Science
Faculty of Science and Environmental Studies,
[1]Department of Physics, Faculty of Science and Environmental Studies,
[2]Department of Land Management, Faculty of Agriculture,
Universiti Putra Malaysia, 43400 UPM Serdang, Selangor, Malaysia

Received: 5 November 1999

ABSTRAK

Penilaian pencemaran air tanah disebabkan pelupusan sisa pepejal telah dibuat melalui penemuan imej kerintangan elektrik di bawah dan sekitar tempat pelupusan di Seri Petaling, Selangor. Perbandingan di antara penemuan dari imej kerintangan 2D dengan keputusan kimia air permukaan dan tanah serta logam berat yang disampel dari tanah tapak pelupusan telah dilakukan. Kajian menunjukkan terdapat dua zon badan sisa terurai yang berkerintangan rendah dan tepu dengan cecair larut resap yang konduktif di sepanjang garis $L\text{-}L_1$ yang dilakukan di permukaan atas tapak pelupusan. Terdapat juga sedikit zon kerintangan rendah yang di perolehi dari imej kerintangan di sepanjang garis $L\text{-}L_2$ di bahagian selatan Sungai Kuyuh bersempadan dengan tapak pelupusan dari arah selatan. Kepekatan logam berat dalam air tanah yang diperolehi dari lubang gerudi di bahagian hilir tapak pelupusan didapati lebih tinggi jika dibandingkan dengan nilai kepekatan dalam air tanah yang diperolehi di bahagian hulu tapak pelupusan. Ion klorida dan natrium didapati lebih tinggi di bahagian hilir tapak pelupusan. Kepekatan logam berat juga didapati lebih tinggi di bahagian hilir tapak pelupusan jika dibandingkan dengan bahagian hulur serta badan utama tapak pelupusan.Umumnya pencemaran didapati mengarah ke bahagian hilir tapak pelupusan.

ABSTRACT

Assessment of ground water pollution due to solid waste disposal has been attempted through the discussion of findings from electrical resistivity imaging survey within and around the landfill site of Sri Petaling located in Selangor. The findings from 2D resistivity imaging surveys were compared with the results from ground and surface water chemistry together with heavy metals in soil samples collected from the landfill. The study showed that there were two low resistivity zones of decomposed waste bodies saturated with highly conducting leachate situated along the resistivity line $L\text{-}L_1$ conducted on the top of the landfill. Other small low resistivity zones were obtained from the resistivity image along line $L\text{-}L_2$ conducted south of Sungai Kuyoh river bordering the landfill from its southern direction. Heavy metals in the ground water from the downstream bore hole were found in higher concentrations compared to their values in the upstream. Chloride and Sodium ions were higher in the downstream. Heavy metals in soil were also more concentrated in the downstream if compared to the upstream and the main body of the landfill. There is a general trend of pollution towards the downstream area of the landfill.

Keywords: electrical resistivity, groundwater pollution, landfill, Malaysia

INTRODUCTION

The electrical resistivity method is one of the most popular geophysical tool used in ground water exploration, it is also used for determining the ground water quality i. e., whether the water is saline, fresh or contaminated (Zohdy 1974; Stollar and Roux 1975; Rogers and Kean 1980; Urish, 1983). Successful monitoring of ground water contamination has been reported by Rogers and Kean (1980) at a fly ash disposal site using surface resistivity. One of the new developments in recent years is the use of 2-D electrical tomography surveys to map areas with moderately complex geology (Griffiths and Barker 1993). Dumping of wastes on land has been widely practiced all over the world, and the most common waste management practice of the mid-1990ís was landfilling (Scrudato and Pagano 1994). One of the adverse impacts of landfilling of municipal solid wastes is the production of which can cause significant impairment of groundwater use for domestic water supply as well as surface waters that receive leachate (Lee and Jones 1996).

MATERIALS AND METHODS

Location and Geological Setting

The Landfill of Sri Petaling is located in Cheras, lying 15 km south of the city center of Kuala Lumpur between latitudes 3° 3.2' and 3° 3.5' N and longitudes 101° 41.73' and 101° 42.6' E, covering an area of 21.1 ha. The landfill started operation in 1979 and was officially closed in 1991 with total amount of waste 7.1 million ton receiving 1500 ton/day. The maximum difference in elevation between the top of the landfill and the surrounding area was estimated to be 28.74 m. This indicated a maximum pressure exerted by the leachate onto the surrounding groundwater and surface water bodies (DOE 1999). *Fig. 1* shows the location and topography of the site. The climate of the area is tropical equatorial characterized by uniform temperature and high rainfall with mean max. annual temperature varying from 24.20 to 32.3°C and mean annual rainfall varying from 2137.9 to 2667.7 mm. Geologically the area entirely lies within the Kenny Hill Formation, (Yin 1961), and believed to be deposited during upper palaeozoic. Lithologically it consists of interbedded sandstones, shales, and mudstones. These formations were thought to have been deposited in a moderately deep marine environment situated near a large supply of reworked sediments. The landfill is located on tin tailing area, and during the geological survey around the landfill, fresh sandstone and phyllite of the Kenny Hill Formation, were outcropping to the north west direction of the northern boarder of the landfill. Three bore holes AH1, AH2, and AH3 were drilled on the upstream, downstream, and within the landfill.

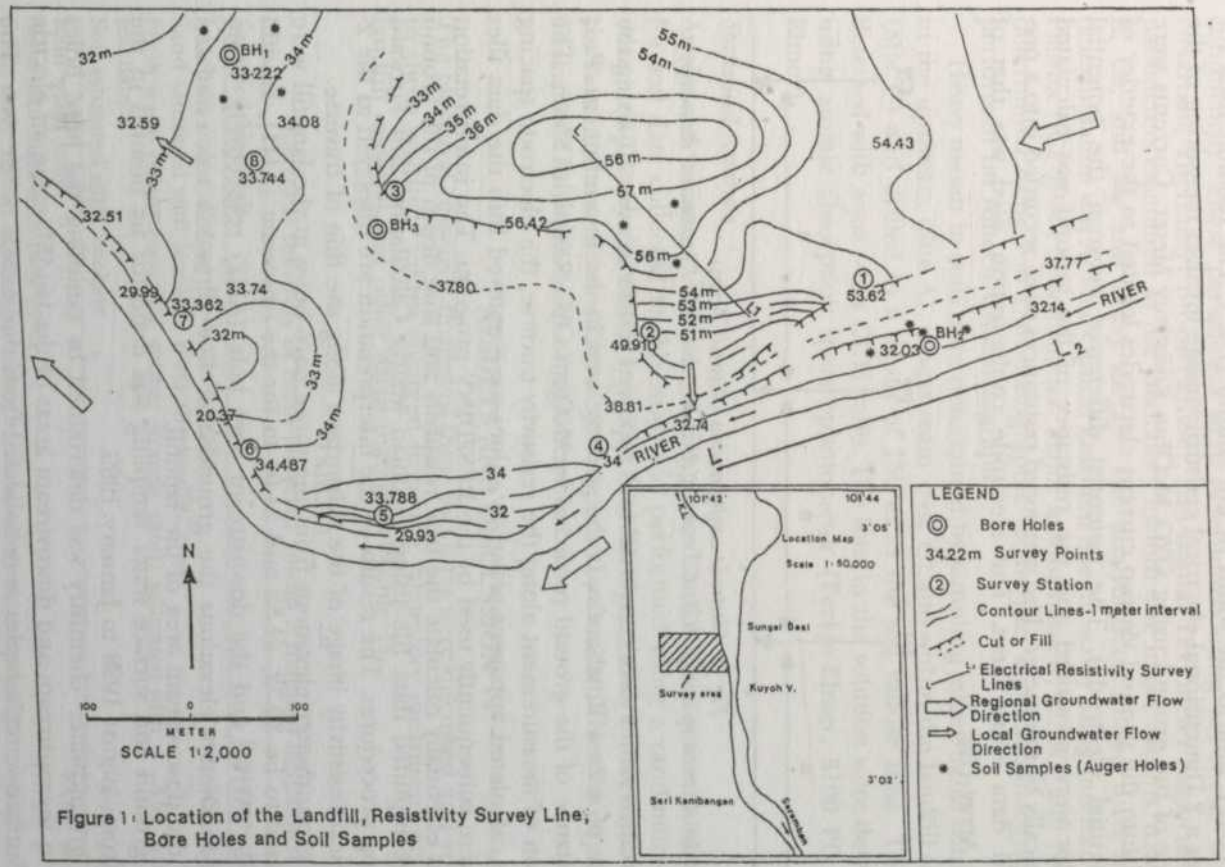

Figure 1: Location of the Landfill, Resistivity Survey Line, Bore Holes and Soil Samples

Fig. 1. Location of the landfill, resistivity survey line, bore holes and soil samples

Resistivity

Two resistivity survey lines were conducted in the central part on the top of the landfill ($L\text{-}L_1$), and to the south of the landfill ($L\text{-}L_2$). The method used for obtaining a 2 Dimensional electrical resistivity image involves measuring of the resistance of the ground using OYO McOhm Resistivity Meter. Currents were injected into the ground via two current electrodes located to the exterior of the potential electrodes. The potential difference between the potential electrodes were measured and the resistance of the ground was calculated automatically by the meter. The measured resistances were recorded into a pre-prepared data entry sheet. The electrode configuration used was that of Wenner Array (*Fig. 2*).

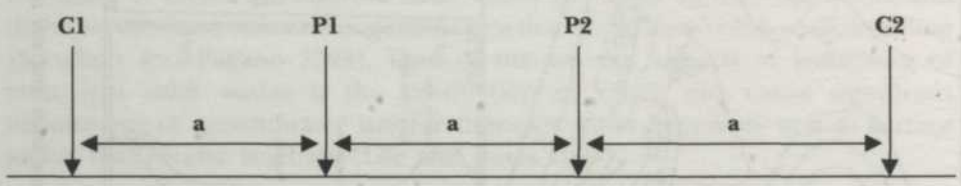

Fig. 2. Electrode configuration (Wenner Array)
(a, is the electrode spacing), (C1, C2 current electrodes, and P1, P2 potential electrodes)

Resistance values were converted into apparent resistivity values ρ_a using the equation: $\rho_a = 2\pi$ a R, where a, is the spacing used in the measurement, R, is the resistance of the ground recorded by McOhm OYO Resistivity Meter. The x position of measurement along the resistivity traverse, the electrode spacing and the calculated apparent resistivity values were entered into the data files which were subsequently used by the RES2DINV program. The interpretation program essentially calculate the true resistivity and true depth of the ground from the inputted data file using Jacobian Matrix Calculation and Forward Modelling procedures. The results of the interpretation are displayed as the 2-D electrical resistivity image of the subsurface along the line of traverse.

The groundwater elevations from the three bore holes at the landfill were determined to be 30.72, 41.58 and 24.04 m for the upstream (AH1), landfill bore hole (AH3), and the downstream bore hole (AH2) respectively. From these groundwater elevations the groundwater flow direction was estimated towards the downstream area of the landfill.

The ground and surface water sampling was done for six months in the period from August 1998 to January 1999.

The groundwater chemistry was determined by sampling the bore holes located in the upstream and downstream areas of the landfill using an electric pump. Surface water samples were collected from the middle of the river. The water samples were collected from the bore holes and the river and stored in 1-liter polyethylene plastic bottle containers. The collected samples were then kept in an ice-box and sent to the laboratory for preservation and chemical analysis. They were preserved under the temperature of 4° C and acidified with concentrated hydrochloric acid to a pH below 2.0 to minimize precipitation

and adsorption on the walls of the container (APHA-AWWA-WEF 1985). The analysis were carried out for in-situ parameters examined in the field and laboratory analysis. In-situ parameters include pH, temperature, and electrical conductivity. These parameters were determined using pH meter with glass electrode, Thermister probe (YSI 58), and Digital TLC meter respectively. The parameters examined in the laboratory include the major cations, namely Na, K, Ca, and Mg and heavy metals. The analytical technique used for their determination was Atomic Optical Emission Spectroscopy using Induced Couple Plasma (ICP-2000) Spectrometer. Major anions namely, Cl, SO_4,and NO_3 were determined using Ion Chromatographic technique, and chromatography was performed on Alltech Chromatograph.

Heavy metals in soils were determined by sampling auger holes constructed in the upstream (Site A), downstream (Site C) and within the landfill site itself (Site C) and drilled to a depth of 150 m in the soil vadose zone. They were detected with aqua regia (X:Y) ratio. The ions in the solution were determined using atomic absorption spectrophotometer (Perkin-Elmer, 5100 PC, Perkin Elmer).

Statistical Analysis

Analysis of variance (ANOVA) of the ground and surface water data, and also for soil data collected in this study was performed using a randomized block design (RCB) by the MSTAT (MSTAT-C, Michigan State University) statistical package, and the mean values were compared by Duncanís New Multiple Range Test (DMRT) at 5% level of significance.

RESULTS AND DISCUSSION

The electrical resistivity images of these two lines were discussed and compared to those resistivity values obtained from the laboratory measurements for the landfill material and other earth materials (Table 1).

TABLE 1
Electrical resistivity of earth materials (mean ± standard deviation)

Sampled Materials	Resistivity (Ohm-m)
Leachate only collected from the landfill	2.99 ± 0.002
Sand saturated with leachate from the landfill area	5 ± 0.04
Fresh waste (plant materials, rubber strands, sand) saturated with leachate	3.51 ± 0.6
Soil saturated with leachate	3.74 ± 0.25
Rain water only	73.82 ± 0.13
Sand saturated with rain water	15.93 ± 1.57
Fresh waste (plant materials, rubber strands, sand) saturated with rain water	20.92 ± 1.43
Soil saturated with rain water	9.98 ± 0.64
Clay saturated with brackish water (Pulau Burung, Nibong Tebal, Southern Seberang Perai)	0.16 ± 0.04

Line L-L$_1$: This line is located on the top of the landfill in the central part with a total length of 250 m and total number of datum points 392 (*Fig. 1*). The most prominent feature in the resistivity image of this line (*Fig. 3*), is the presence of three low resistivity zones of decomposed waste body saturated with highly conductive leachate. The large zone found at a distance of 145-175 m from the base point (first electrode position) on the right part of the resistivity image. It is situated between a depth of about 10 to 25 m from the top surface with a thickness of about 15 m. The other two small zones were found on the left side of the resistivity image approximately situated on the same depth and at about 90 m from the base point. The decomposition of the waste materials decrease as we move away and around these zones. There are relatively higher resistivity materials reaching up to 20 Ωm probably composed of soil and sand saturated with leachate beside fresh waste materials (plant materials, rubber strands and sand) saturated with leachate and rain water. The bed rock is represented by the high resistivity materials greater than 100 Ωm on the bottom of the section at a depth of about 38 m from the top of the landfill. There is a narrow thin layer of high resistivity on the top surface interpreted as a dry layer of weathered materials and hard rocks with sand materials. These materials were brought about for the process of beautification of the landfill for the Commonwealth Games held at Bukit Jalil in September 1998.

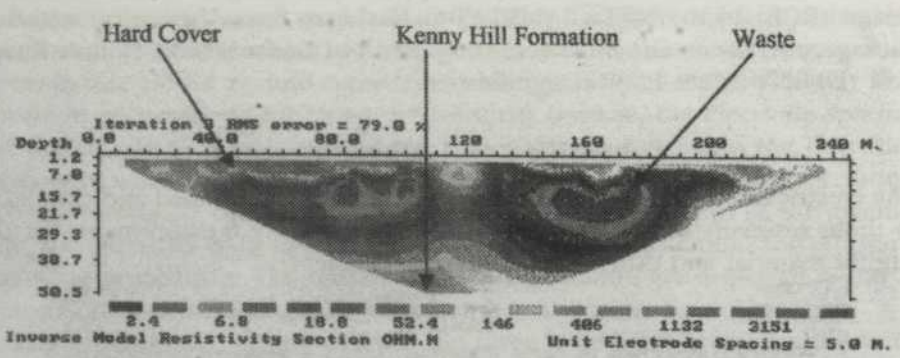

Fig. 3. Resistivity image along Line L-L$_1$

Line L-L$_2$: This line has a length of 300 m and total number of datum points equal 552 and trending east-west direction. It was conducted just to the south of Sungai Kuyoh river (*Fig. 1*). The most prominent feature in its resistivity image *Fig. 4*, is the lateral discontinuities in resistivity where there were two highly resistive zones of more than 100 Ωm at the bottom left and upper right parts of the image. The middle part of the image and the top right are low resistive zones of less than 60 Ωm probably representing the aquifer materials of sandstone and clay materials of Kenny Hill Formation. Within the wide low resistivity zone there are small scattered low resistivity zones which possess low resistivity of less than 30 Ωm. These zones are probably clay lenses or saline water zones due to the effect of high chloride in the downstream area which

is probably released from the waste body during the acidic phase of the landfill development (Arneth *et al* 1989). The lateral discontinuities of high-low-high resistivity as we move from the left bottom to the upper right of the image may reflect a structural, faulting, rock facies changes or differences in porosities (Brown 1987).

GROUNDWATER POLLUTION

The groundwater pollution was detected from the elevated values of EC, Na, K and Cl in the groundwater of the downstream bore hole (Table 2). These values were exceeding the values set by WHO (1984) for drinking water. No guideline values set for K. These elevated values can be related to the movement of leachate towards the downstream direction following the direction of groundwater movement. This movement was facilitated by the high difference in topography between the landfill and the surrounding ground and surface water bodies.

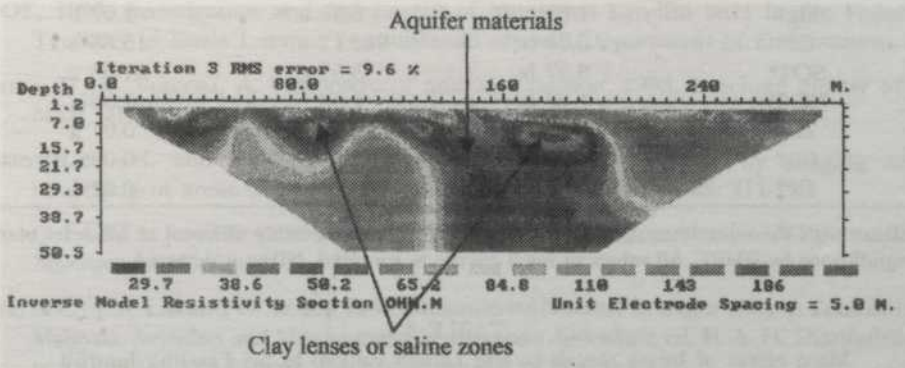

Fig. 4. Resistivity image along Line L-L$_2$

Ca and Mg ions were also higher in the groundwater of the downstream bore hole. The high values of these ions in the downstream is probably due to the release of contaminants during the acidic phase of the landfill development (Arneth *et al,* 1989). The landfill now in its methanogenic phase due to alkaline pH downstream (Fatta *et al.* 1998). No sign of heavy metal pollution in the ground and surface water since the values of Zn, Cu, and Cr were below the permissible levels of the WHO (1984) and below the Malaysia standards set for drinking water (Ministry of Health 1983).

SOIL POLLUTION

Based on statistical analysis the soil heavy metal concentrations in the area were within the normal range and did not reflect any sign of soil pollution by heavy metals (Table 3). The concentrations of Cu, Zn, and Pb were significantly higher in soil samples from the downstream while Ni, and Cd were showing

variable concentrations in different sites. The concentrations of Cu, Zn, and Ni were within the range of background levels in different soil series as reported by Lee *et al.* (1992), while the concentrations of Pb and Cd were below the levels in Kuala Lumpur soils and streetdust which were 895 mg/kg and 2466 mg/kg for Pb and 2.38 mg/kg and 2.96 mg/kg for Cd as reported by Ramlan and Badri (1989).

TABLE 2
Chemical composition of groundwater and surface water

Parameter	Upstream	Downstream	River water
pH* (Standard units)	5.58 c	8.05 a	7.37 b
Temperature* (°C)	29.92 b	31.88 ab	33.82 a
Conductivity* (mS/cm)	0.11 b	7.16 a	0.41 b
Na*	3.97 b	438.51 a	13.02 b
K*	3.20 b	383.45 a	6.52 b
Ca*	9.52 b	31.32 a	31.07 a
Mg*	1.62 c	8.53 a	2.67 b
Cl*	6.06 b	983.12 a	15.68 b
SO4*	8.37 b	3.57 c	21.05 a
NO3*	1.67 b	1.38 b	7.56 a
Zn*	0.014 a	0.015 a	0.01 a
Cu*	0.003 b	0.012 a	0.005 b
Cr*	0.002 b	0.01 a	0.01 a

* Means with the same letter (s) along each row are not significantly different at 5% level of significance by DMRT. All values in mg/l except as specified, ND, not detected.

TABLE 3
Main effect of heavy metals in soil (mean values) at Sri Petaling landfill (concentrations in mg/Kg soil)

Parameter	Site A	Site B	Site C
Cu*	1.83 b	5.52 a	6.49 a
Cd*	0.92 b	1.07 a	1.01 a
Zn*	3.97 c	8.02 b	20.44 a
Cr*	12.61 a	9.92 b	5.71 c
Pb*	5.79 ab	3.42 b	7.67 a
Ni*	2.89 a	2.2 b	2.38 ab

(* Means with different subscripts in the same row are significantly different at 5% level of significance by Duncan Multiple Range Test (DMRT).

CONCLUSION

There are three low resistivity zones of highly conductive leachate within the main body of the landfill. The leachate migrated towards the downstream areas of the landfill following the direction of groundwater movement. The leachate was detected in the groundwater of the downstream bore hole by the elevated

values of Na, K, Cl and EC. The high values of resistivity in the resistivity image of line $L\text{-}L_2$ suggest that the leachate did not affected the area south of Sungai Kuyoh river. This also suggests that the leachate did not migrated south of the river. The concentrations of heavy metals in soil samples from the landfill area did not show any sign of inorganic pollution.

REFERENCES

APHA-AWWA-WEF, 1985. *Standard Methods for the Examination of Water and Waste Water.* 19th ed. Washington D.C.

Arneth, J-D, G. Milde, H. Kerndorff, R. Schleyer, 1989. Waste deposit influences on groundwater quality as a tool for waste type and site selection for final storage quality. In *The Landfill- Reactor and Final Storage*, ed. P Baccini. Lecture notes in earth Sciences 20, p. 399-415. Berlin: Springer Verlag.

Brown, C. E. 1987. Modeling and analysis of direct-current electrical resistivity in the Durham Triassic Basin, North Carolina, *J. of Geoexploration* **24**: 429-440.

DOE, 1999. Investigation and Assessment of Municipal Landfill Sites in the Federal Territory of Kuala Lumpur (unpublished report). Department of Environment.

Fatta, D., C. Voscosa, A, Papadopoulos and M. Loizidou. 1998. Laechate quality of a MSW landfill. *J. of Environ. Sci. and Health* **A33 (5):** 749-763.

Griffith, D. H. and R. D. Barker. 1993. Two-dimensional resistivity imaging and modelling in areas of complex geology: *J. Applied Geophysics* **29**: 211-226.

Lee, G. F. and A. Jones-Lee. 1996. Landfill leachate management: overview of issues. *MSW Management* **(6):** 18-23.

Lee, S. C., J. S. Lim and O. Wahid 1992. Miconutrients status in major soils in Peninsular Malaysia. *Secondary and Micronutrients in Malaysian Agriculture*, ed. H. A. H. Sharifuddin, p. 131-148. Kuala lumpur: Malaysian Society of Soil Science.

Loke, M. H. and R. D. Barker. 1996. Rapid least-squares inversion of apparent resistivity pseudosections by a Quasi-Newton method. *Geophysical Prospecting* **44:** pp 131-152.

Ministry of Health. 1983. National Guidelines for Drinking Water Quality. Kuala Lumpur: Government Printers.

Ramlan, M. N. and M. A. Badri. 1989. Heavy metals in tropical city street dust and roadside soils: A case of kuala Lumpur, Malaysia. Environ. *Technol. Lett.* **10:** 435-444.

Rogers, R. B. and W. F. Kean. 1980. Monitoring groundwater contamination at a fly ash disposal site using surface electrical resistivity methods: *Ground Water* **18:** 472-478.

Scrudato, R. J. and J. Pagano. 1994. Landfill Leachate and Groundwater contamination.í In *Groundwater Contamination and Control*, ed. U. Zolle, p. 169-187, New York: Marcell Dekker, Inc.

Stollar, R. and P. Roux. 1975. Earth resistivity surveys-a method for defining ground water contamination: *Ground Water* **13:** 145-150.

Urish, D. W. 1983. The practical application of surface electrical resistivity to detection of ground water pollution: *Ground Water* **21:** 144-152.

YEAP, E. B. 1969. Geology of Petaling Jaya-Salak South area, Selangor. Unpublished B.Sc. Thesis, University of Malaya.

YIN, E. H. 1961. Geology and Mineral Resources of the Kuala Lumpur area (unpublished work), Malaya Geological Survey Department.

ZOHDY, A. A. R. 1974. Application of Surface Geophysics to Groundwater Investigations. In *Electrical Methods, Techniques for Water Resource Investigations of the U.S. Geological Survey.*

Pertanika J. Sci. & Technol. 9(2): 207 - 217 (2001)
ISSN: 0128-7680

Shear Strength of Brick Aggregate Web Reinforced Concrete Beams

Md. Hazrat Ali[1]*, M. Monjur Hossain[2], and M. Shamim Z. Bosunia[3]

[1]Assistant Professor, Dept. of Civil Engineering, Bangladesh Institute of Technology (BIT), Chittagong, Bangladesh

[2]Professor, Dept. of Civil Engineering, Bangladesh Institute of Technology (BIT), Khulna, Bangladesh

[3]Professor, Dept. of Civil Engineering, Bangladesh University of Engineering and Technology, Dhaka-1000, Bangladesh

Received: 26 November 1999

ABSTRAK

Kajian ini membincangkan tentang kekuatan ricih alur konkrit agregat batu bata yang diperkukuh dengan jaringan bagi nisbah jarak-kedalaman ricih yang berbeza-beza. Secara sendiri, alur diperkukuh dengan rangkaian keluli yang masing-masing bernisbah ρ_b = 0.0248, 0.0371, dan 0.0495 bagi 14 MPa (2000 psi), 21 MPa (3000 psi), dan 28 MPa (4000 psi), dengan kekuatan ricih 6mm (#2) diameter stirup menegak. Sejumlah 28 alur konkrit yang diperkukuh telah diuji bagi mengkaji kapasiti ricih di bawah bebanan dua-titik. Catatan telah dibuat pada corak-corak rekahan dan jenis-jenis kerosakan semasa alur dihentak. Hasil ujian bagi kekuatan ricih alur telah dibandingkan dengan hasil ujian menggunakan persamaan ACI dan kaedah-kaedah yang dicadangkan oleh para penyelidik lain. Secara umum, kelakuan alur yang diuji bersesuaian dengan persamaan ACI dan juga persamaan-persamaan lain. Didapati kapasiti alur berkurangan dengan peningkatan kadar *a/d* bagi kedua-dua stres keretakan pepenjuru dan stres muktamad.

ABSTRACT

This study deals with the shear strengths of web-reinforced brick aggregate concrete beams for different shear span-depth ratios. The beams were singly reinforced with main steel ratios ρ_b = 0.0248, 0.0371, and 0.0495 for 14 MPa (2000 psi), 21 MPa (3000 psi), and 28 MPa (4000 psi) series, respectively and with shear reinforcement of 6mm (#2) diameter vertical stirrups. A total of twenty-eight reinforced concrete beams were tested to investigate the shear capacities under two-point loading. Crack patterns and types of failures during crushing of beams were recorded. The test results for ultimate shear strengths of beams were compared with results using the ACI equation and with methods proposed by other researchers. The behavior of the test beams in general, agreed well with the ACI equation and other equations. It is found that shear capacity decreases with increasing *a/d* ratio for both diagonal cracking stress and ultimate stress.

Keywords: concrete beams, two-point loading, shear span-depth ratio, type of failure, ultimate shear strength

INTRODUCTION

Reinforced concrete beams are part and parcel of buildings and foundations. With the robust growth of construction work in many Southeast Asian countries, beam design is a subject of considerable relevance. The strength of concrete is strongly related to the phenomenon of primary fissure propagation, always present in the concrete bulk, as a result of concrete setting. Inevitable defects and non-homogeneity occurring in the concrete structure produce stress concentration. In regions of highest stress concentration, the initiation of cracks leads to their propagation and consequently ultimate failure of the structure (Prokopski 1993).

Gravel and crushed rock are generally used as course aggregate in concrete construction. Since gravel and crushed rock are not sufficient to meet the construction demands in Bangladesh and are more costly, crushed first class burnt brick of 25mm-downgrade size, locally called khoa, is used. In Bangladesh, about 90% of concrete construction works are done using khoa and its usage is also popular in India and Pakistan. Since the present code provisions followed in Bangladesh are prepared on the basis of study on conventional coarse aggregate concrete in general, the present work might play a role in future code formulation and/or its modification.

The shear strength of structural elements, especially in concrete beams, is an important factor to be considered in design. If not carefully designed, shear cracks may initiate and propagate, causing unexpected ultimate failure of structures. Vertical stirrups have been commonly used as shear reinforcement for a long time and a considerable number of experimental data on the shear strength of beams with variety of stirrup type, size, and spacing are available (Habibullah 1967; and Shamim-uz-Zaman 1986). However, its effectiveness with regards to the shear span-depth ratio of brick aggregate concrete beams has not yet been studied, and indeed, no consideration has been given in the existing code. This study deals with the shear capacity of brick aggregate web-reinforced simply supported rectangular concrete beams with varying shear span-depth ratios.

MATERIALS AND METHODS

Ordinary Portland cement was used in the construction of the test specimens. The specific gravity, normal consistency, initial and final setting time of cement were found to be 3.15, 26.38%, 1h 13.5min, and 5h 30min, respectively.

The fine aggregate was taken from Bangladesh Institute of Technology (BIT), Khulna stack and the coarse aggregate was the 25mm downgrade size khoa. The physical properties of coarse and fine aggregates, namely, the fineness modulus (F.M.); loose unit weight (kN/m^3); compacted unit weight (kN/m^3); absorption capacity (%); and bulk specific gravity (saturated surface dry, SSD condition); were obtained to be 6.75 and 2.56; 13.12 and 10.59; 14.20 and 15.52; 6.67 and 1.09; and 2.08 and 2.64; respectively. Detail of the concrete mix designs using the ACI method is shown in Table 1. The beams were

TABLE 1
Details of concrete mix design by the ACI method

Design strength f_c' (MPa)	Ratio by weight (Cement:Sand:Stone:Water)	Ratio by volume (Cement:Sand:Stone:Water)	Density of concrete (kN/m3)	Entrapped air (%)
14	1 : 2.37 : 5.14 : 0.82	1 : 2.81 : 7.76 : 2.58	19.79	2.5
21	1 : 1.79 : 4.26 : 0.68	1 : 2.05 : 6.20 : 2.06	19.78	2.5
28	1 : 1.36 : 3.67 : 0.57	1 : 1.55 : 5.20 : 1.73	19.84	2.5

TABLE 2
Design details of beams

Beam size	f_c (MPa)	f_y (MPa)	Steel ratio ρ_b	Main reinforcement detail		Stirrup detail		$V_{c(allow)}$ (kN)	V_s (kN)	Total design shear $V_n = V_c + V_s$ (kN)
				Top	Bottom	Size (mm)	c/c Spacing (mm)			
927 × 102 × 203*mm*	14	276	0.025	One 10mm dia. bar	One 22mm dia. bar	6	76	9.56	17.47	27.03
2134 × 102 × 203*mm*	14	276	0.025	One 10mm dia. bar	One 22mm dia. bar	6	76	9.56	17.47	27.03
927 × 102 × 203*mm*	21	276	0.037	One 10mm dia. bar	One 29mm dia. bar	6	76	11.70	17.47	29.17
2134 × 102 × 203*mm*	21	276	0.037	One 10mm dia. bar	One 29mm dia. bar	6	76	11.70	17.47	29.17
927 × 102 × 203*mm*	28	276	0.050	One 10mm dia. bar	One 32mm dia. bar	6	76	13.52	17.47	30.99
2134 × 102 × 203*mm*	28	276	0.050	One 10mm dia. bar	One 32mm dia. bar	6	76	13.52	17.47	30.99

designed by Ultimate Strength Design (USD) method and 6mm (#2) diameter stirrup with design nominal spacing of center to center was used (Table 2). Two sizes of beams, namely, 927 × 102 × 203*mm* (36.5" × 4" × 8"), and 2134 × 102 × 203*mm* (84" × 4" × 8") with mild steel plate anchored at both ends and standard cylinders for each concrete mix design, were constructed. The cylinders and beams were cured for 28 days prior to testing whence the following investigations were carried out:

(a) Tests for design compressive strengths; six specimens for each design mix were tested. Paskova and Meyer (1994) reported that an optimum of five specimen readings is best suited for averaging purposes,
(b) Tests of beams under two-point loading for varying shear span-depth ratios, and
(c) Comparison of shear capacity with the ACI equation and with several other proposed equations.

Experimental failure ultimate and diagonal cracking stresses were compared with predictions using the ACI equation, Bresler and Scordelis formula, Clark formula, and Zsutty equation. The relevant equations are listed in the following as Eq. (1) through Eq. (7). The Zsutty's equations are in SI systems, while the other equations for V_c and V_s are in F.P.S. systems. Probably, the best known equations for and are the ACI Eqs. (2) and (3). Using dimensional analysis and statistics, Zsutty proposed Eq. (5) for computing V_c of ordinary beams, and Eq. (6) for deep beams. The ACI equation, and Zsutty equation, impose a separation in the shear strength of reinforced beams by splitting the shear contribution into two parts, namely, v_c (shear contribution by concrete) and v_s (shear contribution by web reinforcement), while the other equations (Clark, Bresler and Scordelis) take account of the composite action of v_c and v_s.

The ACI's code equations (1995)

$$V_c = \left(1.9\sqrt{f_c'} + 2500\rho_w \frac{V_u d}{M_u}\right) b_w d \quad \text{but } \frac{V_u d}{M_u} \le 1.0$$

$$V_c \le 3.5\sqrt{f_c'} b_w d \quad \text{or } V_c = 2\sqrt{f_c'} b_w d \tag{1}$$

$$V_s = \frac{A_v f_y d}{s} \qquad V_n = (V_c + V_s) \le 8\sqrt{f_c'} b_w d \tag{2}$$

Bresler and Scordelis's (1963) formula

$$V_u = \left(1.9\sqrt{f_c'} + 2500\rho \frac{Vd}{M} + rf_y\right) bd$$

or (3)

$$V = \left(2\sqrt{f_c'} + rf_y\right) bd$$

Clark's (1951) equation

$$V_u = 7000\rho + 0.12 f_c' \frac{d}{a} + 2500\sqrt{r} \tag{4}$$

Zsutty's (1968, 1971) equations

$$V_c = \left[2.174\left(\frac{f_c'\rho d}{a}\right)^{1/3}\right]bd \tag{5}$$

$$V_c = \left(\frac{2.5}{a/d}\right)\left[2.174\left(\frac{f_c'\rho d}{a}\right)^{1/2}\right]bd \tag{6}$$

$$V_s = \frac{A_v f_{yv} d}{s_v} \tag{7}$$

RESULTS AND DISCUSSION

At different stages of loading, different types of cracks were formed at different locations. Typical flexural cracks generally appeared first in the pure bending zone, followed by flexural and/or diagonal tension cracks in the shear span at increased loading. Diagonal tension cracks generally occur at the middle third of the overall depth above the bottom face of the beam, extending simultaneously toward the loading and support points. In general, for all beams, fine vertical flexural cracks are formed first, usually in the mid-span regions. On further loading increment, diagonal cracks occurred independently near the middle of the shear spans, crossing the mid-depth of the beam instantly. The flexural cracks, which occurred earlier, then stabilized and stopped propagating. Inclined cracks formed in the shear span widen and progress in the load-support direction until ultimate failure took place. *Fig. 1* illustrates the typical cracking pattern of the test beam under loading. The behavior of test beams, in general, agreed well with reported results (ACI equation 1995; Bresler and Scordelis 1963; Clark 1951; and Zsutty 1968 & 1971). The test results and cracking loads, including the mode of failure for beams of different concrete compressive strengths are shown in Table 3. Critical diagonal tension cracks appeared at an average loads equal to 78%, 76%, and 81% of ultimate loads for 14 MPa, 21 MPa, and 28 MPa, respectively. The beams exhibited considerable reserve strength after diagonal cracking. In conventional concrete and deep beams, Tan et al. (1995) reported that the diagonal cracking strength is between 20

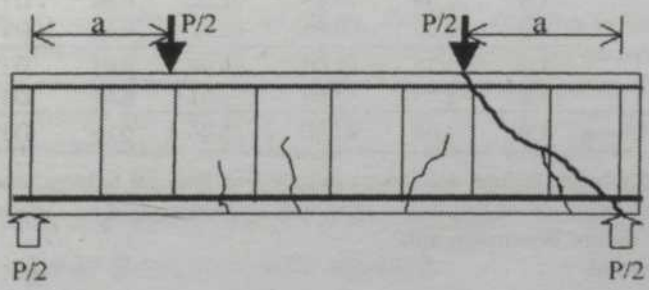

Fig. 1. Typical cracking pattern of beams under two-point loading

TABLE 3
Test results and cracking patterns for beams with different concrete compressive strengths

Beam size	Beam ID	a/d ratio	Diagonal tension cracking load, P_c (KN)	Ultimate load, P_u (kN)	Ratio P_c/P_u	Failure mode	Remarks
Test data for 14 MPa web-reinforced concrete beams							
927 × 102 × 203*mm*	A1	1.50	63.64	85.66	0.74	DT	L
	A2	1.50	54.29	70.31	0.77	DT	L
	A3	1.50	53.84	63.64	0.85	DT	L
	A4	2.50	44.50	66.75	0.67	DT	L
	A5	2.50	51.20	61.19	0.84	DT	L
	A6	2.50	59.63	68.09	0.88	DT	L
	A7	2.75	44.50	53.40	0.83	DT	L
	A8	2.75	42.28	48.95	0.86	DT	L
2134 × 102 × 203*mm*	A9	4.00	22.25	37.82	0.59	**	F
Test data for 21 MPa web-reinforced concrete beams							
927 × 102 × 203*mm*	B1	1.50	61.41	82.33	0.75	DT	L
	B2	1.50	66.76	95.23	0.70	**	F
	B3	1.50	74.32	97.90	0.76	DT	L
	B4	2.50	63.19	73.87	0.86	DT	L
	B5	2.50	63.64	84.11	0.76	DT	L
	B6	2.50	67.64	80.99	0.84	DT	L
	B7	2.75	50.73	72.09	0.70	DT	L
	B8	2.75	57.86	76.54	0.76	DT	F
	B9	2.75	50.73	60.08	0.84	DT	L
2134 × 102 × 203*mm*	B10	4.00	42.27	64.97	0.65	**	F
Test data for 28 MPa web-reinforced concrete beams							
927 × 102 × 203*mm*	C1	1.50	57.85	73.43	0.79	DT	L
	C2	1.50	51.17	69.42	0.74	DT	L
	C3	1.50	73.78	92.56	0.80	DT	L
	C4	2.50	50.29	66.75	0.75	DT	L
	C5	2.50	73.43	91.22	0.80	DT	L
	C6	2.50	69.86	82.32	0.85	DT	L
	C7	2.75	52.00	56.96	0.91	DT	L
	C8	2.75	44.50	54.51	0.82	DT	L
2134 × 102 × 203*mm*	C9	4.00	44.50	53.40	0.83	DT	L

DT = Diagonal tension failure dominant, initiated by flexural tension cracks,
L = Failure of concrete at the top of diagonal tension cracks, i.e., shear failure,
F = Flexural failure dominant, and
** = Not recorded.

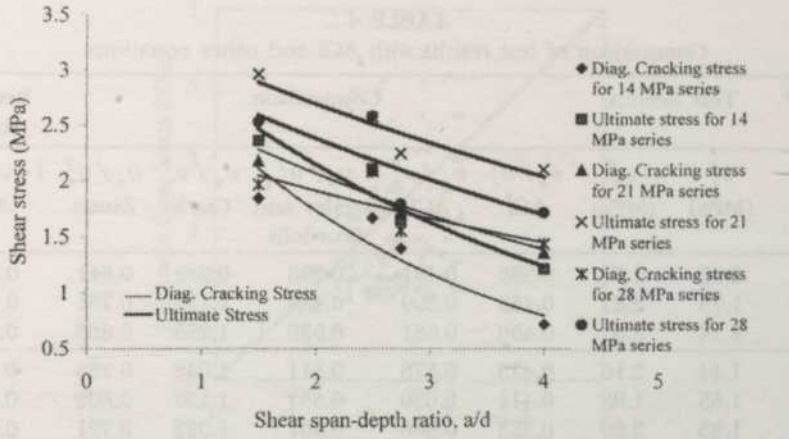

Fig. 2. Ultimate and diagonal cracking stresses with varying shear span-depth ratio

and 35 percent of the ultimate shear strength. The higher test P_c/P_u values recorded in this study are mainly due to the higher tensile capacity of brick aggregate concrete. Shamim-uz-Zaman (1986) also observed higher tensile capacity of brick aggregate concrete. It is also observed that with increasing *a/d* ratio, the failure modes were mixed, with flexure becoming more dominant. Beams A7, B8, and B10 resulted in ultimate flexure failures (Table 3).

The variations in diagonal cracking and ultimate stresses with increasing *a/d* ratio are shown in *Fig. 2*. The variation in v_c^T with increasing *a/d* is small, except for the 14 MPa series. In deed, if extrapolations are allowed, both v_u^T and v_c^T will converge at higher *a/d* (*Fig. 2*). This makes sense that with increasing *a/d* ratio, flexural failure dominates and formation of diagonal cracks would lead to ultimate beam failure.

The test results were compared with four design methods as shown in Table 4 and *Fig. 3*. The ratio v_n/v_u^T, where v_n is the calculated ultimate stress using the proposed equations and v_u^T the measured ultimate stress, is an indication of the agreement between the two stresses. Points those fall below the 45° line, i.e., line, i.e., $v_n = v_u^T$ line (*Fig. 3*), are conservative and those above are non-conservative, i.e., overestimated. Although, the ACI equation is the best known among the other equations, it is found that the Bresler and Scordelis equation has the lowest standard deviation of 0.128 (Table 4) amongst the four methods, and the predictions are the most conservative. In the order from lowest to highest standard deviations, as well as in the ranking from highest to lowest in terms of conservative results are the Bresler and Scordelis, ACI, Zsutty, and Clark equations, respectively. Using the ACI equation, the relative v_n/v_c^T and the reserve capacity $\left(1-v_n/v_u^T\right)$ were obtained.

TABLE 4
Comparison of test results with ACI and other equations

Beam*	Test Results		Comparison					Reserve stress
	v_c^T (MPa)	v_n^T (MPa)	v_c/v_c^T ACI	v_n/v_n^T ACI	v_n/v_n^T Bresler and Scordelis	v_n/v_n^T Clark	v_n/v_n^T Zsutty	$1-v_n/v_n^T$ ACI
A1	2.05	2.77	0.386	0.491	0.398	0.932	0.641	0.509
A2	1.75	2.27	0.453	0.599	0.485	1.136	0.781	0.401
A3	1.74	2.05	0.456	0.661	0.536	1.255	0.863	0.339
A4	1.44	2.16	0.473	0.578	0.511	1.042	0.735	0.422
A5	1.65	1.98	0.411	0.630	0.557	1.137	0.802	0.370
A6	1.93	2.20	0.353	0.566	0.501	1.022	0.721	0.434
A7	1.44	1.72	0.462	0.713	0.639	1.276	0.901	0.287
A8	1.36	1.58	0.486	0.778	0.697	1.392	0.982	0.222
A9	0.72	1.22	0.857	0.967	0.902	1.686	1.176	0.033
B1	1.98	2.66	0.528	0.606	0.458	1.346	0.806	0.394
B2	2.16	3.07	0.485	0.524	0.396	1.163	0.697	0.476
B3	2.40	3.16	0.436	0.510	0.385	1.131	0.678	0.490
B4	2.04	2.39	0.429	0.604	0.510	1.293	0.795	0.396
B5	2.05	2.72	0.426	0.531	0.448	1.136	0.698	0.469
B6	2.18	2.61	0.401	0.551	0.466	1.179	0.725	0.449
B7	1.64	2.33	0.520	0.609	0.523	1.296	0.796	0.391
B8	1.87	2.47	0.456	0.574	0.493	1.221	0.750	0.426
B9	1.64	1.94	0.520	0.731	0.628	1.555	0.956	0.269
B10	1.36	2.10	0.571	0.641	0.580	1.338	0.812	0.359
C1	1.87	2.37	0.708	0.797	0.573	2.012	1.073	0.203
C2	1.65	2.24	0.801	0.843	0.606	2.128	1.135	0.157
C3	2.38	2.99	0.555	0.632	0.455	1.596	0.851	0.368
C4	1.62	2.16	0.675	0.771	0.631	1.874	1.037	0.229
C5	2.37	2.95	0.462	0.564	0.462	1.371	0.759	0.436
C6	2.26	2.66	0.486	0.625	0.511	1.519	0.841	0.375
C7	1.68	1.84	0.634	0.886	0.739	2.141	1.187	0.114
C8	1.44	1.76	0.741	0.926	0.772	2.238	1.240	0.074
C9	1.44	1.72	0.673	0.889	0.788	2.104	1.156	0.111
Mean	1.790	2.288	0.530	0.671	0.559	1.447	0.878	0.329
Standard Deviation	0.384	0.481	0.130	0.136	0.128	0.382	0.176	0.136

* The beam notations possess the same design compressive strength, beam size, and *a/d* ratio as in Table 3.

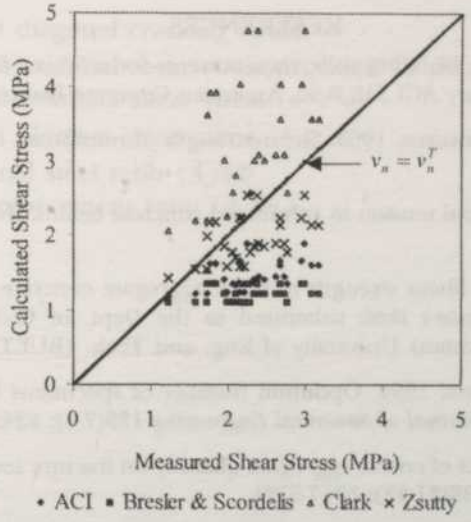

Fig. 3. Comparison of measured ultimate stress with ACI equation and other researchers

CONCLUSIONS

Experimental ultimate and diagonal cracking stresses were compared with predictions using the ACI equation, Bresler and Scordelis formula, Clark formula, and Zsutty equation. The behavior of the test beams in general, agreed well with the reports from other investigators. It is found that the critical diagonal tension crack appeared at an average loads P_c at 78%, 76%, and 81% of the ultimate loads P_u for 14 MPa, 21 MPa, and 28 MPa, respectively. The beams exhibited considerable reserve strength after diagonal cracking. The web shear diagonal tension crack is the dominant type of crack for shear failure. It is observed that with increasing a/d ratio, the failure modes were mixed, with flexure becoming more dominant. Although, the ACI equation is the best-known equation, it is found that the Bresler and Scordelis equation has the lowest standard deviation of 0.128 amongst the four methods, and the predictions are most conservative. It is also found that the shear capacity decreases with increasing a/d ratio for both diagonal cracking stress and ultimate stress.

ACKNOWLEDGEMENTS

The authors would like to acknowledge Bangladesh Institute of Technology (B.I.T.), Khulna, for financial support and technical assistance. The authors are highly grateful to Mr. Sk. Muzakka Zaher and Mr. Sazzad Ahmed for their contribution during this research. Sincere gratitude is due to Prof. Abdus Salim (Civil), BIT, Khulna and Prof. G. M. Habibullah, Director, BIT, Rajshahi, for their valuable suggestions and encouragement.

REFERENCES

ACI COMMITTEE 318 1995. Building code requirements for reinforced concrete (ACI 318-95) and Commentary ACI 318 R-95. American Concrete Institute, Detroit, pp. 369.

BRESLER, B., and A.C. SCORDELIS, 1963. Shear strength of reinforced concrete beams. *ACI Journal* **60:** 51-72.

CLARK, A.P. 1951. Diagonal tension in reinforced concrete beams. *ACI Journal* **23(2):** 145-156.

HABIBULLAH, G.M. 1967. Shear strength of brick aggregate concrete beams without web reinforcement. *Master's thesis* submitted to the Dept. of Civil Eng., Bangladesh (erstwhile East Pakistan) University of Eng. and Tech. (BUET), Dhaka-1000.

PASKOVA, T., and C. MEYER. 1994. Optimum number of specimens for low-cycle fatigue tests of concrete. *Journal of Structural Engineering* **120(7-9)**: 2242-2247.

PROKOPSKI, G. 1993. Effect of coarse aggregate quantity on fracture toughness of concrete. *J. Materials Science* **28(21-22):** 5717-5721.

SHAMIM-UZ-ZAMAN, M. 1986. Use of crushed brick aggregates in concrete construction. In *The Asia-pacific Concrete Technology Conference Proceedings*, p. 6.1-6.13, Jakarta, Indonesia.

TAN, K.H., F.K. KONG, S. TENG, and L. GUAN, 1995. High-strength concrete deep beams with effective span and shear span variations. *ACI Structural Journal* **92(4):** 395-405.

ZSUTTY, T.C. 1968. Beam shear strength prediction analysis of existing data. *ACI Journal* **65(11):** 943-951.

ZSUTTY, T.C. 1971. Shear strength prediction for separate categories of simple beam tests. *ACI Journal* **68(2):** 138-143.

NOTATIONS

a = shear span measured from center of support to center of loading point
A_s = area of longitudinal reinforcing bars on flexural tension side of beam
A_v = area of shear reinforcement
b_w, b = width of beam
d = effective depth (distance from extreme compression fiber to centroid of longitudinal tension reinforcement
f'_c = specified concrete compressive strength
f_y = yield strength of reinforcement
f_v, f_{yv} = Yield strength of vertical reinforcement
M, M_u = ultimate moment taken as positive
P_c = initial diagonal tension cracking load
P_u = ultimate failure load
r = Ratio of web-reinforcement (A_v/bs)
s, s_v = spacing of shear reinforcement
V, V_u = ultimate shear taken as positive
v_c = calculated nominal shear stress provided by concrete

v_c^T = measured diagonal cracking stress
v_s = calculated nominal shear stress provided by shear reinforcement
v_n = calculated nominal shear stress $(v_c + v_s)$
v_n^T = measured ultimate shear stress
ρ_w, ρ = longitudinal steel ratio (A_s/bd)
ρ_v, ρ_{yv} = shear reinforcement ratio (A_v/bs_v)

Pertanika J. Sci. & Technol. 9(2): 219 - 227 (2001)
ISSN: 0128-7680

Piezoelectric and Photoacoustic Detection for Power Meter Measurement

C.Y.J. Fanny, W.M. Mat Yunus and M.M. Moksin
Department of Physics
Faculty of Science and Environmental Studies
Universiti Putra Malaysia
43400 UPM Serdang, Selangor, Malaysia

Received: 8 June 2000

ABSTRAK

Teknik piezoelektrik dan gas-mikrofon yang berasaskan kesan fotoakustik ditunjukkan untuk mengkaji kuasa alur laser dalam julat (2-16) mW. Dalam setiap kes, isyarat akustik didapati berkadar terus dengan kuasa laser sehingga 16 mW. Tindakan kuasa meter bagi teknik fotoakustik sel tertutup didapati lebih sensitif terhadap perubahan modulasi frekuensi daripada teknik fotoakustik sel terbuka bagi frekuensi, f < 110 Hz. Akan tetapi, kedua-dua teknik mempunyai tindakan kuasa meter yang hampir sama selepas 110 Hz. Bagi teknik piezoelektrik, pergantungan nisbah isyarat-kuasa terhadap modulasi frekuensi adalah sama dalam kedua-dua kes filem perak dan kepingan brass.

ABSTRACT

The piezoelectric and gas-microphone detection techniques based on the photoacoustic effect in an absorbing material were demonstrated to monitor the laser power in the range of (2-16) mW. In each case, the photoacoustic signals were found to be linear up to the laser power of 16 mW. The power meter responsivity for closed photoacoustic cell detection is more sensitive to frequency changes compared to open photoacoustic cell at chopping frequency, f < 110 Hz. However, both detection exhibited the same signal-to-power ratio after 110 Hz. In piezoelectric detection, the dependence of signal-to-power ratio on chopping frequency is similar for both cases, i.e. silver film and brass disc.

Keywords: laser beam, power meter, photoacoustic detection, piezoelectric

INTRODUCTION

In the mid-1970s, variant of absorption spectroscopy was developed which exploited the photothermal effect. It was called photoacoustic spectroscopy because the photothermal heating effect was detected by an indirect acoustic method. Basically, there are three schemes that can be identified for the detection of the thermal waves: acoustic, optical and thermal (cited in Almond and Patel 1996). In this paper focus on the acoustic detection techniques which include the use of a microphone for the detection of pressure variations in photoacoustic cell and a piezoelectric transducer for the detection of thermoelastic waves in solid media. (Satheeshkumar and Vallabhan 1985; Rai *et al.* 1987; Guthrie and Medina 1984).

In this work, a comparison is made between different absorbing material in piezoelectric detection and between open photoacoustic cell (OPC) and closed photoacoustic cell (CPC) detection as a sensitive laser power meter on the principal of the photoacoustic effect. From the previous study, similar experiment had been conducted by Peralta, *et al.* (1988). They measured the cw Argon-ion laser powers up to 1000 mW by using piezoelectric transducer. The PA signal is proportional to the power of the incident beam. In 1996, Cai, et al. demonstrated the use of piezoelectric to detect the PA signal in an enclosed cell. They used a 4 W Argon-ion laser and obtained the same result as done by Peralta *et al.* (1988). In our case, we have carried out a measurement at low laser power (< 16 mW) of argon-ion laser by using piezoelectric, OPC and CPC detections.

METHOD

Piezoelectric Detection

Piezoelectric (PZT) detection is a scheme to detect the thermoelastic waves in the sample resulted by the incident light heating. Applying the PZT-PA theory proposed by Jackson and Amer (1980), the increasing temperature of the sample leads to the expansion of the region illuminated by incident light. The expansion of the heated region causes displacement of the sample surface whose magnitude is proportional to the average temperature gradient in the sample. This displacement is then sensed by the PZT in which converts the stress into a measurable voltage. Expression of this voltage can be described as

$$V \infty M\alpha_t \frac{1}{(pc)_s} \frac{P}{\omega} \tag{1}$$

$\frac{P}{\omega}$ is the energy deposited per cycle, $\frac{1}{(pc)_s}$ converts the energy to a temperature, α_t transforms the temperature rise to a strain and M is a voltage for a given strain. From equation (1), the signal amplitude is proportional to the incident power and therefore PZT is found to be useful as laser power meter.

Fig. 1 shows the schematic of the laser power measurement apparatus. The light source consists of a 150 mW argon-ion (Omnichrome's 543) laser beam which is mechanically chopped and filtered before being focused onto the piezoelectric transducer (Newport product HC524). The laser power output was monitored by a power meter from Control Optics (OPM-9601). The generated photoacoustic signal is detected and analyzed by a lock-in amplifier (SR530). The piezoelectric detector which is used in the experiment consists of a ceramic PZT bonded to the thin brass disc 0.40 mm in thickness and at the other side of the PZT was coated with a thin silver film (*fig. 1*). The laser beam is illuminated on the thin brass disc or the silver film surface which acts as the absorbing material. The measurement has been carried out by monitoring the photoacoustic signal as a function of chopping frequency at various laser power level for both thin brass absorbing disc and silver film.

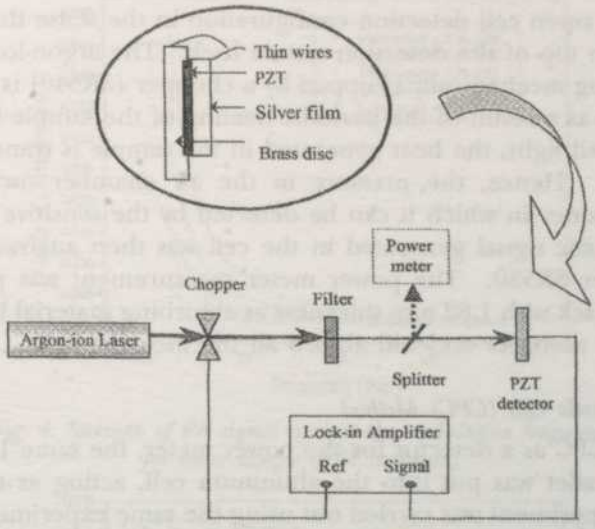

Fig. 1. Experimental set-up for the use of a PZT as a laser power meter

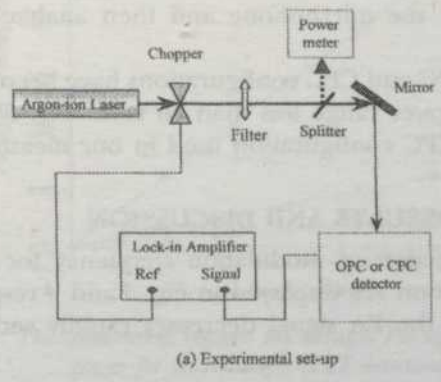

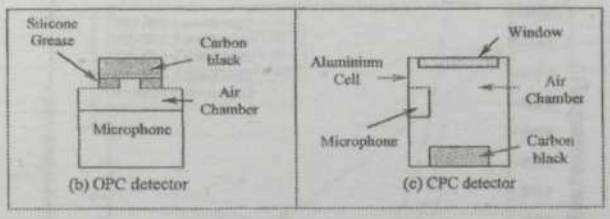

Fig. 2. (a) Experimental set-up for microphone photoacoustic detection, (b) OPC configuration and (c) CPC configuration

Microphone Detection

Open Photoacoustic Cell (OPC) Method

The schematic cross section of the OPC configuration is shown in *Fig. 2(a)*. It consists of mounting the sample directly onto an electret microphone (Cirkit product, UK) with a circular hole of 2 mm diameter by employing vacuum

grease. It is an open cell detection configuration in the sense that the sample is placed on the top of the detection system itself. The argon-ion laser beam, which after being mechanically chopped by a chopper (SR540) is focused onto the sample. As as a result of the periodic heating of the sample by absorption of the modulated light, the heat generated in the sample is transferred to the gas in contact. Hence, the pressure in the air chamber oscillates at the chopping frequency in which it can be detected by the sensitive microphone. The photoacoustic signal generated in the cell was then analyzed by using a lock-in amplifier SR530. The power meter measurement was performed by using carbon black with 1.82 mm thickness as absorbing material because it acts as a black-body absorber and will absorb all the incident light.

Closed Photoacoustic Cell (CPC) Method

When using a CPC as a detector for the power meter, the same 1.82 mm thick carbon black pallet was put into the aluminum cell, acting as the absorbing sample. The experiment was carried out using the same experimental set up as shown in *Fig. 2(a)*. The heat generated in the sample is transferred to the surface of the sample and heated the air in the cell. Again, the photoacoustic signals were detected by the microphone and then analyzed by the lock-in amplifier.

In our work, these OPC and CPC configurations have been used to monitor the laser power in the power range less than 16 mW. *Fig. 2(b)* and *2(c)* show the different OPC and CPC configuration used in our measurement.

RESULTS AND DISCUSSION

The PA signals as a function of modulation frequency for brass and silver samples using PZT detection are displayed in *Fig. 3* and *4* respectively. At low frequencies, $f < 100$ Hz the PA signal decreases rapidly with the increasing

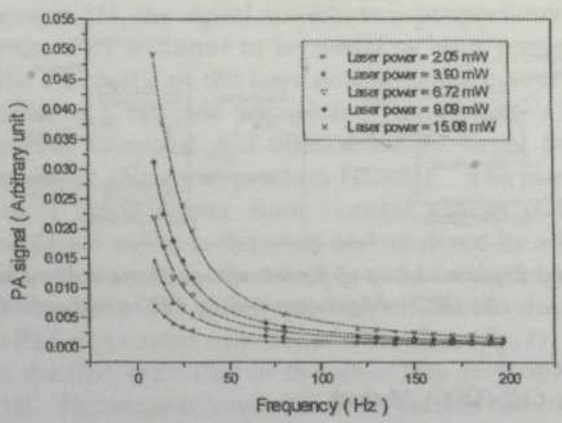

Fig. 3. Strength of PA signal against the modulation frequency for brass sample (PZT detection)

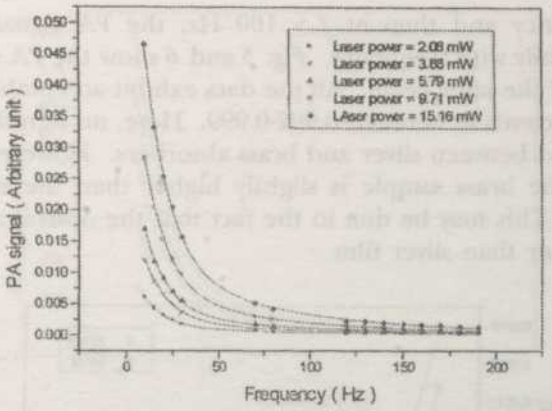

Fig. 4. Strength of PA signal against the modulation frequency for silver sample (PZT detection)

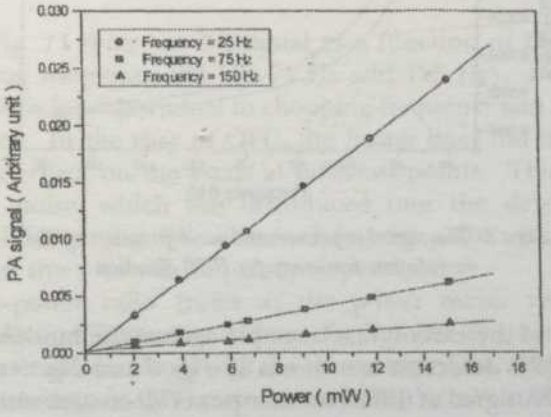

Fig. 5. The relationship between the strength PA signal and laser power for brass sample (PZT detection)

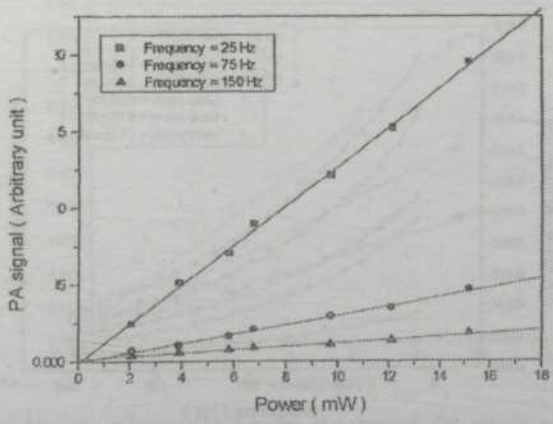

Fig. 6. The relationship between the strength PA signal and laser power for silver sample (PZT detection)

chopping frequency and then at $f > 100$ Hz, the PA signal was observed decreasing gradually with frequency. *Fig. 5* and *6* show the PA signal increases with the power of the laser beam. All the data exhibit acceptable linearity with correlation coefficients in between 0.992-0.999. Here, no significant difference has been observed between silver and brass absorbers. However, the signal-to-power ratio of the brass sample is slightly higher than the silver sample as shown in *Fig. 7*. This may be due to the fact that the optical absorptance for brass disc is higher than silver film.

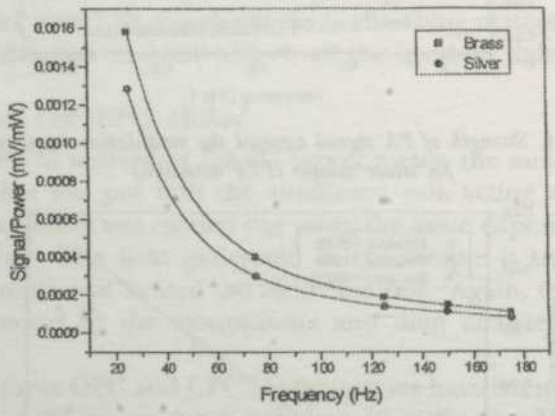

Fig. 7. The signal-to-power ratio as a function of the modulation frequency for PZT detection

The PA signal of the carbon black sample against the modulation frequency using OPC and CPC detection are shown in *Fig. 8* and *Fig. 9* respectively. In both figures, the PA signal at different laser power decreases with the increasing of the chopping frequency. It is noted that the PA signal in CPC detection decreases very rapidly for $f < 70$ Hz.

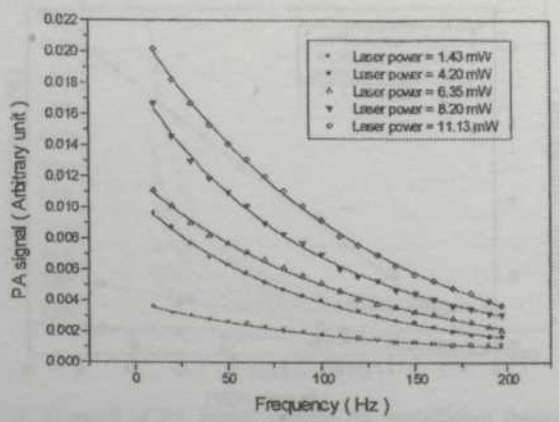

Fig. 8. Strength of PA signal against the modulation frequency for carbon black sample (OPC detection)

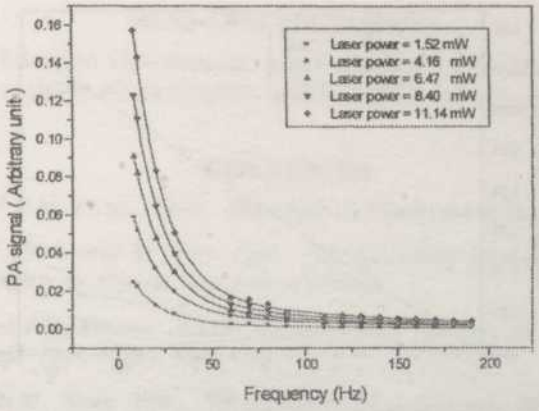

Fig. 9. Strength of PA signal against the modulation frequency for carbon black sample (CPC detection)

Fig. 10 and *Fig. 11* show the PA signal as a function of the laser power at different chopping frequency (25 Hz, 75 Hz and 125 Hz). In both cases, the PA signals are inversely proportional to chopping frequency and are proportional to the laser power. In the case of OPC, the fitting lines did not pass through the origin but intercept on the y-axis at different points. This may be due to the background noise, which was introduced into the detection system at higher gain amplifier setting. We observed that the point where the respective line intercepts on the y axis is frequency dependent.

The signal-to-power ratio (refer as the power meter responsivity) as a function of modulation frequency is shown in *Fig. 12*. The curves showed that the signal-to-power ratio decreases with the increasing of the chopping frequency. The signal-to-power ratio of OPC varied from 5.70 μV/mW at 25 Hz to 0.40 μV/mW at 174 Hz. For CPC detection, the signal-to-power ratio changed from 1.44

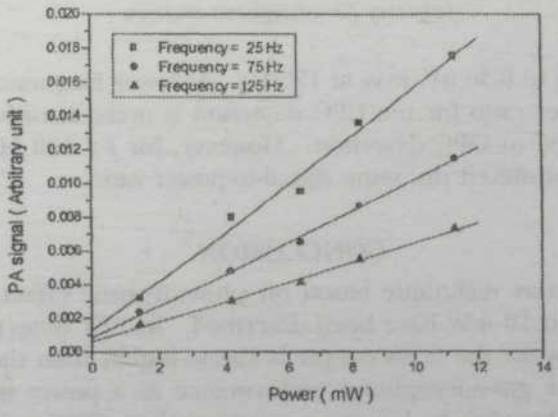

Fig. 10. The relationship between the strength PA signal and laser power for carbon black sample (OPC detection)

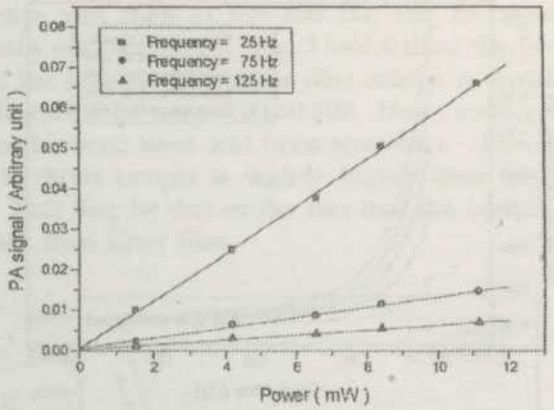

Fig. 11. The relationship between the strength PA signal and laser power for carbon black sample (CPC detection)

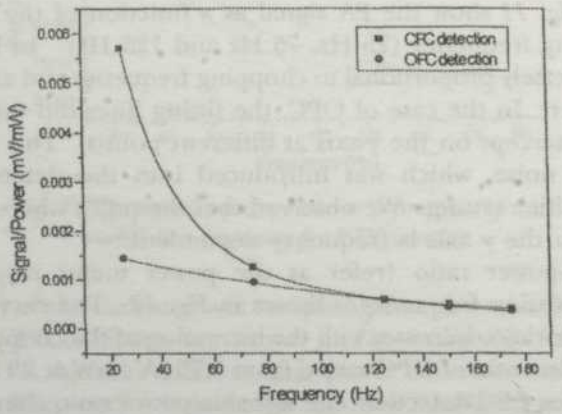

Fig. 12. The signal-to-power ratio as a function of the modulation frequency for microphone detection

μV/mW at 25 Hz to 0.36 μV/mW at 175 Hz. At lower frequencies, $f < 110$ Hz, the signal-to-power ratio for the CPC detection is more sensitive to frequency changes compared to OPC detection. However, for $f > 110$ Hz the CPC and OPC detection exhibited the same signal-to-power ratio.

CONCLUSION

Three power meters technique based on photoacoustic effect for measuring laser power, up to 16 mW have been described. In PZT detection, the power meter responsivity for the brass sample is always higher than the silver sample. In comparing the gas-microphone performance as a power meter, the CPC technique was observed to be more sensitive than OPC technique at low frequency. At high modulation frequency, there is no preference in between OPC and CPC technique.

ACKNOWLEDGEMENTS

We thank the Malaysian Government and Universiti Putra Malaysia for research support through IRPA 09-03-04-0065 and postgraduate Pasca (CYJF).

REFERENCES

ALMOND, D.P. and P.M. PATEL. 1996. *Photothermal Science and Techniques.* UK. Press.

CAI, H.T., P.C.W. FUNG and W. ZHU. 1996. Photoacoustic phenomenon in emulsion solution. *Progress in Natural Science* **6:** s577-s580.

GUTHRIE, R.W. and F.D. MEDINA. 1984. Photoacoustic cell for use as an optical power meter. *J. Appl. Phys.* **57(9):** 4485-4486.

JACKSON, W and N.M. AMER. 1980. Piezoelectric photoacoustic detection: theory and experiment. *J. Appl. Phys.* **51:** 3343-3353.

PERALTA, S.B., H.H. AL-KHAFAJI and A.W. WILLIAMS. 1988. Photoacoustic optical power meter using piezoelectric detection. *J. Phys. E: Sci Instrum.* **21:** 195-196.

RAI, V.N., S.N. THAKUR and D.K. RAI. 1987. A simple laser power meter dependent on photoacoustic effect. *J. Phys. E: Sci Instrum.* **20:** 1472-1476.

SATHEESHKUMAR, M.K. and C.P.G. VALLBHAN. 1980. Use of a photoacoustic cell as a sensitive laser power meter. *J. Phys. E: Sci Instrum.* **18:** 434-436.

Pertanika J. Sci. & Technol. 9(2): 229-235 (2001)
ISSN: 0128-7680

Citric Acid Method for the Preparation of $LiMn_2O_4$ Cathode for Rechargeable Li-ion batteries

M. Amin Idrees[1], M. Hashim[2], Abang Abdullah Abang Ali[3] and W. Mahmood Mat Yunus[4]

Institute of Advanced Technology
Universiti Putra Malaysia
43400 UPM, Serdang, Selangor Darul Ehsan, Malaysia

[4]Department of Physics
Universiti Putra Malaysia
43400 UPM, Serdang, Selangor Darul Ehsan, Malaysia

Received: 17 July 2000

ABSTRAK

$LiMn_2O_4$ berfasa tunggal telah disintesiskan menggunakan kaedah sol-gel dengan asid sitrik sebagai agen pembentukan gel. Keistimewaan kaedah ini adalah keadaan homogen diperolehi daripadda masa rawatan suhu yang lebih singkat, saiz kristal yang lebih kecil, lebih stabil, saiz zarah yang lebih kecil dan morfologi yang lebih baik. Suhu pembentukan $LiMn_2O_4$ diperolehi serendah 242 °C. Kesan keadaan kristal dan kestabilan $LiMn_2O_4$ terhadap rawatan suhu dikaji menggunakan analisis struktur (XRD) dan terma (DTA/TGA). Ketulenan dan morfologi bahan ini dianalisis menggunakan EDAX.

ABSTRACT

Single-phase $LiMn_2O_4$ has been synthesized using a citric acid method from citric acid solution, lithium carbonate solution and manganese nitrate solution. Homogeneous in a less heat treatment time, smaller crystalline size, better stability, smaller particle size and better morphology are the advantages of using this method. The formation temperature of $LiMn_2O_4$ has been found to be as low as 242 °C. The effect on crystallinity and stability of $LiMn_2O_4$ with heat treatment has been studied using structural (XRD) and thermal (DTA/TGA) analysis. The impurity and morphology of this material has been investigated with EDAX.

Keywords: *$LiMn_2O_4$*, sol-gel method, chelating agent, structural (XRD), thermal (DTA/TGA) analysis and EDAX

INTRODUCTION

$LiMO_2$ (M = Co, Mn, Ni) type compounds with layer structures such as $LiCoO_2$ (Dickens *et al.* 1992), $LiMn_2O_4$ (Thackeray 1992) and $LiNiO_2$ (Delmas *et al.* 1995) have been of great interest as cathode material for rechargeable lithium batteries. Enormous interest has been shown in the $LiMn_2O_4$ system in the past few years (Scrosati 1992). $LiMn_2O_4$ material is cheaper than $LiCoO_2$ and $LiNiO_2$, it is easy to produce and less toxic for the environment. In this study, a method has been developed to synthesize lithium manganese oxide directly

using citric acid as chelating agent. This method is simple and inexpensive. By controlling the Li / Mn ratio and the synthesis temperature, single-phase $LiMn_2O_4$ can be obtained.

MATERIALS AND METHODS

Li_2CO_3 (lithium carbonate pure grad BDH) and Mn $(NO_3)_2$. $4H_2O$ (Fluka) with a molar ratio of 1:1 were dissolved in an aqueous solution of citric acid (Fluka). The molar ratio of citric acid to total metal ions was 1.5. The mixture was stirred on a magnetic stirring plate for 3h to ensure that the reagents were uniformly mixed and the homogeneous solution was achieved, and also the complex reaction between Mn^{2+} and citric acid was accomplished. Ammonium hydroxide solution was slowly added until the required pH value of around 5 was achieved. This range of pH controls the formation of metal-

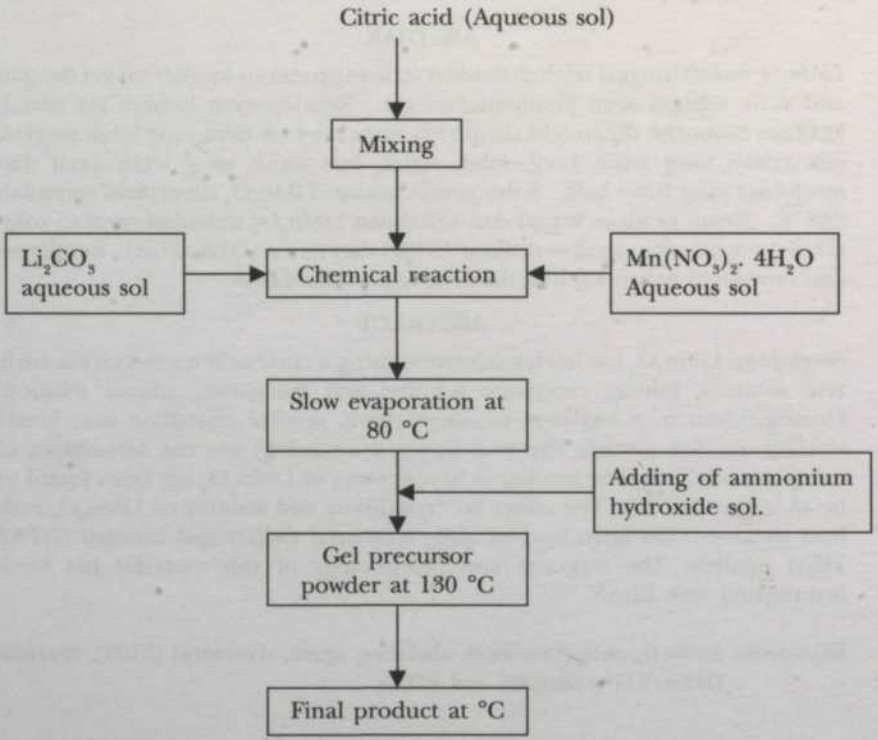

Fig. 1. The flow chart showing the synthesis of $LiMn_2O_4$

acid complex and the dissociation of carbolic acid (In-Hwan *et al.* 1997). The solution was evaporated at 80 °C on a magnetic stirring hot plate until a transparent gel precursor was formed. The precursor was further dried at 130 °C for two hours to obtain the powder mass for DTA and TGA analysis. Further the precursor was kept for decomposition in air at 200 °C until it was fired completely. During this process oxidation reaction takes place and finally the polycrystalline $LiMn_2O_4$ product was obtained.

In order to analyze the material as a host for battery applications, thermal characteristics of the cathode material under study were done by means of differential thermal analysis using Perkin Elmer DTA 7 and thermogravimetric analysis was carried out using Rheometric Scientific TGA 1000. Structural analysis was done using X-ray Diffractometer (XRD, Philips PW 1840). Energy dispersive X-ray analyzer (EDAX) was carried using Philips Model PV 3800, to identify the materials synthesized.

RESULTS AND DISCUSSION

Fig. 2 shows the DTA analysis of $LiMn_2O_4$ precursor complex in the temperature range of 50 °C to 800 °C. An exothermic transformation begins to appear onset at around 242 °C indicating the formation of the compound and this huge exothermic reaction shows the decomposition of organic moieties present in the precursor, which burned in the presence of atmospheric oxygen. The powder under study was self-burning once ignited because the decomposed nitrate ions are oxidizers (Kumar *et al.* 1995). This temperature formation is less than that reported by Barboux *et al.* (1991). The reason for the lower formation temperature might be due to the homogeneous mixing of the materials by constant stirring at low calcination temperature and the suppression

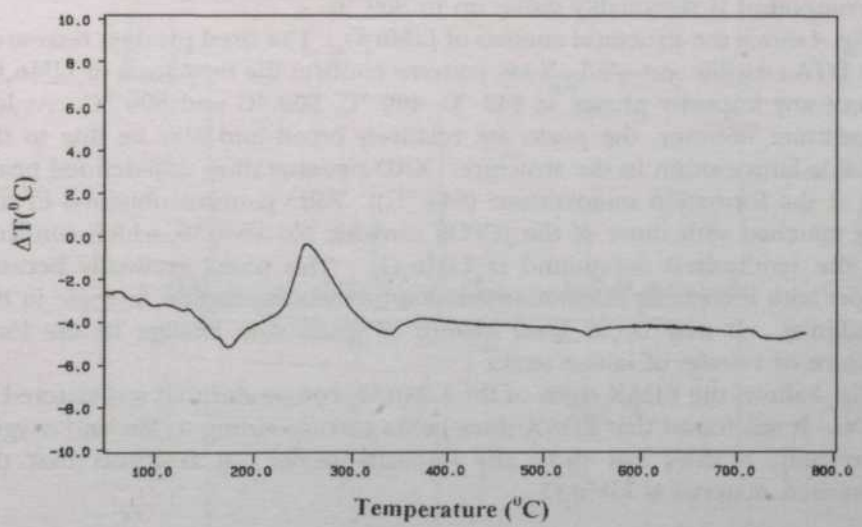

Fig. 2. DTA trace for $LiMn_2O_4$ of the gel precursor at a heating rate of 10 °C m

of the formation of precipitates by the chelating agent. It suggests that the homogeneity of the complex and chemical bond formation is better in citric acid for the preparation of $LiMn_2O_4$. Citric acid also acted as a fuel during the process and hence helps to lower the formation temperature.

Fig. 3 shows a TGA plot of $LiMn_2O_4$ precursor complex. A sharp decrease in mass is observed around 242 °C, which corresponds to the decomposition of the chemicals constituents leading to the formation of the compound. This is

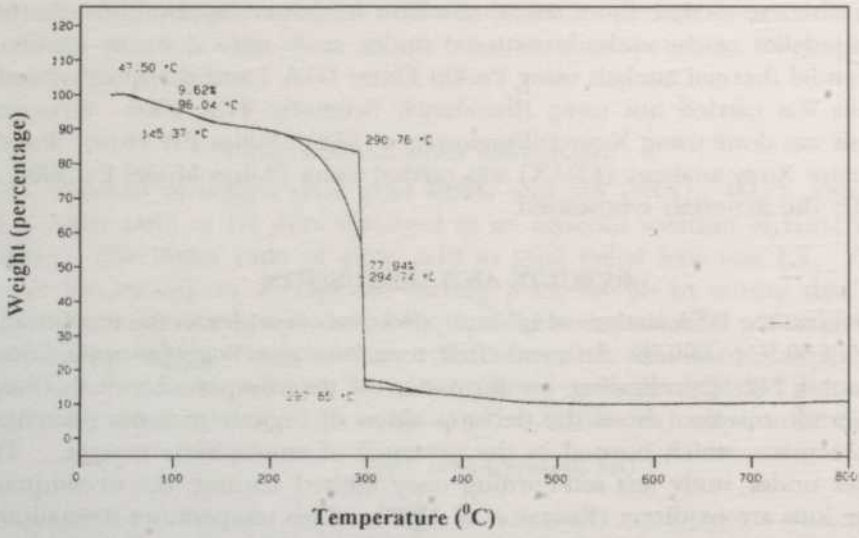

Fig. 3. TGA plot of $LiMn_2O_4$ analysis of the gel precursor at a heating rate of 10 °C m^{-1}

in agreement with the DTA results. DTA and TGA studies have confirmed that the compound is reasonably stable up to 800 °C.

Fig. 4 shows the structural analysis of $LiMn_2O_4$. The fired product recovered from DTA crucible was used. X-ray patterns confirm the formation of $LiMn_2O_4$ without any impurity phases at 242 °C, 400 °C, 600 °C and 800 °C. At low temperature however, the peaks are relatively broad and may be due to the probable lattice strain in the structure. XRD patterns show well-defined peaks even at the formation temperature (242 °C). XRD patterns obtained in this study matched with those of the JCPDS card file No 18-0736, which confirms that the synthesized compound is $LiMn_2O_4$. The peaks gradually became sharper with increasing calcination temperatures, indicating an increase in the crystallinity. It may occur from growth of grain size, change in the local structure or release of lattice strain.

Fig. 5 shows the EDAX study of the $LiMn_2O_4$ compound that was sintered at 800 °C. It was found that EDAX show peaks corresponding to Mn and oxygen atoms only, it does not show any impurity peaks. It confirms that the synthesized material is $LiMn_2O_4$.

CONCLUSION

Bulk amounts of $LiMn_2O_4$ precursor powders were prepared using citric acid as chelating agent. DTA studies show that the temperature of formation of $LiMn_2O_4$ is below 242 °C, the lowest temperature reported so far from such a route for the preparation of $LiMn_2O_4$. XRD results show that the product is single-phase at low temperature EDAX study confirms the purity of the compound.

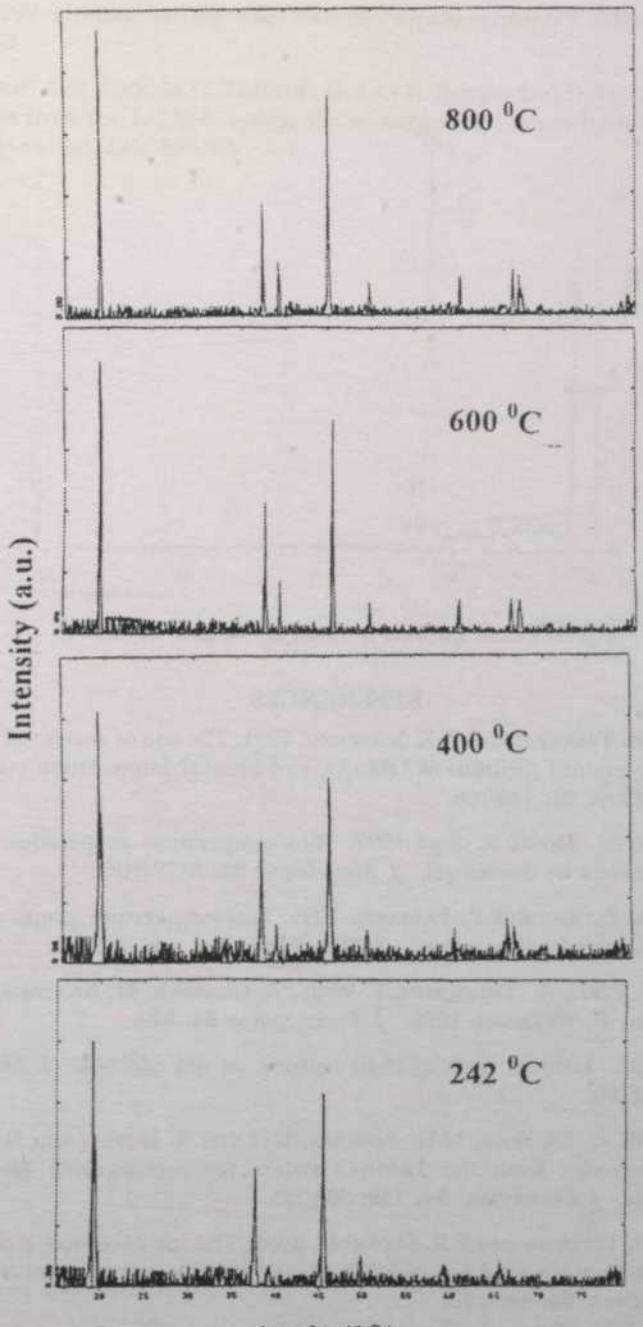

Fig. 4. X-ray diffraction patterns of the gel-derived materials $LiMn_2O_4$ sintered at 242 °C, 400 °C, 600 °C and 800 °C

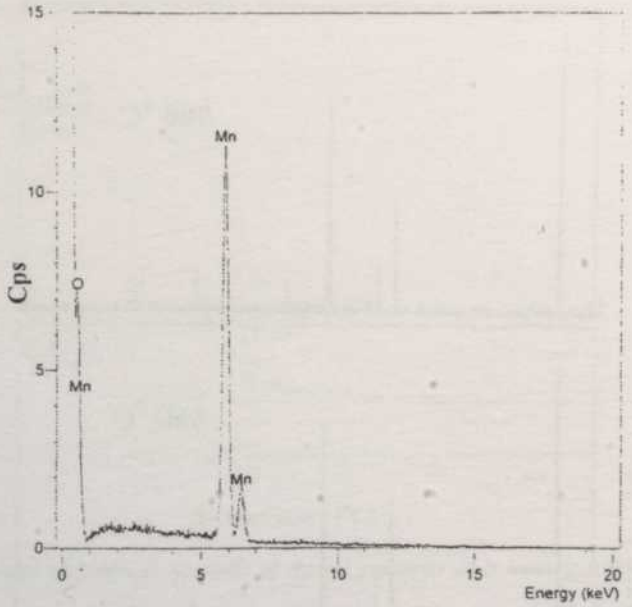

Fig. 5. EDAX spectrum of $LiMn_2O_4$ sintered at 800 °C

REFERENCES

Barboux. P., J. M. Tarascon and F. K. Shokoohi. 1991. The use of acetate as precuors for he low-temperature synthesis of $LiMn_2O_4$ and LiCoO2 intercalation compounds. *J. Solid State Chem.* **94:** 185-196.

In-Hwan Oh, S. A. Hong, K. Sun. 1997. Low-temperature preparation of ultrafine $LiCoO_2$ powders by the sol-gel. *J. Mat. Science* **32:** 3177-3182.

Kumar, S. S., A. Pathak and P. Pramanik. 1995. Low-temperature preparation of fine particles of mixed oxide system. *J. Mat. Science Lett.* **14:** 35-37.

Delmas, C., J. P. Peres, A. Demourges, F. Weill, A. Chadwick, M. Broussely, F. Perton, Biensan Ph., P. Willmann. 1995. *J. Power Sources* **54:** 329.

Scrosati, B. 1992. Lithium rocking chair battries: an old concept? *J. Electrochem. Soc.* **139:** 2776-2780.

Thackeray M. M., A. De Kock, M.H. Rossouw, D. Lilies R. Bittihn and D. hoge. 1992. Spinel electrodes from the Li-Mn-O system for rechargeable lithium battery applications. *J. Electrochem. Soc.* **139:** 363-365.

P. Barboux, J.M. Tarascon and F.K. Shokoohi. 1991. The use of acetate a precursors for the low-temperature synthesis of $LiMn_2O_4$ and $LiCoO_2$ intercalation compounds. *J. Solid State Chem.* **94:** 185-196.

In-Hwan Oh, Seong-Ann Hong, Yang-Kook Sun. 1997. Low-temperature preparation of ultrafine LiCoO2 powds by the sol-gel method. *J. Mat. Science.* **32:** 3177-3182.

S. Kumar Saha, A. Pathak and P. Pramanik. 1995. Low-temperature preparation of fine particles of mixed oxide system. *J. Mat. Science Lett.* **14:** 35-37.

B. Scrosati. 1992. Lithium rocking chair batteries: an old concept? *J. Electrochem. Soc.* **139:** 2776-2780

M.M. Thackeray, A.de Kock, M.H. Rossouw, D. Lies R. Bittihn and D. Hoge. 1992. Spinel electrodes from the Li-Mn-O system for rechargeable lithium battery applications. *J. Electrochem. Soc.* **139:** 363-365.

Pertanika J. Sci. & Technol. 9(2): 237 - 244 (2001)
ISSN: 0128-7680

Sifat Dielektrik Getah Asli Terepoksida (ENR50)

Mohd Noor Mat, W.M. Daud W. Yusoff, Zainul Abidin Hassan dan W. Mahmood Mat Yunus

Jabatan Fizik
Fakulti Sains dan Pengajian Alam Sekitar
Universiti Putra Malaysia
43400 UPM Serdang
Selangor

Diterima: 20 Julai 2000

ABSTRAK

Kertas ini melaporkan pengukuran sifat dielektrik getah asli terepoksida (ENR50) yang menggunakan spektrometer dielektrik pada suhu 303, 313, 333, 353 dan 373K di dalam julat dari 10^{-2} ke 10^{6} Hz. Hasil eksperimen menunjukkan kapasitan kompleks berubah dengan frekuensi dan meningkat dengan peningkatan suhu dan peratus komposisi karbon. Hasil eksperimen diperihalkan dengan model rangkaian litar setara yang dicadangkan oleh Joncher.

ABSTRACT

This paper reports the measurement of dielectric properties of epoxydized natural rubber (ENR50) by using dielectric spectrometer at the temperature 303, 313, 353 and 373K in the frequency range from 10^{-2} to 10^{6} Hz. The experimental result has shown that the complex capacitance varies with frequencies and increases with increasing temperature and carbon percentage. The experimental result has been described with the equivalent circuit network model proposed by Joncher.

Kata kunci: pengutuban, ketelusan, litar siri, litar selari dan masa kelambatan

PENGENALAN

Sifat dielektrik bahan dicirikan oleh ketelusan dielektrik dan tangen kelesapan (Hill 1979). Bahan dielektrik adalah suatu bahan yang mempunyai rintangan tinggi dengan nilai konduktans yang rendah. Apabila bahan dielektrik diletakkan di antara dua plat kapasitor selari, didapati keupayaan menyimpan cas bertambah (Livingston 1999). Ini disebab berlakunya pengutuban dielektrik (Joncher 1983) dan ditulis sebagai (Joncher 1983)

$$P = (\varepsilon - \varepsilon_0)E \qquad (1)$$

dengan P, ε, ε_0 dan E merujuk kepada pengutuban, ketelusan relatif, ketelusan ruang bebas dan medan elektrik. Di dalam medan elektrik ulang alik, proses pengutuban akan mengalami kelambatan di dalam mencapai keseimbangan (Joncher 1983). Kelambatan ini dirujuk sebagai masa santaian.

Ketelusan dielektrik diperolehi dengan mengukur kapasitan (Hill & Pickup 1985) iaitu $C^*(\omega) = C'(\omega) - jC'(\omega)$

$$= \varepsilon_0 \frac{A}{d}\left(\varepsilon'(\omega) - j\varepsilon''(\omega)\right) \quad (2)$$

di mana dan merupakan ketelusan dielektrik nyata dan faktor kelesapan manakala A dan d ialah luas permukaan elektrod dan tebal sample. Bagi kes unggul (rajah 1a), kapasitan kompleks boleh ditulis

$$C^*(\omega) = \frac{\left(\frac{1}{\omega^2 C}\right) - j\left(\frac{1}{\omega G}\right)}{\left(\frac{1}{G}\right)^2 + \left(\frac{1}{\omega C}\right)^2} \quad (3)$$

dengan G adalah konduktans.

Oleh kerana kapasitans yang diperolehi melalui kaitan (3) hanyalah sesuai untuk sample cecair elektrolit, menyebabkan perlunya mengubahsuai formula empirik untuk menyesuaikan kes-kes yang tidak unggul khususnya sampel pepejal. Oleh itu dengan menggunakan kapasitor yang diperkenalkan oleh Joncher (1983), C*(ω) boleh ditulis sebagai

$$C^*(\omega) = A(j\omega)^{p-1} = C_o\left(\frac{f}{f_c}\right)\left(\sin\left(p\frac{\pi}{2}\right) - j\cos\left(p\frac{\pi}{2}\right)\right) \quad (4)$$

dengan A ditakrifkan sebagai $A = C_o\left(\frac{1}{\omega_c}\right)^{p-1}$ dengan $\omega_c = 2\pi f_c$, penyelesaian kepada masalah ini menjadi mudah, bila p mengambil nilai di antara 0 dan 1.

Bagi litar bersiri di antara kapasitor dan konduktans (rajah 1 a), kapasitan setara ialah

$$\frac{1}{C_d^*} = \frac{1}{A(j\omega)^{p-1}} + \frac{1}{C - B(j\omega)^q}$$

$$C_d^* = \left(\frac{\frac{a_1}{a_1^2+b_1^2} + \frac{a_2}{a_2^2+b_2^2}}{\left(\frac{a_1}{a_1^2+b_1^2} + \frac{a_2}{a_2^2+b_2^2}\right) + \left(\frac{b_1}{a_1^2+b_1^2} + \frac{b_2}{a_2^2+b_2^2}\right)}\right) - j\left(\frac{\frac{b_1}{a_1^2+b_1^2} + \frac{b_2}{a_2^2+b_2^2}}{\left(\frac{a_1}{a_1^2+b_1^2} + \frac{a_2}{a_2^2+b_2^2}\right) + \left(\frac{b_1}{a_1^2+b_1^2} + \frac{b_2}{a_2^2+b_2^2}\right)}\right) \quad (5)$$

dengan a_1, a_2, b_1 dan b_2 ditakrifkan sebagai $a_1 = C - C_o\left(\frac{f}{f_c}\right)^q \cos\left(q\frac{\pi}{2}\right)$, $a_2 = C_o\left(\frac{f}{f_c}\right)^{p-1} \cos\left(p\frac{\pi}{2}\right)$, $b_1 = C_o\left(\frac{f}{f_c}\right)^q \sin\left(q\frac{\pi}{2}\right)$, $b_2 = C_o\left(\frac{f}{f_c}\right)^{p-1} \sin\left(p\frac{\pi}{2}\right)$ serta A dan B ditakrifkan sebagai $A = C_o\left(\frac{1}{\omega_c}\right)^{p-1}$ dan $B = C_o\left(\frac{1}{\omega_c}\right)^q$ serta p dan q mengambil nilai di antara 0 dan 1.

Bagi litar dua kapasitor selari (rajah 1b), kapasitan kompleks boleh dinyatakan sebagai

$$C_{qdc}^*(\omega) = C_1^*(\omega) + C_2^*(\omega) = F(j\omega)^{m-1} + L(j\omega)^{n-1}$$

$$= C_o\left(\frac{f}{f_c}\right)^{m-1} \sin\left(m\frac{\pi}{2}\right) + C_o\left(\frac{f}{f_c}\right)^{n-1} \sin\left(n\frac{\pi}{2}\right)$$

$$-j\left(C_o\left(\frac{f}{f_c}\right)^{m-1} \cos\left(m\frac{\pi}{2}\right) + C_o\left(\frac{f}{f_c}\right)^{n-1} \cos\left(n\frac{\pi}{2}\right)\right) \quad (6)$$

yang mana F dan L ditakrifkan sebagai $F = C_o\left(\frac{1}{\omega_c}\right)^{m-1}$ dan $L = C_o\left(\frac{1}{\omega_c}\right)^{n-1}$ serta m dan n mengambil nilai di antara 0 dan 1.

Seterusnya bagi litar selari (rajah 1 c). kapasitan kompleks boleh dinyatakan sebagai

$$C^*(\omega) = C^*_{qdc} + C^*_d + C_{inf} \quad (7)$$

dan bagi litar selari (rajah 1d), kapasitan kompleks boleh dinyatakan sebagai

$$C^*(\omega) = C^*_{qdc} + C^*_d + C_{inf} - j\frac{G}{\omega}$$

yang mana C^*_{qdc} dan C^*_d dalam kaitan (7) dan (8) ditakrifkan sama seperti dalam kaitan (5) dan (6), manakala C_{inf} dan G ialah kapasitan infiniti dan konduktans.

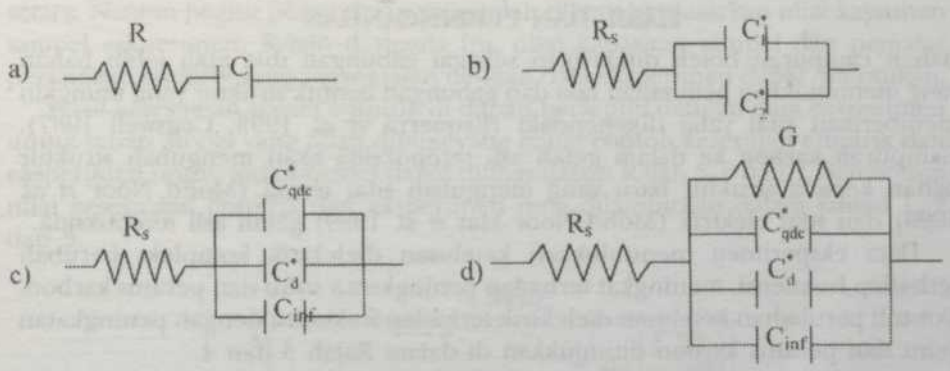

Rajah 1 : a) Kombinasi RC secara siri b) Kombinasi kapasitor semesta secara selari
c) Kombinasi kapasitor semesta dan dwikutub secara selari
d) Kombinasi kapasitor semesta, dwikutub, infiniti dan konduktans secara selari

KAEDAH EKSPERIMEN

Sampel getah asli (ENR50) dengan komposisi karbon hitam 0, 25, 50 dan 75 peratus (kemudian dirujuk sebagai sampel: a_1, a_2, a_3 dan a_4) yang digunakan dalam kajian ini telah divulkankan pada suhu 423K dalam satu bekas besi yang dibuat khusus bersaiz dalaman 17.6cm x 17.6cm dengan ketebalan 0.05, 0.1 dan 0.2cm dengan masa 16, 9, 10 dan 10 minit untuk setiap sampel a1, a2, a3 dan a4 (Mohd Noor Mat *et al.* 1999). Litar pengukuran di dalam eksperimen ini ditunjukkan oleh rajah 2.

Sampel getah asli diletakkan di antara dua elektrod dalam sel yang boleh dikawal suhunya. Pengukuran kapasitan komplek getah asli dilakukan dengan

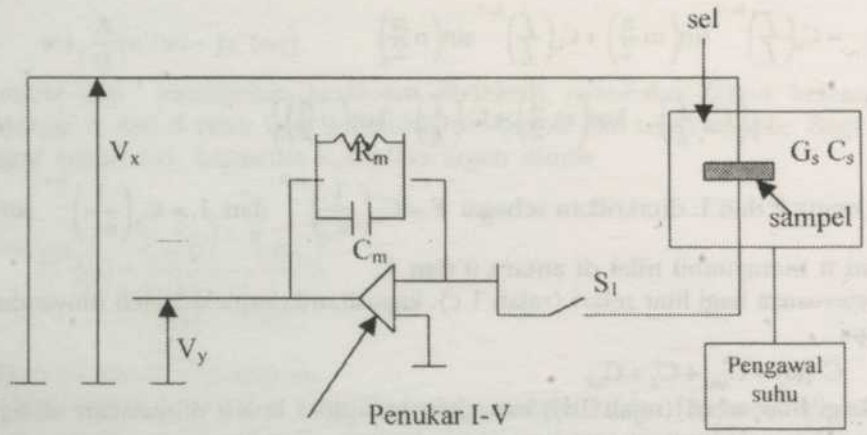

Rajah 2: Litar pengukuran

teknik piawai menggunakan Spektrometer Dielektrik pada suhu 303, 313, 333, 353 dan 373K dengan julat frekuensi 10^{-2} ke 10^{6} Hz.

HASIL DAN PERBINCANGAN

Bahan campuran boleh ditakrifkan sebagai gabungan dua atau lebih bahan yang menunjukkan pemisahan fasa dan gabungan bentuk struktur yang mungkin memberikan sifat yabg dikehendaki (Ezquerra *et al.* 1993; Cogswell 1987). Campuran karbon ke dalam getah asli terepoksida akan mengubah struktur bahan kepada struktur baru yang mengubah sifat terma (Mohd Noor *et al.* 1999) dan sifat elektrik (Mohd Noor Mat *et al.* 1999) getah asli terepoksida.

Data eksperimen menunjukkan ketelusan dielektrik kompleks berubah terhadap frekuensi, meningkat terhadap peningkatan suhu dan peratus karbon. Contoh perubahan ketelusan dielektrik terhadap frekuensi dengan peningkatan suhu dan peratus karbon ditunjukkan di dalam Rajah 3 dan 4.

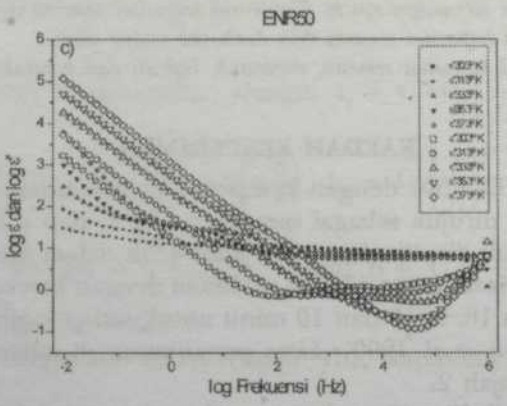

Rajah 3: Contoh plot perubahan ketelusan dielektrik kompleks terhadap frekuensi sampel ENR 50 tanpa karbon pada suhu 303, 313, 333, 353 dan 373K

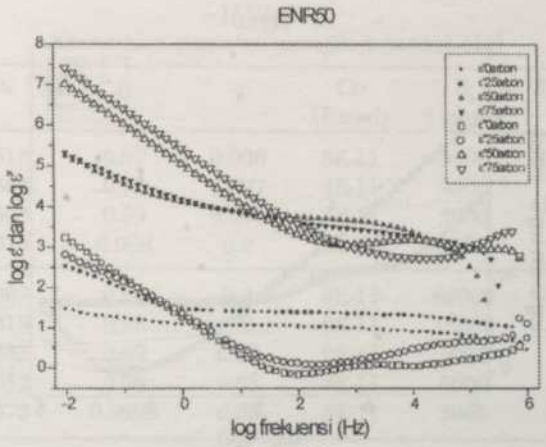

Rajah 4: Contoh plot perubahan ketelusan dielektrik terhadap frekuensi sampel ENR50 dengan komposisi karbon 0, 25, 50 dan 75 peratus pada suhu 303K

Penentusahan pengutuban yang terlibat dalam perjumlahan pengutuban bagi setiap sampel pada setiap suhu dapat dikenalpasti melalui model litar setara. Namun begitu permodelan yang telah dibuat berdasarkan nilai kapasitan sampel eskperimen. Selain daripada itu, nilai kapasitan sampel dan pemalar persamaan empirik yang bersesuaian dengan data eksperimen dapat ditentukan.

Hasil kesesuaian secara empirik di dapati bersetuju dengan data eksperimen untuk setiap model yang telah dibuat yang mana contoh kesesuian empirik dan eksperimen untuk setiap model dapat dilihat dalam Rajah 5, 6 dan 7. Sementara nilai kesesuaian empirik dan eksperimen pula dilampirkan dalam jadual 1, 2 dan 3.

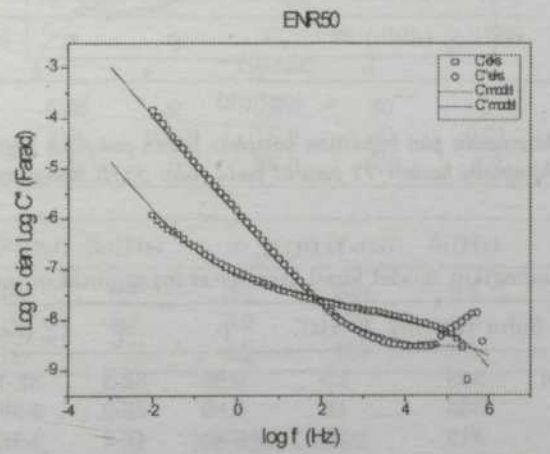

Rajah 5: Contoh kesesuain plot kapasitan kompleks lawan frekuensi bagi sampel ENR50 dengan komposisi karbon 75 peratus pada suhu 303K menggunakan model (1b)

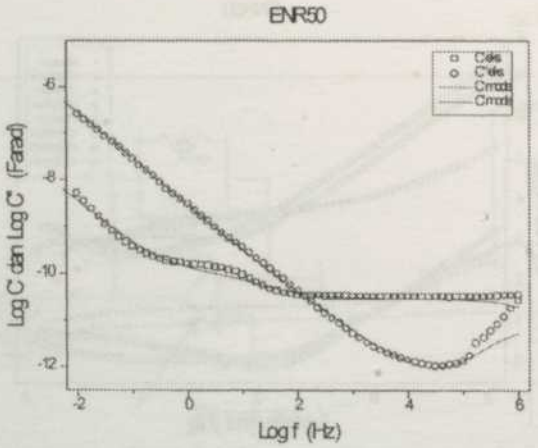

Rajah 6: Contoh kesesuian plot kapasitan kompleks lawan frekuensi bagi sampel ENR50 tanpa karbon pada suhu 353K menggunakan model (1c)

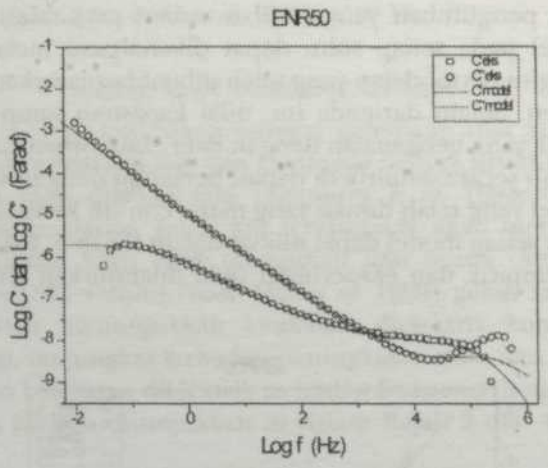

Rajah 7: Contoh kesesuaian plot kapasitan kompleks lawan frekuensi bagi sampel ENR50 dengan komposisi karbon 75 peratus pada suhu 353K menggunakan model (1d)

JADUAL 1
Kesesuaian mengikut model kuasi arus terus menggunakan modal (1b)

Sampel	Suhu (Kelvin)	f_c (Hz)	p	q	C_0 (Farad)	R_s (ohm)
ENR50, O% karbon	303	1.5	0.95	8E-3	5E-11	10000
ENR50, 50 %	303	12	0.89	2E-2	3.3E-8	300
	313	26	0.89	4E-2	3.3E-8	300
ENR, 75 % karbon	303	35	0.8	8E-3	3.3E-8	50
	313	50	0.8	8E-3	5.5E-8	50

JADUAL 2
Kesesuaian pemalar mengikut model (1c)

Sampel	Suhu (K)	p	q	Co (Farad)	R_s (ohm)	Fc (Hz)	C_{inf} (Farad)
ENR50	313	0.97	0.006	5E-11	5000	6	5E-12
0% karbon	333	0.98	0.007	4E-11	5000	30	5E-12
	353	0.99	0.008	2E-11	2000	150	1E-11
	373	0.998	0.2	3E-11	2000	220	1E-13
ENR50	303	0.97	0.2	9E-11	60000	1	1E-13
25% karbon	313	0.98	0.2	9E-11	15000	4	1E-13
	333	0.99	0.03	9E-11	5000	12	1E-13
	353	0.98	0.03	8E-11	5000	35	1E-13
	373	0.9999	0.03	8E-11	3000	90	1E-13

C (Farad)	C_m (Farad)	Fm (Hz)	m	C (Farad)	Fn (Hz)	n	Co (Farad)
200	10	0.3	0.2	200	0.3	0.3	5E-13
200	10	4	0.2	200	4	0.3	6E-13
200	10	10	0.2	200	10	0.3	4E-13
200	10	20	0.2	200	20	0.3	7E-13
200	10	0.1	0.2	200	0.1	0.3	7E-12
200	10	0.1	0.2	200	0.1	0.3	3E-12
200	10	1	0.2	200	1	0.3	5E-12
200	10	1	0.2	200	1	0.3	9E-11
200	10	1	0.2	200	1	0.3	2E-11

JADUAL 3
Kesuaian pemalar menggunakan model (1d)

Sampel	Suhu(K)	p	q	C_0 (Farad)	Rs (ohm)	f_c (Hz)	G_s (S)	C_{int} (Farad)
ENR50,	333	0.85	0	9E-8	30	5	3E-5	1E-13
75%	353	0.9	0.001	1E-8	50	0.01	6E-5	1E-13
karbon	373	0.9	0	3E-8	100	0.9	1.3E-4	1E-13

C (Farad)	C_m (Farad)	fm(Hz)	m	C (Farad)	fn(Hz)	n	C_0 (Farad)
200	10	0.5	0.2	200	0.5	0.3	3E-8
200	10	0.5	0.2	200	0.5	0.3	1E-8
200	10	0.5	0.2	200	0.5	0.3	4E-9

KESIMPULAN

Pengukuran nilai kapasitan kompleks getah asli terepoksida dilakukan dalam julat frekuensi 10^{-2} ke 10^{6} Hz. Sementara nilai pemalar dielektrik kompleks pula diperolehi dari kapasitan kompleks melalui kaitan (Livingston 1999). Hasil

eksperimen menunjukkan penyerahan ketelusan kompleks terhadap frekuensi meningkat dengan peningkatan suhu dan peratus karbon. Pengesahan pengutuban yang terlibat yang menyumbang kepada jumlah pengutuban dikenalpasti melalui model litar setara yang bersetuju dengan data eksperimen.

RUJUKAN

COGSWELL. F.N. 1987. *Thermoplastic Structural Composites.* Philadelphia: Institute of Physics Conference Series.

EZQUERRA. T. A., F. KREMER. dan G. WEGNER. 1992. *AC Electrical Properties of Insulator-Conductor Composites.* New York: Dielectric Properties of Haterogeneous Materials, Progress in Electromagnetics Research.

HILL. R.M. 1979. Characterisation of dielectric loss in solids and liquids. *Nature* **275:** 96-99.

HILL. R.M. dan C. PICKUP. 1985. Barrier effect in dispersive media. *J. of Materials Science.* **20:** 4431-4444.

HIPPEL, A.R.V. 1954. *Dielectric and Waves.* New York: John Wiley and Sons.

JONCHER. A.K. 1977. The 'Universal' dielectric response. *Nature* **267:** 673-679.

JONCHER. A.K. 1983. *Dielectric Relaxation in Solids.* London: Chelsea Dielectrics Press.

LIVINGSTON. J.D. 1999. *Electronic Properties of Engineering Materials.* New York : John Wiley and Sons.

MOHD NOOR MAT, ZAINUL ABIDIN HASSAN, W. M DAUD W. YUSOFF dan W. MAHMOOD MAT YUNUS. 1999 9 (b). Kekonduksian elektrik dalam getah asli (SMR5) dibentangkan di *Seminar Sains dan Keadaan Pepejal (MASS)*, Prince Crown Hotel, Pulau Pinang.

MOHD NOOR MAT, W. MAHMOOD MAT YUNUS, ZAIDAN ABDUL WAHAB, ZAINUL ABIDIN HASSAN dan MOHD MAAROF MOKSIN. 1999 9 (a). Pengukuran pekali resapan terma getah asli terepoksida dengan kaedah lindapan. *J. Solid St. Sci. and Technol.* **7 (1):** 148-155.

Pertanika J. Sci. & Technol. 9(2): 245 - 251 (2001)
ISSN: 0128-7680

Antimicrobial and Cytotoxic Activity of Cholesterol and β-Sitosterol from Chloroform Extract of the Leaves of *Vitex quinata*

Hassan Abdalla Almahy, Mawardi Rahmani, Mohd Aspollah Sukari and Abd. Manaf Ali[1]
Department of Chemistry, Universiti Putra Malaysia, 43400 UPM, Selangor, Malaysia
[1]Department of Biotechnology, Universiti Putra Malaysia, 43400 UPM, Selangor, Malaysia

Received: 22 September 2000

ABSTRAK

Dua sebatian fitosterol telah berjaya dipencil daripada daun *Vitex quinata* dengan menggunakan kaedah kromatografi lajur ekstensif. Kedua-duanya telah dikenalpasti secara spektroskop sebagai kolestrol dan β-sitosterol, dan aktiviti biologi kedua-duanya telah juga dinilai. Kedua-duanya memberi keputusan ujian yang positif menentang dua spesies bakteria (*Bacillus cereus dan Pseudomonas aruginosa*), serta keputusan yang negatif terhadap empat spesies kulat. Ujian terhadap kedua-duanya juga memperlihatkan aktiviti sitotoksik menentang garis sel leukemia T-limfoblas dengan nilai IC_{50} masing-masing sebanyak 10 dan 25 μg/ml.

ABSTRACT

Two phytosterols were efficiently isolated from the leaves of *Vitex quinata* using extensive column chromatographic method. They were spectroscopically identified as cholesterol and β-sitosterol and their biological activity was also evaluated. The two compounds gave positive test results against two species of bacteria (*Bacillus cereus* and *Pseudomonas aeruginosa*) and negative results against four species of fungi. Both of them gave cytotoxic activity against T-lymphoblastic leukemic cell line with IC_{50} values of 10 and 25 μg ml respectively.

Keywords: antibacterial, antimicrobial, disc difussion method, cytotoxic activity

INTRODUCTION

Vitex quinata (heterophylla) (Hegnauer 1963) is a moderate-sized tree found in the central part of Peninsular Malaysia and India (Wagner 1984) belonging to the family Verbenaceae (Smith 1976; Corner 1952). The local name of the plant is called "Orange-barked Vitex" (Nagiton 1978). The leaves of *V. glabrata* (Apichart 1993), *V. pinnata* (Apichart and Chatriwat 1993) and *V. canescens* (Suksamrarn 1997) have been reported to contain turkesterone. Pinnatasterone as the major ecdysteroids of the *Vitex* species (Kubo and Ayafor 1984). We now wish to report the isolation of cholesterol and β-sitosterol from *V. quinata* together with their antimicrobial and cytotoxic activity. This is the first report on the leaves of *V. quinata*.

MATERIALS AND METHODS

Plant material

The plant was collected in April 1998, from Perak (North of Malaysia) and a voucher specimen has been deposited at the Herbarium, Biology Department, Universiti Putra Malaysia.

Extraction and isolation

The ground air-dried leaves of *Vitex quinata* (1.133 kg) was extracted successively with petroleum ether, chloroform and methanol by maceration. The extraction was repeated three times for each solvent for three days. The concentrated chloroform extract (14.0g) was subjected to column chromatography (Merck silica gel 70-230 mesh) eluting with petroleum ether, chloroform and chloroform-methanol as eluents. Fractions eluted with petroleum ether: chloroform (3:7) were combined and repeatedly rechromatographed in the same manner to afford compound (1) and recrystallised with ethanol to give white needles melting point 150-151°C (Yamaguchi, 197°C, 149°C).
IR (KBr, cm^{-1}): 3402 (OH), 2973 (CH).
UV λ_{max} nm, EtOH: 273 (0.09), 240 (0.11), 227 (0.01), 213 (0.02).
^{1}H-NMR (270 MHz, CDd_3) δ = 5.4 (1H, *t*, H-6), 3.5 (1H, br, 3-OH), 0.6-0.1 (methyl protons).
^{13}C-NMR (100 MHz, $CDCl_3$) ppm: 140.7 (C-5), 121.7 (C-6), 71.8 (C-3), 56.7 (C-14), 56.1 (C-17), 50.1 (C-9), 42.3 (C-13), 39.7 (C-12), 39.5 (C-24), 37.2 (C-1), 36.5 (C-4), 36.2 (C-22 & C-10), 35.7 (C-20), 31.9 (C-8), 31.6 (C-7), 28.2 (C-16), 28.0 (C-25 & C-2), 24.2 (C-15), 23.8 (C-23), 22.8 (C-27), 22.5 (C-26), 21.0 (C-11), 19.3 (C-19), 18.7 (C-21), 11.8 (C-18).
MS m/e (% intensity): 386 (M^+, 5.5), 371 (6.4), 326 (1.8), 301 (7.3), 275 (6.4), 247 (7.3), 231 (0.9), 213 (6.4), 173 (6.4), 145 (11.8), 119 (18.2), 95 (28.2), 81 (29.1), 57 (57.3), 43 (100).

Further elution with petroleum ether: chloroform (4: 9) gave a semipurified fraction which was rechromatographed to yield compound (2) as white powder, melting point 137-138°C (It ill et al., 1991, 136-137°C).
IR (KBr, cm^{-1}): 3424 (OH), 2938 (CH).
UV λ_{max}nm, EtOH: 290.0 (0.24), 277.0 (0.01).
^{1}H-NMR (300 MHz, CDd_3) δ = 5.3 (1H, *d*, J=0.78, Hz, H-6), 3.5 (1H, br, 3-OH), 0.6=2.3 (m, aliphatic protons).
^{13}C-NMR (100 MHz, $CDCl_3$) ppm: 140.8 (C-5), 121.7 (C-6), 71.8 (C-3), 56.8 (C-14), 56.1 (C-17), 50.2 (C-9), 45.9 (C-8), 44.9 (C-13), 42.3 (C-4), 39.8 (C-12), 37.3 (C-1), 36.5 (C-10), 36.2 (C-20), 35.5 (C-24), 34.0 (C-22), 31.9 (C-7), 31.7 (C-2), 29.2 (C-23), 28.3 (C-16), 26.1 (C-25), 24.3 (C-15), 23.1 (C-28), 21.1 (C-11), 19.8 (C-27), 19.4 (C-19), 19.1 (C-29), 18.8 (C-26), 12.0 (C-18), 11.9 (C-21).
MS m/e (% intensity): 414 (M^+, 11.1), 396 (4.4), 354 (4.4), 342 (4.4), 329 (4.4), 329 (4.4), 303 (5.6), 289 (4.4), 273 (5.6), 255 (4.4), 231 (4.4), 213 (4.4), 187 (3.3), 163 (10.0), 159 (15.6), 145 (20.0), 133 (21.1), 119 (21.1), 107 (31.1), 95 (18.9), 81 (30.0), 69 (30.0), 57 (57.8), 55 (40.0), 43 (100).

The isolated compounds were tested for their activity using two bacteria (*Bacillus cereus* and *Pseudomonas aeruginosa*) and their cytotoxic activity were also evaluated using T-Lymphoblastic leukemic (CEM-SS) cell line.

Microorganisms

The microorganisms were obtained from the culture collection of the Department of Biotechnology, the stock cultures were grown on Potato Dextrose Agar (PDA) for 24 hours at 28°C at which time the cells were harvested by centrifugation (4°C, 2000 rpm, 3min.). The cells were washed and suspended in sterile 0.9% saline to give a final concentration of 10^5-10^6 CFU/ml using a haemocytometer (Bergeys, 1957)

The microbial strain used were: *Bacillus cereus* NRRLUI-1447, *Pseudomonas aeruginosa* UI-60690; and four fungi (*Aspergillus ochraceus* NRRL 398, *Candida lipolytica* ATCC 2075, *Sacchromyces cerevisiae* NRRL 2034. and *Sacchromyces alipolytica*).

Disc Diffusion Method

Antibacterial activity of the isolated compounds were tested using disc diffusion method (Bauer *et al.* 1966). The discs were prepared by impregnating them in ethanolic solution of each sample (10 mg/ml). They were then evenly spaced out on the agar surface previously inoculated with the suspension of each microorganism to be tested. Standard discs of nystatin (50g/discs) and streptomycin 24 hours and the antimicrobial was recorded by measuring the width of the clear inhibition zones around each disc.

Minimum Inhibition Concentration

The effectiveness of the antibacterial activity of the samples was quantified using the tube dilution method (Hufford *et al.*, 1975). Samples at different concentrations (30-1000 g/ml) were added to 5 ml broth. Cultures containing between 10^5-10^6 CFU were inoculated in 5 ml broth tubes and incubated for 24 hours at 37°C. Nystatin was used as standard for comparison with the activities of the samples against the microbial species. Minimum inhibitory concentration (MIC, g/ml) was recorded as the highest dilution which was free from microbial growth.

Assay for Cytotoxic Activity

Stock solutions were prepared by dissolving the samples in 90% ethanol at 10 mg/ml for crude and 10 mg/ml for pure compounds, the stock solution was diluted in RPMI-1640 medium at different concentrations.

Cultivation of Cells

Stock of (CEM-SS) cells were obtained from National Cancer Institute and cultivated in RPMI-1640 (Sigma, USA) medium supplemented with 10% of fetal calf serum, pencillin unit/ml and streptomycin unit/ml as a complete growth medium (CGM). Cells were maintained in 25 cm^2 flask (Nunck, Denmark) with

10 ml of (CGM) in CO_2 incubator at 37°C with 5% CO_2 until confluence (Weilew *et al.* 1989).

Cytotoxicity Assay

The assay was performed by using (CEM-SS) cells in 96 wells plate (Nunck, Denmark). Aliquots of the sub-stock was adjusted and mixed with medium to give a total volume of 50 µl/well at chosen dilution. The cell concentration was adjusted to 2×10^5 cells/ml. Aliquot of 50 µl cell suspension was added to each well. The culture plate was kept in CO_2 incubator (Sanyo, Japan) at 37°C with 5% CO_2 for 3 days. This was followed by the addition of 20 µl of MTT solution (5 mg/ml in PBS). The plate was incubated at 37°C for 4 hours in CO_2 incubator. 80 µl of the medium from each well was removed after 4 hours and 100 µl of DMSO was added into each well and the plate was left at room temperature for about 30 mins. The remaining crystals were dissolved by resuspension and the optical density was recorded using an ELISA reader (Biotek EL340) at wavelengths of 570 nm. Controls consisted of untreated cells. Absorbance values were compared with values obtained for controls and percentage cell viability was determined by using the microtitration assay (Ali *et al.*, 1997). Cytotoxicity was recorded as the 50% inhibition concentration (IC_{50}) with reference to the untreated control cells (Ali *et al.* 1998).

RESULTS AND DISCUSSION

Preliminary screening of the isolated compounds of *V. quinata* for antimicrobial investigation was performed qualitatively using the disc diffussion assay. The two compounds were isolated after extensive chromatographic procedures and identified spectroscopically. Compound (**1**) was identified as cholesterol by comparing their melting point and spectral data with those from literature. The data obtained from compound (**2**) was in very close agreement to the literature values for β-sitosterol. The biological activity of these compounds were evaluated against Gram-positive and Gram-negative bacteria. (Table 1) both compounds gave medium inhibition activity with *Bacillus cereus* and strong inhibition with *Pseudomonas aeruginosa.*

Both compounds gave cytotoxic activity against T-Lymphoblastic leukemic (CEM-SS) cell line with an IC_{50} values of 10 and 25µg/ml respectively (Figs. 1 and 2).

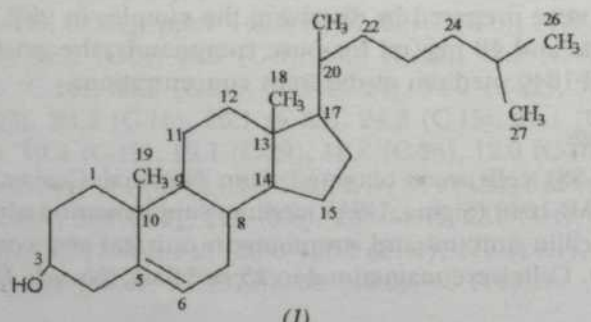

(1)

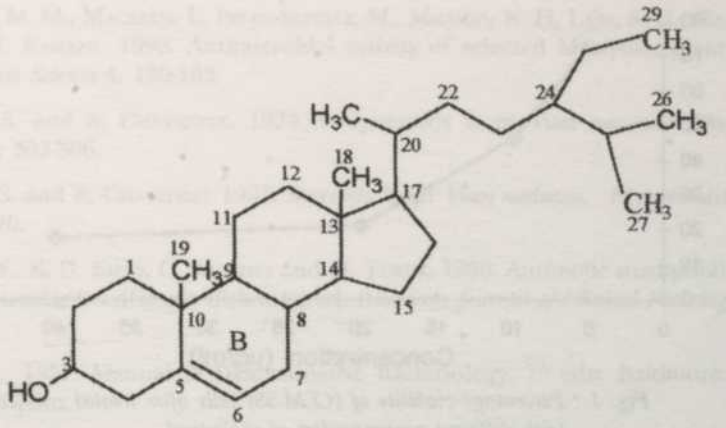

(2)

TABLE 1
Antimicrobial activity of cholesterol and β-sitosterol against bacteria and fungi

Compound	Bacteria		*Fungi*			
	B.cer.	*P..aeri*	*A.och*	*C. lip*	*S. are*	*S. lip*
cholesterol	++	+++	-	-	-	-
β-sitosterol	++	+++	-	-	-	-

concentration used = 100 µg/ml, methanol
B.cer = *Bacillus cereus* *P. aeri* = *Pseudomonas aeriugenosa*
A.och = *Aspergillus ochraceus* *C. lip.* = *Candida lipolytica*
S.are = *Sacchromyces cerevisiae* *S. lip* = *Sacchromyces alipolytica*
- no inhibition ++ medium inhibitin +++ strong inhibition

This is the first report on the isolation of cholesterol from Verbenaceae, but for β-sitosterol it has been isolated previously from *V. negundo* (Fabian *et al.*, 1982) and *V. fisheri* (Kubo *et al.* 1990) without records of their biological and cytotoxic activity.

Based on antimicrobial screening studies on bacteria and fungi, it can be inferred that the chlorofrom-soluble extracts and the pure isolated compounds of *V. quinata* are effective against bacteria but had no effect against fungi. The activity of the compounds ranged between moderate and strong in the antibacterial tests towards the two microorganisms (*Bacillus cereus* and *Pseudomonas aeruginosa*). However, cholesterol and β-sitosterol gave the same encouraging results compared to crude chloroform extract.

CONCLUSION

In general, it is quite difficult and time consuming to fully characterised the structure of steroids. The ^{1}H-NMR and ^{13}C-NMR with various experimental

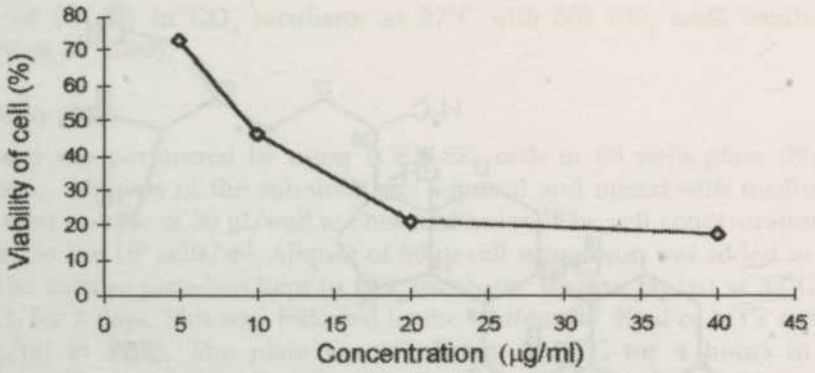

Fig. 1 : Percentage viability of (CEM-SS) cells after treated with different concentration of cholesterol

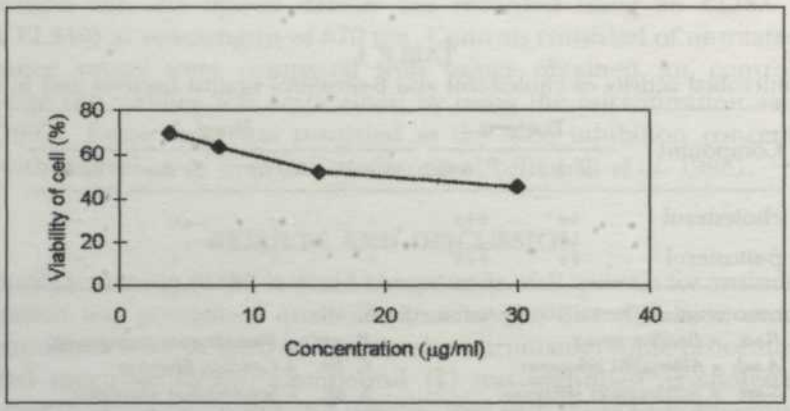

Fig. 2 : Percentage viability of (CEM-SS) cells after treated with different concentration of β–sitosterol

procedures are very useful tools in determining the whole structure of steroids. The ambiguity of the spectra obtained could be resolved by examining the individual specrta for various protons overlapped.

ACKNOWLEDGEMENTS

The authors wish to thank Univerity of Juba (Sudan) and Government of Malaysia for the research grant through IRPA program.

REFERENCES

Ali. A. M., M. Mackeen, L. Intan-Safinar, M., Mhamid, N. H, LAJIS, S. H., El-Sharkawy and M Murakoshi. 1997. Antitumour promoting and antitumour activities of the crude extract from the leaves of *Juniperus chinensis*. *Journal of Ethnopharmacognosy* **53**: 165-167.

ALI. A. M., M. M., MACKEEN, L, INTAN-SAFINAR, M., MHAMID, N. H, LAJIS, S. H., EL-SHARKAWY and K. KAWAZU. 1998. Antimicrobial activity of selected Malaysian plants. *Natural Products Science* **4**: 180-183.

APICHART, S. and S. CHATRIWAT. 1993. Ecdysteroids from *Vitex negundo. Phytochemistry* **32(2)**: 303-306.

APICHART, S. and S. CHATRIWAT 1993. Steroids from *Vitex medensis. Phytochemistry* **33(3)**: 418-420.

BAUER, A.W., K. D. KIRBY, C. SHERRIES and M. TURCK. 1966. Antibiotic susceptibility testing by a standardized single disk method. *American Journal of Clinical Pathology* **45**: 493-496.

BERGEYS, P., 1957. Manual of Determinative Bacteriology. 7th edn. Baltimore: Williams and Wijkins.

CORNER, H. J., 1952. *Wayside Trees of Malaya*, **Vol 2**: p. 752-753. Kuala Lumpur, Malaysia: United Selangor Press.

FABIAN, M. D., M. L. ROSARIO, V. J, CAGAMPANG and G. L. LOLIT. 1987. Phytochemical studies on the leaves of *Vitex negundo*, L.(Lagundi). *The Phillippine Journal of Science* 403-410.

HEGNAUER, R. 1963. Chemical Plant Taxonomy p. 389. London: Academic Press

HILL, R. A., D. N. KIRK, H. L. MAKIN and G. M. MURPHY. 1991. *Dictionary of Steroids Chemical Data, Structures and Bibliographies,* p 825. London: Chapman and Hall.

HUFFORD, C. D., J. M., FUNDERBURK, J. M., MORGAN, and L. W., ROBRTSAN. 1975. Steroids from four species of *Liliaceae Journal of Pharmaceutical Science* **64**: 789-792.

KUBO, I., Y., ASAKA, J. M. STOUT and T. NAKATSU. 1990. Structure of a novel phytoecdysteroid from *Vitex fisharii. Journal of Chemical Ecology* **16(8)**: 2581-2588.

KUBO, M., and F. AYAFOR. 1984. Chemical constituents of *Vitex negundo. Agricultural Biological Chemistry* **48**: 1684.

NAGITON, P. S., 1978. *Tree Flora of Malaya: A Manual for Foresters.* Kuala Lumpur, Malaysia: Longman Malaysia Sdn. Bhd.

SMITH, P. M. 1976. *The Chemotaxonomy of the Plant.* London: Edward Arnoid Ltd.

SUKSAMRARN, A., N. PROMRANGSAN, C. BORDIN, S. HOMVISASEVONISA and S. ACHARA. 1997. Ecdysteroids of the root and bark of *Vitex canescens. Phytochemistry* **45(6)**: 1149-1152.

WAGNER, H., E. BLODT and M. ZGAINSKI, 1984. *Plant Drug Analysis.* p. 170. Berlin: Springer-Verlag.

WEILOW, O. S., R., KISER, D. L., FINE, J. P. BADER, R. H., SHOEMAKER, and M. R. BOYD. 1989. ^{13}C-NMR spectra of some C-19 hydroxy, C-5, 6 epoxy and C-24 ethyl steroids. *J. Nat. Cancer Inst.* **81**: 577-586.

YAMAGUCHI, K. 1970. *Spectral Data of Natural Products.* Vol. 1: p 194 & 203. New York: Elsevier.

Pertanika Journal of Science and Technology

Subject Index for Vol. 9, Nos. 1 and 2, 2001

Pertanika Journal of Science & Technology

Author Index for Volume 9, Nos. 1 & 2, 2001

ACKNOWLEDGEMENT

The Editorial Board acknowledges the assistance of the following reviewers in the preparation of Volume 9, Numbers 1 & 2 of this journal

Prof. Ir. Abang Abdullah Abang Ali
Prof. Madya Dr. Abdul Kariem Hj. Mohd. Arof
Dr. Ashok Kumar
Dr. K. R. Desai
Prof. Brian Fisher
Prof. Dr. Kamel Arrifin Mohd. Atan
Prof. Lee Chnoong Kheng
Dr. Lee Teang Shui
Prof. Dr. Li Changkuan
Dr. Majidah Ariffin
Prof. Madya Ir. Dr. Mohd. Amin Mohd Soom
Prof. Madya Dr. Mohd. Kamil Yusoff
Prof. Dr. Muhammad Mat Salleh
Prof. Dr. Muhammad Yahya
Dr. Noriah Bidin
Prof. Dr. T.C Ralph
Prof. Madya Dr. Sim Chiaw Hock
Dr. Siwulan Adji
Dr. Tan Hui Boon
Prof. R. Weavers

Preparation of Manuscript

General
The manuscript, including footnotes, tables, and captions for illustrations, should be typewritten double spaced on paper 210 x 297 mm in size, with margins of 40 mm on all sides. Three clear copies are required. Typing should be on one side of the paper only. Each page of the manuscript should be numbered, beginning with the title page.

Title page
The title of the paper, name of author and full address of the institution where the work was carried out should appear on this page. A short title not exceeding 60 characters should be provided for the running headline.

Abstract
Abstracts in Bahasa Melayu and English of not more than 200 words each are required for full articles and communications. No abbreviation should appear in the abstract. Manuscripts from outside of Malaysian may be submitted with an English abstract only.

Keywords
Up to a maximum of ten keywords are required and they should be placed directly below the abstract.

Footnotes
Footnotes to material in the text should not be used unless they are unavoidable. Where used in the text, footnotes should be designated by superscript Arabic numerals in serial order throughout the manuscript. Each footnote should be placed at the bottom of the manuscript page where reference to it is made.

Equations
These must be clearly typed, triple-spaced and should be identified by numbers in square brackets placed flush with the right margin. In numbering, no distinction is made between mathematical and chemical equations. routine structural formulae can be typeset and need not be submitted as figures for direct reproduction but they must be clearly depicted.

Tables
Tables should be numbered with Arabic numerals, have a brief title, and be referred to in the text. Columns headings and descriptive matter in tables should be brief. Vertical rules should not be used. Footnotes in tables should be designated by symbols or superscripts small italic letters. Descriptive materials not designated by a footnote may be placed under a table as a *note.*

Illustrations & Photographs
Illustration including diagrams and graphs are to be referred to in the text as 'figures' and photographs as 'plates' and numbered consecutively in Arabic numerals. All photographs (gloosy black and white prints) should be supplied with appropriate scales.

Illustrations should be of print quality; outputs from dotmatrix printers are not acceptable, Illustrations should be on separate sheets, about twice the size of the finished size in print. All letters, numbers and legends must be included on the illustration with the author's name, short title of the paper, and figure number written on the vereso. A list of captions should be provided on a separate sheet.

Unit of Measure
Metric units must be used for all measurements.

Citations and References
Items in the reference list should be referred to in the text by inserting, within parentheses, the year of publication after the author's name. If there are more than two authors, the first author should be cited followed by '*et al*'. The names of all authors, however, will appear in the reference list.

In the case of citing an author who has published more than one paper in the same year, the papers should be distinguished by addition of a small letter, e.g. Choa (1979a); Choa (1979b); Choa (1979c).

In the reference list, the names should be arranged alphabetically according to the name of the first author. Serials are to be abbreviated as in the *World List of Scientific Periodicals.*

The abbreviation for Pertanika Journal of Science and Technology is *Pertanika J. Sci. Technol.*

The following reference style is to be observed:

Monograph
Alefed, G. and J. Herzberger. 1983. *Introduction to Interval Computations.* New York: Academic Press.

Chapter in Edited Book
Muzzarell, R.A.A. 1980. Chitin. In *Polymers in Nature,* ed. E.A. MacGregor and C.T. Greenwood, p. 417-449. New York: John Wiley.

Serials
Kamaruzaman Ampon. 1991. The effect of attachment of hydrophobic imidoesters on the catalytic activity of trypsin. *Pertanika* **14(2)**: 18-185.

Proceedings
Mokhtaruddin, A.M. and L.M. Maene. 1981. Soil erosion under different crops and management practices. In *Agricultural Engineering in National Development,* ed. S.L. Choa, Mohd Zohdie Bardaie, N.C. Saxena and Van Vi Tran, p. 245-249. Serdang, Malaysia: Universiti Pertanian Malaysia Press.

Unpublished Materials (e.g. theses, reports & documents)

Sakri, 1. 1990. Proper construction set-up of Malaysian Fish Aggregating Devices (Unjam). Ph.D. Thesis, Universiti Pertanian Malaysia, Serdang, Selangor.

Pertanika Journal of Science & Technology

Volume 9 No. 2, 2001

Contents

ISSN 0128-7680

07

9 770128 768083